

***IN SITU* FORMING HYDROGELS USING SELF-  
ASSEMBLY OF FLUOROALKYL-ENDED  
POLY(ETHYLENE GLYCOL)S**

**Thesis by  
Giyoong Tae**

In Partial Fulfillment of the Requirements

for the degree of  
Doctor of Philosophy

California Institute of Technology

Pasadena, California

2002

(Submitted November 12, 2001)

© 2002

Giyoong Tae

All Rights Reserved

Dedicated to My Parents and Family for their love and support

## Acknowledgements

I would like to appreciate the former and current members in Julie Lab for their help and the good environment I had. I really enjoyed the life in this lab, and I don't think I can find this kind of open-minded lab in any other place. First, former members, Zhongren, Guru, Weijun, Sunil, Ani, Bhavana, Deniz, Jagdish, Ravi, Chris, and Hee-Hyun; they were all highly talented and helpful to solve many detailed problems I faced in my experiments, and they were willing to spend any time for me. Current members, Anne, Mike, Wei, Eric, Derek, Lucia, Charles, Young Bok, Rob, Maria, Fred; I am grateful that I was together with them and wish them great achievements.

I also would like to thank the former and current members in Jeff Lab. Insup, Cheng-Yun, Don, John, Thomas, Sven, Alison, Natalie, Shelly; even though I did not spend a long time with them, they helped the initiation of my experiments in my first year and also my short visit to ETH, Zurich. Yong, Hugo, Ronald, Alessandro; without them, I couldn't do anything during my visit there.

I should mention that I got several essential experimental data from the help of several people in other places. First of all, Dithelm Johannsmann at MPI in Mainz, Germany, provided me the facilities for SPR and QCR experiments. He was really supportive of my experiments, and he also showed a warm heart to make me feel easy during my visit there. Prof. Thio E. Hogen-Esch, and former student Huashi Zhang, at USC showed me his lab and synthesis protocol so that I could make my samples. Jyotsana Lal and Ed Lang at ANL in Illinois helped me to get the SANS data. Also, A.F. Parlow in National Hormone & Pituitary Program provided human growth hormone for my release experiments.

I would like to appreciate to my committee members, Professor Mark Davis and Zhen-Gang Wang for their valuable time and effort on my research.

Luckily, I have had two wonderful advisors, Julie Kornfield and Jeff Hubbell. They both showed a great patience for my inefficient progress and insufficient communication skill. Julie tried to help me in every way, and guided me into the right direction with her brilliant physical insight. More importantly, she kept cheering me up and made me feel optimistic about my progress. Her encouragement was essential for me to finish my study here. Jeff amazed me by his vast knowledge and excellency in various areas, as well as effective and critical guidance in spite of infrequent contacts. Both of them were also very generous to support my short-term visits to several places and participation in numerous conferences.

Finally, I would like to thank to my family. As the youngest, I only received love from all my family. My parents provided me their endless love and support. They kept giving me their special care, and it was a driving force for my study. My brother and sister had concern for my studies, too. Fortunately, I got the most important thing, my own family, during my study here. Whijihn, my lovely wife, and Sangwook, my son; with them, I could overcome the hard times during my final years. I also acknowledge my parents-in-law for their concern and help.

## Thesis Abstract

Telechelic polymers with hydrophilic midblocks (poly(ethylene glycol), PEG) and hydrophobic end groups (fluoroalkyl,  $R_f$ ) are synthesized and explored as candidates for in situ forming hydrogels for biomedical applications. Relevant physical properties, including phase behavior, rheology and erosion kinetics, are characterized to guide rational design of polymers for specific applications, including controlled release of therapeutic proteins and deposition of biocompatible surface layers. Disruption of the aggregation of the end groups using biocompatible complexing agents or solvents produces a low viscosity liquid that is injectable; self-assembly of the gel once inside the body can be achieved gently by diffusion of the complexing agent or solvent out into the surrounding tissue. By modulating molecular structure, the mechanical and erosion properties of these hydrogels can be systematically varied over a wide range for desired applications.

With increasing fluoroalkyl length relative to PEG length, the phase behavior of these fluoroalkyl-ended PEGs ( $R_f$ -PEGs) polymers in aqueous solution changes from single-phase behavior (continuous transition in properties from solution-like to gel-like with increasing concentration), to sol-gel coexistence, to an insoluble precipitate (Chapter 2). For sol-gel coexisting polymers, the equilibrium gel concentration and the modulus of the gel phase are governed by the length of the PEG midblock, whereas the relaxation time is determined by the hydrophobe length. The erosion characteristics of these hydrogels correlate with their phase behavior: the gels of sol-gel coexisting species exhibit surface erosion in an open system with slow dissolution rate controlled by the end-group length, whereas gels showing single-phase behavior exhibit bulk erosion that is relatively fast.

Aqueous solutions of  $R_f$ -PEGs exhibit ordering transitions with increasing concentration (Chapter 3). The hydrophobic cores of the micelle-like aggregates order into a body-centered-cubic (BCC) structure. The aggregated state of the hydrophobic core is determined by the length of the hydrophobic end group, and is insensitive to the concentration of the polymer solution or the temperature. A shorter PEG length for a given end group produces a much enhanced ordering compared to a longer one. This micelle packing effect is manifested in changes in the viscoelastic properties: the single-relaxation behavior evolves to the appearance of a new low frequency elastic plateau in the dynamic moduli, and a linear response changes to a yielding behavior in creep.

The gel phase of sol-gel coexisting polymers can be transformed into an injectable state by the addition of a bio-tolerable organic solvent, such as N-methyl pyrrolidone (NMP), and this solution can be restored to a hydrogel state quickly after injection by removal of the organic solvent by diffusion. Release of Human growth hormone (hGH) using this injectable formulation (Chapter 4) reveals that hGH remains stable inside the hydrogel formed, and more than 2 weeks of prolonged release of hGH pretreated with zinc is obtained using the injectable formulation without irreversible aggregation. For the  $R_f$ -PEGs examined here, the release rate of hGH is determined by the rate of diffusion through the hydrogel.

The telechelic  $R_f$ -PEGs that exhibit sol-gel equilibrium or precipitated gel phase behavior provide a facile route to hydrophilic modification of poly(tetrafluoroethylene) (PTFE) surfaces that are frequently encountered in biomedical devices (Chapter 5). Dip coating of PTFE into 1 wt %  $R_f$ -PEGs in ethanol, followed by immersing into water,

converts the surface of PTFE from hydrophobic to hydrophilic. The lifetime of this modification is correlated to the phase behavior of the bulk gel state, and stable in the various ranges of shear rates. An  $R_f$ -PEG that is insoluble in water gave a stable modification over a period of weeks in the absence of shear, and persisted for days when subjected to the highest shear stresses encountered in arteries (3-4Pa). Telechelic  $R_f$ -PEGs are effective, while monofunctional PEGs with a single fluoroalkyl group are not.

The swelling and drying behaviors of thin films of  $R_f$ -PEGs ( $\sim 0.1 \mu\text{m}$ ) show abnormalities relative to glassy and semi-crystalline films (Chapter 6). In a humidity ramp test starting from a dry state, thin films of  $R_f$ -PEGs show a distinctive hysteresis behavior; as humidity increases, little swelling occurs until  $\sim 85\%$  humidity, then the film swells rapidly; as the humidity decreases, a rapid deswelling occurs near  $\sim 75\%$  humidity. In a humidity step test, following a step-up the mass increase shows an overshoot, followed by a gradual approach to the equilibrium value, whereas the film tracks the equilibrium state very rapidly and monotonically following a step down from high to low humidity.



## Contents

Acknowledgements	iv
Thesis Abstract	vi
Contents	ix
<b>1 Introduction</b>	<b>1</b>
Objectives of Research	1
Associative Polymers	2
Phase behavior	3
Pheological properties	5
Aggregation number of the junction site	6
Lyotropic ordering transition	7
Polymers for Drug Delivery	8
<i>In situ</i> Transition Systems	10
Thesis Organization	13
References	14
<b>2 Phase Behavior and Erosion Properties of <math>R_f</math>-PEGs</b>	<b>19</b>
Introduction	20
Experimental Section	23
Synthesis of end-group modified PEGs	23
Characterization of sol-gel equilibria	26
Mechanical property measurements	27
Characterization of erosion of gel phases	27
Results	28
Phase behavior	28
Mechanical properties of gel phases of sol-gel coexisting species at $C_{gel, eq.}$	30
Erosion characteristics	32
Discussion	36
Comparison to prior studies of $R_f$ -PEGs	36
Implications for biomedical applications	37
Implications for theory	38
Conclusions	44
References	46
<b>3 Ordering Transition of <math>R_f</math>-PEGs: Rheology and SANS</b>	<b>60</b>
Introduction	61
Experimental Section	64
Synthesis of PEGs with fluorocarbon end-groups ( $R_f$ -PEGs)	64
Rheological measurements	64
SANS measurements	65
Results	66
Phase behavior	66
Linear viscoelastic properties of non-phase separating species	66
Linear viscoelastic properties of gels for sol-gel coexisting species	67

Comparison of Rf-PEG to bare PEG .....	68
Creep behavior .....	69
Lyotropic ordering of the gel phase .....	70
Aggregation number of the hydrophobic core .....	71
Discussion .....	73
Characteristics of single-phase species .....	73
Ordering transition .....	75
Plateau modulus .....	76
End-group dissociation mode .....	78
Conclusions .....	79
References .....	80
<b>4 <i>In situ</i> Transformation and Protein Release from Injectable Formulation</b> .....	<b>98</b>
Introduction .....	99
Experimental Section .....	102
Synthesis of end-group modified PEGs (R <sub>f</sub> -PEGs) .....	102
Mechanical properties .....	102
<i>In situ</i> transition experiments .....	103
Protein release experiments .....	103
Results and Discussion .....	104
Hydrogel with controlled, surface erosion characteristics .....	104
<i>In situ</i> transition using cyclodextrin complexation .....	105
<i>In situ</i> transition using organic solvents .....	108
The sustained release of hGH from the injection formulation .....	109
Conclusions .....	112
References .....	114
<b>5 Surface Modification of Poly(Tetrafluoroethylene)(PTFE) Using R<sub>f</sub>-PEGs</b> .....	<b>123</b>
Introduction .....	124
Experimental Section .....	126
Materials (R <sub>f</sub> -PEGs) .....	126
Surface modification of PTFE with R <sub>f</sub> -PEGs .....	126
Characterization of surface properties of PTFE .....	127
Stability of R <sub>f</sub> -PEG adsorption under flow condition .....	128
Electron Spectroscopy for Chemical Analysis (ESCA) .....	128
Results and Discussion .....	128
R <sub>f</sub> -PEG adsorption onto PTFE .....	128
Characterization of R <sub>f</sub> -PEG adsorption by ESCA .....	131
Conclusions .....	133
References .....	134
<b>6 Swelling Behavior of Thin Films of R<sub>f</sub>-PEGs under Controlled Humidity</b> .....	<b>141</b>
Introduction .....	142
Experimental Section .....	144
Materials (R <sub>f</sub> -PEGs) .....	144
Mass determination by QCR with control of humidity .....	145

Results .....	146
Humidity ramp test .....	146
Humidity step test .....	147
Discussion .....	147
Sorption isotherm .....	147
Transient sorption .....	149
Conclusions .....	151
References .....	153

## List of Figures

1.1	Schematic diagram of chain association for the associative polymers in weak association regime as a function of concentration. ....	17
1.2	The rheological properties of associative polymers in weak association regime. ....	18
2.1	Schematic diagram of the surface plasmon resonance (SPR) experiment in contact with a flowing system. ....	51
2.2	Single relaxation behavior of the equilibrium gel for the sol-gel coexisting species. ....	52
2.3	Dynamic moduli of gel phases of sol-gel coexisting species at equilibrium compositions. ....	53
2.4	Change of surface plasmon resonance angle with time for 10KC8 film of initial dry film thickness 0.55 $\mu\text{m}$ . ....	55
2.5	Dissolution time as a function of the initial dry thickness of 10KC8 gels. ....	56
2.6	Lyotropic phase transition of one-end modified PEG solutions. ....	57
2.7	Phase diagram of the end-group modified PEG systems. ....	58
2.8	Schematic representation of dissolution of the polymer gel in an open environment. ....	59
3.1	Dynamic moduli of 20KC10 solutions. ....	83
3.2	Concentration dependence of material properties of 20KC10 solutions. ....	84
3.3	Dynamic moduli of 10KC8 solutions at $C > C_{\text{gel,eq}}$ at 25 $^{\circ}\text{C}$ ....	85
3.4	Development of the low-frequency plateau with time after loading. ....	87
3.5	Dynamic moduli of 10KC8 12 wt % solution at various temperatures. ....	88

3.6	Creep responses (a) as a function of molecular structure for fixed concentration (17 wt %, $\sigma = 500$ Pa), and (b) as a function of applied shear stress (for 10KC10 17 wt %)	89
3.7	SANS pattern of 10KC8 solutions as a function of concentration at 25 °C.	91
3.8	SANS pattern of 10KC8 12 wt % as a function of temperature.	92
3.9	Comparison of SANS patterns for various species at 12 wt % at 25 °C.	93
3.10	SANS pattern of 10KC10 15 wt % solution at 25 °C.	94
3.11	SANS pattern of dilute (0.5 wt %) monofunctional R <sub>f</sub> -PEG solutions.	95
3.12	Concentration dependence of the (a) “effective fraction,” $G_0/nkT$ , and (b) relaxation time of the end-group dissociation mode, $\tau_{e,d}$ .	97
4.1	Decrease in viscosity of 10KC8 in aqueous solution, induced by addition of NMP to disrupt association.	116
4.2	Restoration of injectable depot into hydrogel state of 10KC8 solution by being exposed to a water reservoir.	117
4.3	BSA release from the pre-made gel state for various R <sub>f</sub> -PEGs at 37 °C.	118
4.4	Schematic depiction of application of the present <i>in situ</i> forming hydrogel system as an injectable depot for sustained release of proteins.	119
4.5	hGH release from 6KC8 hydrogel without Zn-pretreatment of hGH.	120
4.6	hGH release from 6KC8 hydrogel with Zn-complexed hGH.	121
4.7	Protein release from the injectable formulation.	122
5.1	The change in the capillary rise by the hydrophobicity of the surface of the capillary that is located at the air-water interface.	136

5.2	The change of the capillary rise of the R <sub>f</sub> -PEG modified PTFE tube with time under flow of water for various wall shear stresses. ....	137
5.3	The schematic representation showing the physical junction state of fluorocarbon engroups of R <sub>f</sub> -PEG molecules. ....	139
5.4	The schematic representation showing the physically aggregated state of R <sub>f</sub> -PEG molecules on PTFE surface. ....	140
6.1	Change of swelling state of 6KC8 thin film ( $\sim 1.0 \times 10^2$ nm when dry) for the change in humidity. ....	155
6.2	Change of swelling state of 6KC8 thin film ( $\sim 1.0 \times 10^2$ nm when dry) for various rates of humidity ramp rates. ....	156
6.3	Changes of swelling states of two different 10KC10 thin films for the change of humidity at 2%/hr.. ....	157
6.4	Changes of swelling states with decreasing humidity for different R <sub>f</sub> -PEGs. ....	158
6.5	Change of swelling state of 6KC8 thin film ( $\sim 1.0 \times 10^2$ nm) for the step change of humidity from 20% to 90%.....	159
6.6	Changes of swelling states of 6KC8 thin films ( $\sim 1.0 \times 10^2$ nm) for the step changes of humidity from 20% to various states.....	160
6.7	Changes of swelling states of 10KC10 thin films of two different thicknesses for the step change of humidity from to 90%.. ....	161

**List of Tables**

2.1	Bifunctional $R_f$ -PEGs. ....	24
2.2	Monofunctional $R_f$ -PEGs. ....	26
2.3	Phase Behavior of Bifunctional $R_f$ -PEGs at 25 °C ....	30
2.4	Mechanical Properties of Gel Phases at $C_{gel,eq}$ . at 25 °C. ....	31
2.5	Dissolution Rates at 25 °C. ....	36
3.1	Aggregation Number of $R_f$ -PEG Solutions. ....	72
4.1	$R_f$ -PEGs with Controlled, Surface Erosion Characteristics. ....	105
5.1	$R_f$ -PEGs. ....	126
5.2	ESCA Analysis of $R_f$ -PEG Modified PTFE Sheet.....	132
6.1	$R_f$ -PEGs. ....	145

# Chapter 1. Introduction

## Objectives of Research

For biomedical applications, there is a general need for materials that are compatible with minimally invasive surgery and other relatively non-invasive procedures. Development of materials that can be non-invasively manipulated *in vivo* presents many unsolved challenges. Materials should be introduced in a liquid state that can be injected through a small opening to create a potentially much larger object in the body. Solidification must be accomplished in a gentle manner that does not harm surrounding tissue or damage the cells or proteins that might be incorporated into the therapeutic material.

This thesis explores the potential of physically associating polymers as a versatile class of materials for biomedical applications. Physical association provides a route to biocompatible materials and methods to induce *in situ* transitions from an injectable state to a hydrogel that is resorbable. However, the molecular design principles to produce hydrogels with desired erosion behavior (e.g., surface *vs.* bulk erosion), desired erosion kinetics, and material properties are not known. First, the relationships between macromolecular structure and the physical structure and properties of associative hydrogels are not known. Second, biocompatible means to transform these polymers from a low viscosity liquid to a gel are not known. Finally, the design of materials for specific biomedical applications needs to be demonstrated.

This thesis sets out to establish these structure-property relations for phase behavior, rheology, and erosion kinetics for the class of physical gels that have hydrophilic, biocompatible midblocks capped with hydrophobic biocompatible end groups.



Poly(ethylene glycol) (PEG) is chosen as the hydrophilic polymer because of its favorable properties of biocompatibility, non-toxicity, and non-immunogenicity. Among hydrophobes, we examine fluoroalkyl segments because of their superior hydrophobicity and chemical and biological inertness. By systematically probing the effects of PEG length and fluoroalkyl length, this research yields new insights into the interplay of interactions mediated by the hydrophilic polymer midblock and aggregation behavior of the end groups. Guided by understanding of the structure property relations of the self-assembled gels, we demonstrate biocompatible means to disrupt aggregation. We also illustrate how integrated understanding of phase behavior and physical properties enables the design of polymers for specific biomedical applications through two examples: controlled release of a therapeutic protein and surface modification of poly(tetrafluoro ethylene) (PTFE).

The prior knowledge that was the foundation for this research was drawn from three areas: the physics of associative polymers, the design of polymers for controlled release applications, and methods for *in situ* solidification of biomedical materials inside the body. A brief review of the literature on associative polymers highlights the physical insight that inspired the present study, as well as indicating the limitations of prior knowledge. Then, we summarize the issues specific to polymers for controlled release applications and methods for *in situ* solidification.

## **Associative Polymers**

Associative polymers are macromolecules with attractive groups at the ends or distributed along the main chain of the molecules. Association among attractive groups

drives formation of inter- and intramolecular physical junctions in solution. Electrostatic interaction, hydrogen bonding (charged or H-bonding polymers in a low polarity solvent), or solvo-phobic interaction (block copolymers in selective solvent, e.g., hydrophobic interaction in an aqueous environment) can be the source of attraction. Since macroscopic solution properties like viscosity can be adjusted dramatically by controlling the physical associations, e.g., by temperature or concentration, these polymers have a wide range of applicability, including rheological thickeners, adhesives, adsorbents, coatings, flocculants, surfactants and stabilizers for heterogeneous polymerization,<sup>1</sup> and DNA sequencing media.<sup>2</sup>

### **Phase behavior**

Most of the studies of associative polymers have examined systems with weakly associating groups at both ends (telechelic structure).<sup>2-13</sup> These polymers exhibit single-phase behavior at all concentrations, with a continuous increase of viscosity and elasticity as concentration increases due to the formation of bridges between the hydrophobic clusters of end-groups (Figure 1.1). This may be regarded as a sol-gel transition, but is not a thermodynamic phase transition.

In contrast, associative polymer systems with strong association between polymer chains by increasing either the strength of attraction of the associating groups or the number of association sites per molecule could result in a first-order phase transition from sol to physical gel.<sup>1,3,4,5</sup> Experimentally, a few cases of phase separation into coexisting sol and gel have been reported for the aqueous solutions of poly(ethylene glycol)s (PEGs) modified with long alkyl groups at both ends.<sup>3,4</sup>

Theorists anticipated that telechelic associative polymers could show a first order phase transitions from sol to gel. Hydrophilic polymers with hydrophobes at both ends would experience the osmotic repulsion among micelle cores that is present in analogous monofunctional chains (diblocks). The new feature that is present in the telechelic case is the ability to form bridges between micelle cores. Semenov et al. recognized that this would provide an entropic driving force toward the formation of a dense phase of micelles, since the number of configurations of the hydrophobes would be greatly increased when the micelles were close enough to permit bridging.<sup>5</sup> This entropic attraction increases with aggregation number. So, when the attraction is sufficiently large to overcome the repulsion, the system separates into two phases. Some important features in his model are the following. 1) Both attraction and repulsion among micelles are determined by aggregation number ( $p$ ) only, not by the midblock length ( $N$ ). 2) The average polymer concentration within the equilibrium gel ( $\phi^*$ ) scales with  $\sim (p^{1/2}/N)^{3\nu-1}$ , where  $\nu$  is the Flory exponent, so both aggregation number and midblock length influence the equilibrium gel concentration. 3) The two phases are a close packed, solid-like phase of micelles and a dilute, gas-like phase of micelles and free chains. Therefore, above the equilibrium gel concentration, stress is relaxed by micelle hopping from site to site in an ordered structure.

In an attempt to describe the phase diagram for associative polymers, Pham et al. extended the model by making an analogy between the associative micelles and adhesive hard spheres, where the “stickiness parameter ( $\tau_s^{-1}$ )” is used to describe the attraction among the “sticky hard spheres”.<sup>4</sup> Important features of this model are the following. 1) This approach provides a general phase diagram in terms of “stickiness parameter” and

volume fraction of micelles, so it has the potential to offer more quantitative predictions than the purely scaling approach of Semenov et al. 2) The “stickiness parameter” is only a function of  $p$ , not  $N$ . So, the phase behavior is determined by  $p$  only, and the equilibrium concentration in terms of volume fraction of each phase in the phase separation regime is also determined by  $p$  alone. 3) Experimentally observed phase concentrations could be explained by the empirically determined “stickiness parameter” with the binodal phase boundary of the sticky hard sphere model.<sup>4</sup> So, phase separation is viewed by Pham et al. as a coexistence of a liquid and a gas of micelles.

### **Rheological properties**

Rheological properties of the associative polymer solutions for the case of weak association (no phase separation) are relatively well understood (Figure 1.2). The most distinct linear viscoelastic property of associative polymer solutions is that they exhibit single relaxation time behavior (Maxwell fluid). Above the overlap concentration, where the micelle-like clusters are connected to each other so that they greatly enhance the viscosity, the stress is relaxed by the breakage of junctions among micelle-like clusters. The relaxation time associated with the breakage of a bridge or super-bridge also changes with topology of the physical network, which is determined by the concentration. The relaxation time increases rapidly at low concentration as the average length of superbridges decreases, but saturates at higher concentration, when the connected topology among micelle-like clusters does not change any more (all links are single-chain bridges).<sup>6</sup> The non-linear viscoelastic properties include a three-region flow curve (viscosity vs. shear rate): a shear-rate-independent region at low shear rates, a modestly

shear thickening region at moderate shear rates, and a shear thinning region at high shear rates. The origin of the unusual shear thickening is not known (hypotheses include shear-induced increase of bridges<sup>7</sup> or increased overlap between stretched elastic strands<sup>1</sup>); the pronounced shear thickening is attributed to shear-induced conversion of bridges to loops.<sup>7</sup> However, little is known about the rheological properties of the gel phase of associating polymers that exhibit sol-gel coexistence.

### **Aggregation number of the junction site**

Both theoretical models of associative polymers in the two phase regime suggest that the aggregation number of the association site is the most important parameter that determines the phase behavior of the associative polymer solution. Therefore, quantitative determination of the aggregation number is very important toward understanding any given system. In spite of a number of prior studies of aqueous solutions of PEG modified with hydrophobes at both ends, knowledge regarding the aggregation number is relatively limited. First, there is ongoing controversy about the effect of concentration on the aggregation number; some results suggest that the aggregation number does not change with concentration,<sup>8</sup> whereas others provide evidence of increasing aggregation number with increasing concentration.<sup>9</sup> Second, while the effect of hydrophobe length on aggregation number for a fixed midblock length has been reported,<sup>4</sup> no experimental data is available either on the effect of midblock length for a fixed hydrophobe, or on the effect of temperature for a fixed concentration. Furthermore, no agreement has been made on the method of analyzing the aggregation number; different methods lead to different aggregation numbers for the same material.<sup>4,9</sup>

The method using fluorescence quenching has the intrinsic limitation coming from the effect of hydrophobic fluorescence dye on the aggregated state,<sup>8</sup> and the method using light scattering has the uncertainty from the intrinsic viscosity data, especially for the system having low equilibrium sol concentration.<sup>4</sup> The method using the scattering pattern of x-ray or neutron<sup>9</sup> beams might give the most reliable data. Therefore, careful, systematic characterization of the aggregation number of a series of samples is required to establish the effects of concentration, hydrophobe lengths and PEG length.

### **Lyotropic ordering transition**

When a phase transition from a disordered to an ordered state is achieved by changing the concentration of a solute, it is referred to as a lyotropic transition. Colloidal suspensions in which interparticle interactions are purely repulsive are known to order into cubic phases at sufficiently high concentration (e.g., micelles formed from diblock copolymers in a selective solvent for one block<sup>10</sup> or star-polymers in solution<sup>11</sup>). Diblock copolymer micelles normally order into a body-centered-cubic (BCC) structure. However, a face-centered-cubic (FCC) structure forms when the corona is sufficiently thin compared to the size of the core.<sup>10</sup> Similarly, star-polymer solutions order into a BCC structure when the number of arms is modest (~30 - ~60), whereas it orders into a FCC structure when this number is higher.<sup>11</sup> For both cases, the soft colloids prefer a BCC structure in their lyotropic ordering, but this tendency shifts toward a FCC structure when the colloidal particles become more rigid.

Considering the micelle-like character of telechelic associative polymers, the solution may display a lyotropic ordering transition, and two cases of lyotropic ordering have been

reported. Cubic order was found for the gel phase of systems with short PEG chains (2k and 4k g/mol) with  $C_{12}H_{25}$  ends,<sup>3</sup> possibly a BCC or a simple cubic (SC) structure. An ordered phase was also observed in a system with relatively long PEG and fluoroalkyl ends (10k with  $C_8F_{17}C_{11}H_{22}$ ), which was assigned as a FCC structure.<sup>12</sup> In contrast, disordered, liquid-like phases were reported for systems with longer PEG (35k or 20k g/mol PEG with alkyl groups). It is noteworthy that even systems that displayed phase separation were reported to have liquid-like order,<sup>4,13</sup> in contrast to Semenov's concept of coexistence between a micellar solution and a micellar solid.<sup>5</sup> The connection between the lyotropic ordering transition and macroscopic viscoelastic properties has not been investigated at all, even though the literature on block copolymers suggests that ordering would have dramatic effects on rheological properties. Thus, there is a need for systematic investigation of the lyotropic ordering transition as a function of molecular structure and concentration of associative polymer.

## **Polymers for Drug Delivery**

Controlled drug delivery systems have been studied and developed extensively to enable the effective use of the target drug, which implies 1) a sustained drug concentration at the desired therapeutic level (without potentially toxic over-dosing or ineffective under-dosing), 2) a potential decrease in the amount of drug needed, 3) a high concentration only at the desired site (local delivery), and 4) improved stability and circulation time of drugs with short half-lives.

Approaches to achieve controlled release profiles of entrapped drug studied so far include the use of micelle,<sup>14</sup> lipid bilayer,<sup>15</sup> aerosol,<sup>16</sup> and polymeric implant systems.

Polymeric implants are distinguished by their broad relevance to tissue engineering,<sup>17</sup> sustained release,<sup>19-22</sup> and mechanical supports.<sup>18</sup> Early work on polymeric implants was initiated by entrapping drug inside solid non-degradable polymers.<sup>19</sup> Then, to avoid the need of removal of implanted polymers, biodegradable polymers such as polyesters<sup>20</sup> and polyanhydrides<sup>21</sup> were developed. Both biodegradable or non-biodegradable systems have been successful in the delivery of hydrophobic, relatively small drugs, but larger molecular weight drugs, such as therapeutic protein drugs, are more difficult to deliver. To overcome the problem of extremely slow release for high molecular weight drugs, porous polymers were developed to enhance the release rate of larger molecules, such as therapeutic proteins.<sup>22</sup> However, additional difficulties remain due to the interaction between the proteins and hydrophobic polymers, such as the instability of proteins located at hydrophilic-hydrophobic interfaces between the aqueous environment and these polymers, e.g., irreversible adsorption of the protein to the polymer surface or irreversible denaturation or aggregation of the protein.<sup>23</sup>

As an alternative approach to protein drug delivery, degradable hydrogel systems have been studied due to their inherent hydrophilicity and biocompatibility.<sup>24</sup> Applying natural hydrogels, such as gelatin, collagen or polysaccharides, has the advantage of exploiting pre-existing and sometimes evolutionarily developed biological interaction and degradation pathways. On the other hand, natural hydrogels are limited by the difficulty of tailoring the degradation rate, as well as uncertain immunological responses and potentially difficult isolation and purification procedures.<sup>25</sup> The majority of synthetic biodegradable hydrogels are based on PEG because of its favorable properties of biocompatibility, non-toxicity, and non-immunogenicity.<sup>26</sup>



Most PEG-based degradable hydrogels developed so far have been made by incorporating a variety of cross-linkers to create a covalent network and degradation sites to induce degradation in the biological environment. In most cases, hydrolytically labile sites such as esters have been incorporated;<sup>27</sup> alternatively, enzymatic degradation sites have been introduced to achieve a degradative response to biological stimuli.<sup>28</sup> However, the majority of PEG-based hydrogels for the protein release developed so far are not injectable depots; they need to be inserted as an implant rather of preformed solids than by injection of liquid precursor of ultimate solids. Therefore, there is a need to develop injectable PEG-based hydrogel systems.

### ***In situ* Transition Systems**

For biomedical applications, there is a need for materials that can be introduced through a small opening to form a desired implant at the intended site of application, in intimate contact with sensitive biological materials. First, the *in situ* formation of material at the implantation site after being delivered as a liquid state has two potential advantages: the ability to match the morphology of a material implant to various complex tissue shapes in the body; and the ability to deliver a large device through a small hole in the body via minimally invasive surgery.<sup>29</sup> Second, this kind of system has various medical applications: as scaffolds for cell transplantation; to modulate interactions at tissue surfaces, such as barriers at the cellular or the protein level to guide tissue regeneration, a barrier for the prevention of thrombosis and intimal thickening after balloon angioplasty, a barrier for preventing postoperative adhesions, or a tissue adhesive; as a delivery carrier for controlled release of drugs or a structural support of

tissue sites to bear mechanical loads during healing or regeneration. In the context of minimally invasive surgery, '*in situ*' and 'in the presence of sensitive biological materials' refers to transition in direct contact with tissues of the body of the recipient. In the context of controlled release or tissue engineering, it also refers to transition in contact with a chemical, drug or cells intended for therapeutic or diagnostic use.

The most extensively developed method so far is to use photopolymerization (photochemically initiated free radical reactions of macromeric gel precursors by UV or visible light irradiation).<sup>30,31</sup> PEG terminated with acrylate groups was developed and applied successfully as mechanical barriers to control wound healing,<sup>31</sup> or to deliver drugs within the artery. By using more hydrophobic macromeric precursors, the transformed materials could bear mechanical load; polyesters formed from fumaric acid and poly(propylene glycol)<sup>32</sup> and acrylated copolymer based on poly(lactic acid and aspartic acid) were developed.<sup>33</sup> These photo-initiated crosslinking methods are very powerful, but they require complex instrumentation for provision of radiation inside the body.

An alternative approach, which obviates the need to perform irradiation in the body, is to mix two reactive precursor solutions, which then react with each other in a multifunctional manner to form a network. PEG terminated with N-hydroxysuccinimidyl (NHS) esters, which is reactive toward amine groups, can form a hydrogel when it is mixed with amine-terminated PEGs.<sup>34</sup> This method can lead to very fast gelation, but it can lead to undesired chemical reactions with surrounding tissues, and the number of highly selective reaction pairs is rather limited.<sup>35</sup>

Enzymatic crosslinking was also developed; transglutaminase was used to enzymatically catalyze formation of amide linkages.<sup>36</sup> This method can form covalent bonds in a controlled manner by adjusting the enzyme concentration, but it also can lead to undesired reactions with surrounding tissues due to the use of primary amines as reacting groups.

Thermodynamic physical transformation was used to achieve *in situ* gelation. Phase transitions of micellar solutions have been employed. Block copolymer solution of poly(propylene glycol) (PPO) and PEG (PPO-PEG-PPO triblock) has a lower critical solution temperature, so it is a liquid at low temperature and can become a gel at body temperature.<sup>37</sup> Also, the solution of certain block copolymers of PEG and poly(lactic acid) (PLA) (either diblock or PEG-PLA-PEG triblock) can form a liquid at high temperature (>40 °C), and then form a gel state at body temperature.<sup>38</sup> These methods are very simple, but the gels that result have weak mechanical strength,<sup>37</sup> and the injection temperature can be high, which might be harmful to the tissue,<sup>38</sup> and the gels frequently demonstrate unacceptably fast degradation rates in open systems.<sup>37,38</sup>

Precipitation of a polymer solution has been used to produce a solid *in situ*; a biodegradable polymer, such as poly(lactic-co-glycolic acid), is dissolved in a biocompatible organic solvent, and when it is injected into an aqueous environment, the polymer precipitates.<sup>39</sup> This method can make use of commercially available polymers, but instead of a hydrogel state, a solid precipitate is obtained. Further, the most widely studied example, poly(lactic-co-glycolic acid), produces strongly acidic conditions in the vicinity of the implant as it degrades, triggering an inflammatory response in the

body.<sup>40,41</sup> Therefore, there is an ongoing need to develop a gentle *in situ* transition method for biomedical materials.

## Thesis Organization

The thesis presents the synthesis, characterization, physics and applications of fluoroalkyl-ended PEG systems. From Chapter 2 to 4, we describe the material properties and method of *in situ* formation of hydrogels using the fluoroalkyl-ended PEG systems: their phase behavior and the erosion properties of R<sub>F</sub>-PEG hydrogels (Chapter 2), their ordering transition using rheology and scattering measurements (Chapter 3), and biocompatible *in situ* transition methods to convert from sol to gel and *in vitro* demonstration of protein release from injectable depots (Chapter 4).

The last two chapters of the thesis present additional interesting discoveries that resulted from this research. Guided by the phase behavior of the R<sub>F</sub>-PEGs, we explored the possibility of using them to conveniently treat the surface of poly(tetrafluoroethylene) (PTFE) to provide a hydrophilic, biocompatible surface on PTFE-encapsulated devices (Chapter 5). Furthermore, due to the semi-crystalline nature of dry PEG and the high hydrophilicity of PEG, the swelling behavior of the present polymers shows unprecedented features relative to either amorphous polymers or previously studied semi-crystalline polymers (Chapter 6).

## Reference

- [1] Rubinstein, M.; Dobrynin, A. V. *Trends Polym. Sci.* **1997**, *5(6)*, 181
- [2] Menchen, S.; Johnson, B.; Winnik, M.A.; Xu, B. *Chem. Mater.* **1996**, *8*, 2205
- [3] Francois, J.; Maitre, S.; Rawiso, M.; Sarazin, D.; Beinert, G.; Isel, F. *Colloids Surf. A* **1996**, *112*, 251
- [4] Pham, Q. T.; Russel, W. B.; Thibeault, J. C.; Lau, W. *Macromolecules* **1999**, *32(9)*, 2996
- [5] Semenov, A.N.; Joanny, J.F.; Khokhlove, A.R. *Macromolecules* **1995**, *28*, 1066
- [6] Annable, T.; Buscall, R.; Ettelaie, R. *J. Rheo.* **1993**, *37(4)*, 695
- [7] Tam, K.C.; Jenkins, R.D.; Winnik, M.A.; Bassett, D.R. *Macromolecules* **1998**, *31(13)*, 4149
- [8] Yekta, A.; Xu, B.; Duhamel, J.; Adiwidjaja, H.; Winnik M.A. *Macromolecules* **1995**, *28*, 956
- [9] Hakansson, B; Hansson, P.; Regev, O.; Soederman, O. *Langmuir* **1998**, *14*, 5730
- [10] McConnel, G.A.; Gast, A.P.; Huang, J.S.; Smith, S.D. *Phys. Rev. Lett.* **1993**, *71(13)*, 2102
- [11] Watzlawek, M.; Likos, C.N.; Lowen, H. *Phys. Rev. Lett.* **1999**, *82(26)*, 5289
- [12] Serero, Y.; Aznar, R.; Porte, G.; Berret, J.-F.; Calvet, D.; Collet, A.; Viguiier, M. *Phys. Rev. Lett.* **1998**, *81(25)*, 5584
- [13] Pham, Q. T.; Russel, W. B.; Thibeault, J. C.; Lau, W. *Macromolecules* **1999**, *32(15)*, 5139
- [14] Lasic, D.D. *Nature* **1992**, *335*, 279
- [15] Oku, N.; Naruse, R.; Doi, K.; Okada, S. *B.B.A.-BIOMEMBRANES* **1994**, *1191*, 389

- [16] Evans, R.M.; Farr, S.J.; Armstrong, N.A.; Chatham, S.M. *Pharmaceut.Res.* **1991**, *8*, 629
- [17] Chaignaud, B.E., Langer, R.S. and Vacanti, Synthetic Biodegradable Polymer Scaffolds Atala A and Mooney D (eds). Birhhauser, Boston, M.A. USA, **1997**
- [18] Slepian, M.J. *Caduil. Clin.* **1994**, *12*, 715
- [19] Fokman, J. and Long, D. *Surgical Research* **1964**, *4*, 139
- [20] Sato, T.; Kanke, M.; Schroeder, H.G. and Deluca, P.P. *Pharmaceut.Res.* **1988**, *5*, 21
- [21] Ron, E.; Turek, T.; Mathiowitz, E.; Chasin, M.; Hageman, M. and Langer, R. *Proc. Natl. Acad. Sci. USA* **1993**, *90*, 4176
- [22] Langer, R. and Folkmanm J. *Nature* **1976**, *263*, 797
- [23] Kim, H.K. and Park, T.G. *Biotech. Bioeng.* **1999**, *65*, 659
- [24] Zaho, X.; Harris, J. M. *J. Pharmaceutical Sci.* **1998**, *87*, 1450
- [25] Deluca, P. P.; Mehta, R. C.; Hausberger, A.G.; Thanoo, B. C. In *Polymeric Delivery Systems*; ACS: Washington, DC, **1993**, pp 53-79
- [26] Harris, J. M., *Poly(ethylene glycol) chemistry. Biotechnical and Niomedical Applications*, Ed., Pletinum: New Yrok, **1992**
- [27] Sawhney, A. S.; Pathak, C. P.; Hubbell, J. A. *Macromolecules* **1993**, *26*, 581
- [28] West, J. L.; Hubbell, J. A. *Macromolecules* **1999**, *32*, 241
- [29] Hubbell, J.A. *MRS Bulletin* **1996**, *Nov.*, 33
- [30] Sawhney, A.S.; Pathak, C.P.; Van, R.J.J.; Dunn, R.C. and Hubbell, J.A. *J. Biomed. Mater. Res.* **1994**, *28*, 831.
- [31] Hill-West, J.L.; Chowdhury, S.M.; Slepian, M.J. and Hubbell, J.A. *Proc. Natl. Acad. Sci. USA* **1994**, *91*, 5967.

- [32] Peter, S.J.; Yaszemski, M.J.; Suggs, L.J.; Payne, R.G.; Langer, R.; Hayes, W.C.; Unroe, M.R.; Alemany, L.B.; Engle, P.S. and Mikos, A.G. *J. Biomater. Sci. Polym. Ed.* **1997**, *8*, 893
- [33] Eliseeff, J.; Anseth, K.; Langer, R. and Hrkach, J.S. *Macromolecules* **1997**, *30*, 2182
- [34] Zhao, X. and Harris, J.M. *J. Am. Chem. Soc. Symp. Ser.* **1997**, *680*, 458
- [35] Elbert, D.L., Pratt, A.B., Lutolf, M.P., Halstenberg, S., Hubbell, J.A. Protein delivery from materials formed by self-selective conjugate addition reactions, *J. Controlled Rel.* **2001**, *76*, 11
- [36] Sperinde, J.J. and Griffith, L.G. *Macromolecules* **1997**, *39*, 5255
- [37] Simons, M.; Edelman, E.R.; DeKeyser, J.L.; Langer, R.; and Rosenberg, R.D. *Nature* **1992**, *359*, 67
- [38] Jeong, B.; Bae, Y.H.; Lee, D.S. and Kim, S.W. *Nature* **1997**, *338*, 860.
- [39] Dunn, R.L.; English, J.P.; Cowsar, D.R. and Vanderbilt, D.D. *US Patent 5 278 202*, **1994**.
- [40] Visscher, G.E.; Pearson, J.E.; Fong, J.W.; Argentieri, G.J.; Robison, R.L. and Maulding, H.V. *J. Biomed. Mater. Res.* **1988**, *22*, 733
- [41] Ignatius, A.A. and Claes, L.E. *Biomaterials* **1996**, *17*, 831

Hydrophobe

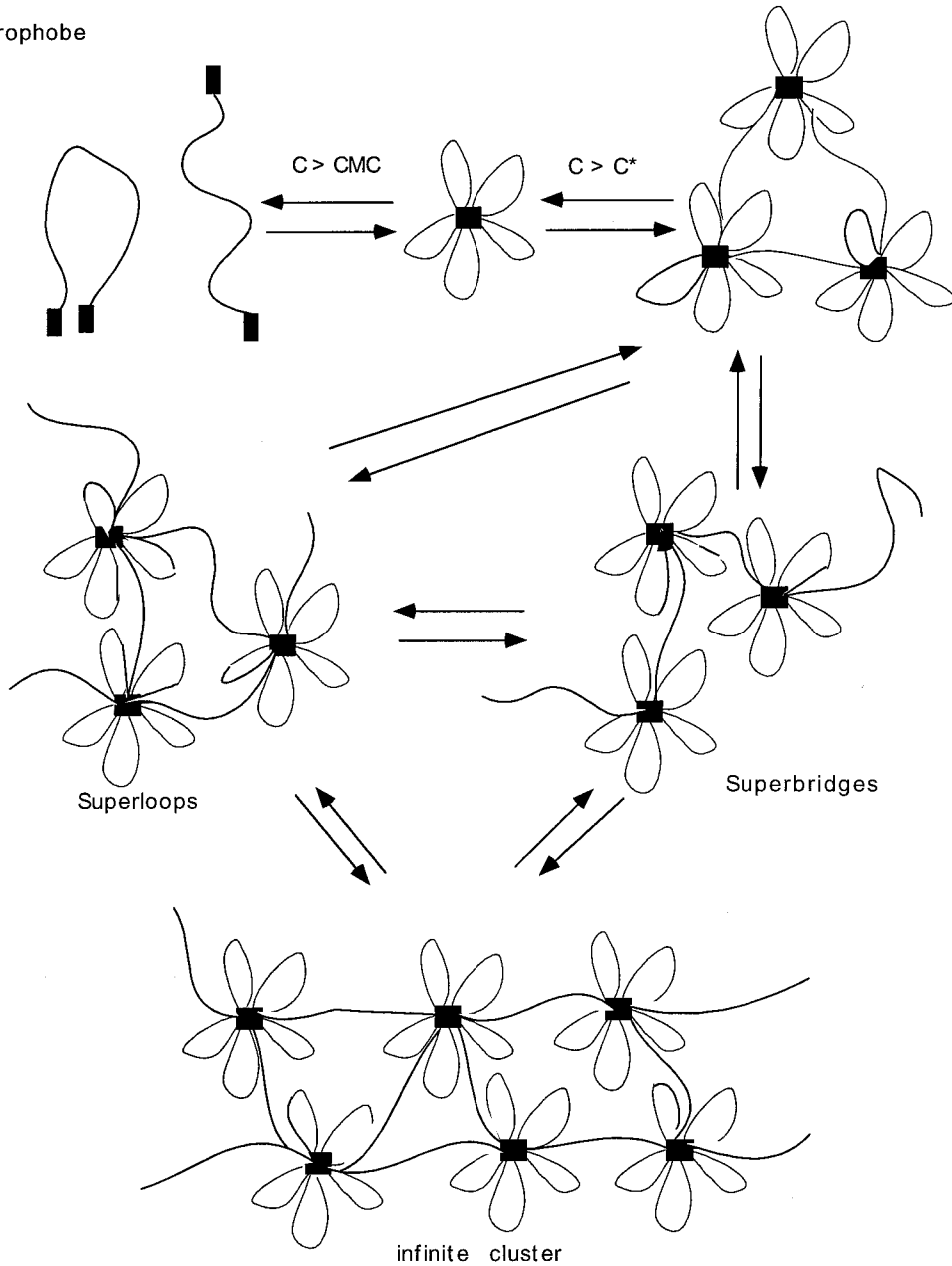


Figure 1.1 Schematic diagram of chain association for the associative polymers in weak association regime as a function of concentration. Above a critical concentration (like CMC), associative polymers self-assemble into micelle-like clusters. When the concentration reaches the overlap concentration, where the micelle-like clusters can touch each other, connections among these clusters start to form. As the concentration increases further, the size of the connected clusters of associative polymers grows continuously, making superloops or superbridges, and finally it forms an infinite gel-like cluster.



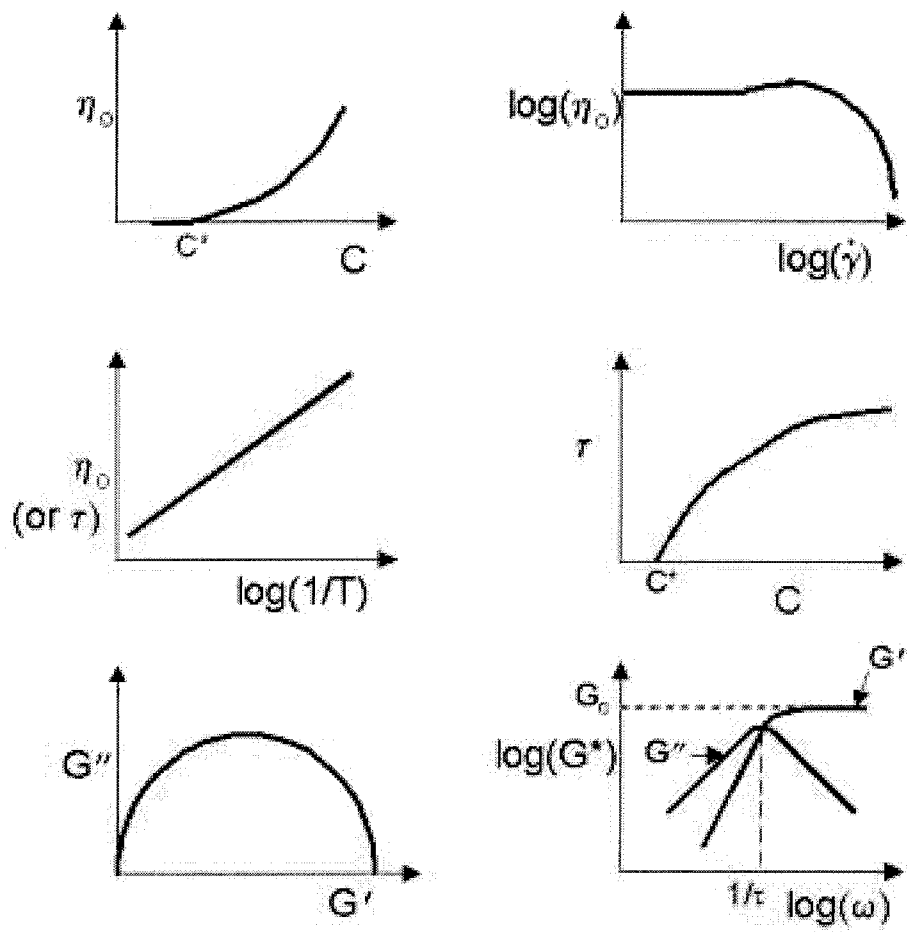


Figure 1.2 The rheological properties of associative polymers in weak association regime.

## Chapter 2. Phase Behavior and Erosion Properties of R<sub>f</sub>-PEGs\*

### Abstract

Poly(ethylene glycol) (PEG) ( $M_w = 6k, 10k, \text{ and } 20k \text{ g/mol}$ ) terminated at both ends by hydrophobic fluoroalkyl segment  $(-(\text{CH}_2)_2\text{C}_n\text{F}_{2n+1})$ ,  $n = 6, 8 \text{ or } 10$ ) was synthesized and demonstrated to self-assemble into hydrogels with phase behavior, mechanical and erosion properties that can be systematically varied by molecular design. With increasing fluoroalkyl length relative to PEG length, the phase behavior of these polymers in aqueous solution changes from the single-phase behavior of familiar associative thickeners, to sol-gel coexistence, to an insoluble precipitate. For those polymers that exhibit sol-gel coexistence, the equilibrium gel concentration (or swelling ratio of the gel phase) and the modulus of the gel phase are governed by the length of the PEG midblock, whereas the relaxation time is determined by the hydrophobe length. The erosion characteristics of these hydrogels correlate with their phase behavior: the gels of sol-gel coexisting species exhibit surface erosion in an open system with slow dissolution rate controlled by the end-group length; in contrast, hydrogels from polymers that show single-phase behavior exhibit bulk erosion that is relatively fast. Therefore, molecular structure of this class of polymers produces hydrogels whose mechanical and erosion properties can be tailored for desired applications.

---

\* The contents of this chapter were published in *Macromolecules* **2001**, *34*, 6409.

## Introduction

Bioerodible and biocompatible polymers are widely used in medicine for drug delivery and medical devices.<sup>1</sup> Relatively hydrophobic biodegradable polymers, e.g., poly( $\alpha$ -hydroxyl esters),<sup>1-3</sup> polyorthoesters,<sup>4</sup> and polyanhydrides,<sup>5</sup> have been successfully developed and used for the controlled release of hydrophobic drugs and as materials in structural supports, such as surgical suture, staples, and meshes. However, there also exists a need for hydrophilic resorbable materials that can incorporate protein drugs or cells,<sup>6</sup> or be used to guide wound healing, e.g., to prevent postoperative adhesion formation.<sup>7</sup> Degradable hydrogel systems have been studied for such purposes due to their inherent hydrophilicity and biocompatibility.<sup>8</sup>

Applying natural hydrogels, such as gelatin, collagen or polysaccharides, has the advantage of exploiting pre-existing and sometimes evolutionarily developed biological interaction and degradation pathways, but is limited by the difficulty of tailoring the degradation rate as well as uncertain immunological responses and potentially difficult isolation and purification procedures.<sup>1,6</sup> The majority of synthetic biodegradable hydrogels are based on poly(ethylene glycol) (PEG) because of its favorable properties of biocompatibility, non-toxicity, and non-immunogenicity.<sup>9</sup>

Most PEG-based degradable hydrogel systems developed so far have been made by incorporating a variety of cross-linkers to create a gel network and degradation sites to induce degradation in the biological environment. In most cases, hydrolytically labile sites such as esters have been incorporated,<sup>6,7,10</sup> alternatively, enzymatic degradation sites have been introduced to achieve a degradative response to biological stimuli.<sup>11</sup>

PEGs modified with hydrophobes at both ends have been investigated widely as model associative polymers.<sup>12-26</sup> These physically crosslinked systems have potential applications as thickeners, adhesives, adsorbents, coatings, flocculants for waste-water treatment, surfactants and stabilizers for heterogeneous polymerization,<sup>12</sup> and DNA separating sequencing media.<sup>14,15</sup> The majority of these systems studied so far do not exhibit phase separation, but form a single phase over the entire concentration range.<sup>13-15,22-26</sup> As the concentration of polymer dissolved in water increases, the size of the connected clusters of associative polymers grows continuously and finally forms an infinite gel-like cluster. This may be regarded as a sol-gel transition, but is not a thermodynamic phase transition.<sup>12</sup> Above a critical concentration, at which the viscosity starts to increase rapidly, all properties of systems existing as a single phase change in a continuous manner with concentration. The rheology of single-phase systems has been modeled in terms of the concentration-dependent topology of aggregation and by breakage of the junction between micelles (bridging chains).<sup>13</sup>

Recently, phase separation has been reported for PEGs modified with long alkyl groups: Francois et al. observed that systems of 2000 g/mol (2 kD) and 4 kD PEG modified with  $-C_{12}H_{25}$  hydrophobes and 20 kD PEG with  $-C_{18}H_{37}$  form quasi-elastic gels at high concentration,<sup>19</sup> and Pham et al. reported that aqueous solutions of 35 kD PEG with C18 alkyl groups or PEGs from 20 kD to 35 kD with C16 alkyl groups separate into a highly viscous lower phase and a low viscosity upper phase.<sup>16-18</sup> Unlike the general phase diagram of physical gel systems showing an upper critical solution temperature (UCST),<sup>27</sup> the equilibrium concentrations of sol and gel of the hydrophobically-modified

PEGs are either temperature-insensitive,<sup>17</sup> or the equilibrium gel phase concentration increases weakly with increasing temperature (LCST behavior was even found for some cases).<sup>19</sup> Temperature-insensitive phase behavior can be explained in terms of an entropically driven association process,<sup>17</sup> and an increase in equilibrium gel concentration or LCST behavior can be explained by the poorer solvation of PEG chains with increasing temperature.<sup>19</sup>

Semenov et al. provided the first theoretical prediction of phase separation of telechelic associative polymer solutions in the limit of high aggregation number.<sup>28</sup> The phase behavior is governed by the competition between osmotic repulsion among micelles composed of the telechelic polymers (analogous to star polymers and diblock micelles) and attraction due to the increase in configurational entropy of the system when bridges form between micelles. The entropic attraction increases with aggregation number. When the attraction is sufficiently large to overcome the repulsion, the system separates into two phases: a close packed “solid” phase of micelles and a dilute “gas” phase of micelles and free chains. Recently, Pham et al. advanced an alternative view in which the phase separation is viewed as a coexistence of a liquid and a gas of micelles.<sup>17</sup> By modeling the associative micelles as adhesive hard spheres, they were able to capture sol-gel coexistence and to qualitatively describe the sol and gel compositions. Thus, this approach has the potential to offer more quantitative predictions than the purely scaling approach of Semenov. However, the discrepancy between the semi-empirically inferred value of the “stickiness parameter” and the theoretical value expected for the observed aggregation number was large (three orders of magnitude). This difficulty is likely to be related to the function describing the intermicelle interaction potential.

Here we explore hydrogels made from self-assembly of PEG modified at both ends with fluoroalkyl end groups ( $R_f$ -PEGs) sufficiently long to exhibit sol-gel coexistence, particularly examining their potential as degradable carriers that have controlled rheological properties and erosion rate. Maintaining the benefits of PEG-based hydrogels and employing physical junctions among chemically inert fluoroalkyl groups, these materials have been designed with biocompatibility in mind. The physical nature of the junction provides a route to surface erosion of hydrogels when exposed to an open environment, in contrast to strategies that incorporate degradation sites. Thus, the gel maintains the modulus of the equilibrium composition and erodes in a predictable manner via desorption of chains and micelles, followed by their diffusion into the reservoir. In addition, moving into the sol-gel coexistence regime by using strong hydrophobic end groups avoids the rapid, bulk erosion characteristic of single-phase systems.

We describe the phase behavior, mechanical properties, and erosion characteristics of a range of materials, including polymers that exhibit sol-gel coexistence. By spanning a wide range of PEG and fluoroalkyl lengths, the results enable molecular design of materials having desired phase behavior (single phase *vs.* sol-gel coexistence) with systematically varied mechanical and erosion properties.


## Experimental Section

**Synthesis of end-group modified PEGs.** Poly(ethylene glycol) (PEG) (with alcohol functionality at both ends) of nominal molecular weight 6000 g/mol (6 kD) (from Fluka, Milwaukee, WI), 10 kD (from Aldrich, Milwaukee, WI), and 20 kD (from Fluka) were used to prepare telechelic  $R_f$ -PEGs. Monomethoxy PEG (i.e., with a methyl terminating

group on one end and alcohol on the other) of nominal molecular weight 2 kD and 5 kD (from Aldrich) were used to prepare monofunctional R<sub>F</sub>-PEGs. Three different fluorinated alcohols (C<sub>n</sub>F<sub>2n+1</sub>CH<sub>2</sub>CH<sub>2</sub>OH, n = 6, 8, 10) were purchased from Lancaster Synthesis Inc. (Windham, NH). Isophorone diisocyanate (IPDI), dibutyltin diacetate and anhydrous tetrahydrofuran (THF) were purchased from Aldrich. Anhydrous ethyl ether was from EM Science (Hawthorne, NY).

**Table 2.1. Bifunctional R<sub>F</sub>-PEGs**

Sample	PEG-bock	End Group <sup>a</sup>	Conversion <sup>b</sup>
20KC8	20 kg/mol	-C <sub>8</sub> F <sub>17</sub>	96 %
20KC10		-C <sub>10</sub> F <sub>21</sub>	97 (92)
10KC8	10 kg/mol	-C <sub>8</sub> F <sub>17</sub>	94
10KC10		-C <sub>10</sub> F <sub>21</sub>	94 (96)
6KC6	6 kg/mol	-C <sub>6</sub> F <sub>13</sub>	99
6KC8		-C <sub>8</sub> F <sub>17</sub>	89
6KC10		-C <sub>10</sub> F <sub>21</sub>	97 (97)

<sup>a</sup> Full end group is -IPDU-(CH<sub>2</sub>)<sub>2</sub>-C<sub>n</sub>F<sub>2n+1</sub>, where IPDU is  -C(O)NH-IPDU-NHC(O)-

<sup>b</sup> Degree of substitution as determined by <sup>19</sup>F NMR (selected values determined by HPLC are in parentheses).

The method of Glass et al.<sup>25</sup> was used to attach fluorinated end groups to the terminal hydroxyls of the polymers. The PEG was dried by azeotropic distillation in toluene and was reacted with a 100-fold molar excess (with respect to end-groups) of vacuum-distilled IPDI in anhydrous THF for 48 hr. This isocyanate-functionalized intermediate was precipitated in anhydrous ethyl ether to remove unreacted IPDI and was subsequently

reacted with a tenfold excess of fluoroalcohol in anhydrous THF for 48 hr with the addition of dibutyltin diacetate. The reaction mixture was precipitated in anhydrous ethyl ether, dissolved in THF and reprecipitated. All reactions were done under argon.


The degree of substitution of PEG termini with  $R_f$  groups was determined by  $^{19}\text{F}$  NMR using  $\text{CF}_3\text{COOH}$  or  $\text{CF}_3\text{SO}_3\text{Na}$  ( $\delta \cong -78$  ppm) as an internal standard and measuring the ratio of the peak intensities of the sample ( $\text{CF}_3$ -  $\delta \cong -83$  ppm) and of the standard, according to the method of Zhang et al.<sup>29</sup> The samples prepared for this study are described in Table 2.1, where the abbreviation nKCM denotes a polymer with a PEG midblock MW of n kg/mol and with m-carbon fluoroalkyl end groups, i.e.,  $\text{C}_m\text{F}_{2m+1}\text{CH}_2\text{CH}_2\text{-PEG-CH}_2\text{CH}_2\text{C}_m\text{F}_{2m+1}$ . To verify the degree of conversion of the ends as determined by  $^{19}\text{F}$  NMR, each sample modified with  $-\text{C}_{10}\text{F}_{21}$  was also characterized using reverse phase HPLC. A C18 column was used with a Waters HPLC system, and eluted using a gradient input of mixed solvent (from 20:80 acetonitrile:water to 100% acetonitrile), which can separate unmodified, one-end modified, and two-end modified PEG. Good agreement between the values obtained by HPLC (shown in parentheses in Table 2.1) and the values obtained by  $^{19}\text{F}$  NMR support the reliability of the NMR method.

Monofunctional  $R_f$ -PEGs were also prepared similarly using monomethoxy PEG of nominal molecular weight 2 kD and 5 kD.



**Table 2.2. Monofunctional R<sub>f</sub>-PEGs**

Sample	PEG-bock	End Group <sup>a</sup>	Conversion <sup>b</sup>
5K-M-C10	5 kg/mol	-C <sub>10</sub> F <sub>21</sub>	91 %
5K-M-C8		-C <sub>8</sub> F <sub>17</sub>	91
2K-M-C10	2 kg/mol	-C <sub>10</sub> F <sub>21</sub>	89

<sup>a</sup> Full end group is -IPDU-(CH<sub>2</sub>)<sub>2</sub>-C<sub>n</sub>F<sub>2n+1</sub>, where IPDU is -NHC(O)-

<sup>b</sup> Degree of substitution as determined by <sup>19</sup>F NMR.

**Characterization of sol-gel equilibria.** In a vial, weighed amounts of fine particles of dried bifunctional R<sub>f</sub>-PEGs were dissolved in deionized water and mechanically shaken for 24 hr. Experiments were performed at a number of concentrations, 1 wt % and greater. For samples that demonstrated phase separation, the gel phase in contact with the dilute phase formed at the bottom of the vial due to the slightly higher density of PEG and fluoroalkyl groups than water.

Gel phase concentrations were obtained by measuring wet and dry weight as follows. After decanting off the dilute phase, the gel phase was weighed; then the gel phase was vacuum-dried and weighed again. The ratio of the two weights was regarded as the concentration of the gel phase.

Concentrations of the dilute sol phase in equilibrium with the gel phase (C<sub>sol,eq.</sub>) were measured using complex formation of PEG with barium and iodine.<sup>30</sup> In 2 mL of sample solution, 0.5 mL of 5 % (w/v) of BaCl<sub>2</sub> in 1 N HCl solution was added. Then, 0.25 mL of standard 0.1 N iodide solution (Aldrich) was added. Ten min. after addition of the I<sub>2</sub> solution, the absorbance at 535 nm was measured. A standard calibration line was

obtained using 1, 5, 10 and 25  $\mu\text{g/mL}$  solutions of PEG; the plot displayed a linear relationship between PEG concentration and absorbance ( $r^2 = 0.9973$ ). To remove any unwanted dispersed gel phase in the sol phase, the dilute phase was removed, and centrifuged, and then the supernatant was used. The supernatant was diluted to the appropriate range of concentration for this analytical method.

**Mechanical property measurements.** Samples were prepared as described above. The mixing time was adjusted to achieve an apparent equilibrium, as determined by the disappearance of light scattering from sample. The prepared samples were centrifuged before loading to remove any entrapped bubbles. A stress-controlled rheometer (SR 5000, Rheometric Scientific), equipped with a solvent trap, was used with a cone-and-plate geometry (0.1 radian cone angle and 25 mm diameter) to obtain the rheological data. With the appropriate solvent trap, drying of the sample was negligible for 12 hr at 25 °C.

**Characterization of erosion of gel phases.** Erosion of the gel phase was observed using surface plasmon resonance (SPR).<sup>31</sup> The surface plasmon resonance angle of a thin gold film is sensitive to the thickness and refractive index of a layer polymer gel in contact with it. On one side of a glass slide, a gold film ( $\sim 50 \text{ \AA}$ ) was deposited and polymers were spin-coated on the gold surface from solution in ethanol. The thickness of the coated film was measured using a profilometer ( $\alpha$ -stepper). A 10% solution of polymer in ethanol was spun at 2000 rpm to give a film of  $\sim 1 \mu\text{m}$  thick; the thickness was increased or decreased by varying the concentration of the polymer solution. The polymer-coated gold slide was assembled into the optical apparatus so that the glass side was facing the prism and the polymer-coated side was exposed to a flowing stream of D.I.

water at 25 °C (Figure 2.1 (a)). The change in resonance angle was recorded as a function of time. The changes in resonance angle reflect changes in film thickness and refractive index that occur during initial swelling and subsequent erosion of the polymer layer (Figure 2.1 (b)). This technique works well for relatively slow erosion rates (so that a thin film of a few microns thick erodes over several hr or more). For faster erosion rates a simple experiment on very thick samples (~1 cm) placed in a vial with an excess of water was used, by simply detecting the dissolved amount in the supernatant which was refreshed at regular intervals.

## Results

**Phase behavior.** The phase behavior of bifunctional  $R_f$ -PEGs is governed by the relative length of the PEG chain and the fluoroalkyl end groups (Table 2.3). Increasing the PEG length increases the solubility of the polymer in water, while increasing the length of the hydrophobe decreases solubility. For a given length of PEG, if the hydrophobe is too short, no phase separation occurs; the polymer simply dissolves into a single phase. For example, 20KC10 and 20KC8 exist as homogeneous solutions over the whole range of concentrations, although the viscosity increases dramatically as the concentration of polymer increases. On the other hand, if the hydrophobe is too long, it may not be possible to dissolve the polymer at all (e.g., 6KC10). Thus, for 6 kD PEG, a C10 fluorocarbon hydrophobe is too long to exist as a sol phase; for 10 kD PEG, both hydrophobes examined, C8 and C10, are in the right range to produce sol-gel phase separation; and for 20 kD PEG, even a C10 fluorocarbon hydrophobe is too short to cause sol-gel phase separation.

For polymers that exhibit sol-gel coexistence, the degree of swelling (the inverse of the concentration of the gel phase) in the equilibrium gel is controlled mainly by the PEG length (Table 2.3). When the PEG length is fixed and hydrophobe length is varied, the swelling ratio is nearly constant (cf. 10KC10 to 10KC8; cf. 6KC8 to 6KC6). The swelling ratio increases with PEG length (cf. 6KC8 to 10KC8), which is analogous to reducing crosslink density.

The phase boundary is insensitive to temperature: increasing the temperature (up to 80 °C) does not lead to any noticeable change of the gel phase concentration for the sol-gel coexisting systems. This insensitivity to temperature is in accord with previously reported hydrocarbon-ended phase-separating systems, as well as with theoretical descriptions<sup>17</sup> in terms of an entropically driven formation of a concentrated phase. The trade-off between the entropy associated with center-of-mass positional freedom in the micelle “gas” and the configurational entropy of the end-groups distributing among multiple micelle cores in the dense phase governs the phase behavior, so the temperature dependence cancels out.

Comparing the behavior in deionized water to that in phosphate-buffered saline (PBS) shows that the gel concentration is slightly higher in PBS than in water; and the sol concentration is consistently lower in PBS than in water (Table 2.3). This difference is due to the decreased solvation of PEG chains due to the salting out effect<sup>32</sup> and the increased aggregation tendency of fluorocarbon end groups due to the added salts in PBS.<sup>29</sup>

The concentrations of the sol phases are very small for all samples (< 0.1 wt %), and, unlike the gel composition, the end group length as well as the PEG length affects the equilibrium sol concentration (Table 2.3).

**Table 2.3. Phase Behavior of Bifunctional R<sub>f</sub>-PEGs at 25 °C**

Sample	Type of phase behavior	Equilibrium compositions in water (wt %)		Equilibrium compositions in PBS (wt %)	
		C <sub>gel,eq.</sub> <sup>a</sup>	C <sub>sol,eq.</sub> <sup>b</sup>	C <sub>gel,eq.</sub>	C <sub>sol,eq.</sub>
20KC8	1 phase	N/A	N/A	N/A	N/A
20K10	1 phase	N/A	N/A	N/A	N/A
10KC8	2 phase	6.5±0.2	0.075±0.005	7.8±0.2	0.055±0.002
10K10	2 phase	6.8±0.7	0.019±0.008	8.1±0.7	0.011±0.003
6KC6	2 phase	9.5±0.5	0.066±0.007	10.5±0.6	0.038±0.002
6KC8	2 phase	11.0±0.3	0.042±0.007	12.5±0.3	0.017±0.001
6KC10	insoluble	N/A	N/A	N/A	N/A

<sup>a</sup> Equilibrium gel phase concentration

<sup>b</sup> Equilibrium sol phase concentration

**Mechanical properties of gel phases of sol-gel coexisting species at C<sub>gel, eq.</sub>** The rheological properties of the gels at their equilibrium compositions show single-relaxation behavior (Figure 2.3), similar to previously examined modified PEG systems.<sup>13-15,18,20-22</sup> The dynamic modulus of 10KC10 at C<sub>gel, eq.</sub> shows a very flat plateau in the storage modulus above the frequency of the maximum G'', ( $\omega_x \sim \text{relaxation time}^{-1}$ ), and its loss modulus drops as  $\omega^{-1}$  with increasing frequency in the same region. Below  $\omega_x$ , terminal

behavior holds ( $G' \sim \omega^2$ ,  $G'' \sim \omega$ ). These features are characteristics of a single relaxation time (or Maxwell) fluid. For a Maxwell fluid, the following relationship holds:

$$G''(\omega) = [G'(\omega)G_0 - G'(\omega)^2]^{-1/2}$$

where  $G_0$  is the plateau modulus. The Cole-Cole plot ( $G''$  versus  $G'$ ) shows a nearly semicircle shape for 10KC10, indicating single-relaxation behavior (Figure 2.2). Over the accessible range of frequency, 10KC8 and 6KC8 at their respective  $C_{\text{gel, eq}}$  appear to behave like 10KC10.<sup>12</sup> As one would expect, 6KC6 has a substantially faster relaxation time, so that in the frequency range measured (100 rad/sec) only terminal regime behavior is observed.

For gels at their equilibrium compositions, the PEG midblock determines the modulus of the gel phase; a similar value in the plateau modulus is observed for 10KC10 and 10KC8 (Figure 2.3), reflecting the similar density of physical junctions in these gels, also evident from the similar values of their swelling ratios (Table 2.3). A higher value was observed for 6KC8, indicating that a higher density of physical junctions is present, which also agrees with its smaller swelling ratio relative to 10KC10 and 10KC8.

**Table 2.4. Mechanical Properties of Gel Phases at  $C_{\text{gel, eq}}$  at 25 °C**

Sample	10KC10	10KC8	6KC8
Composition (%)	6.8	6.5	11.0
Relaxation time ( $\tau_r$ )(s)	1.2	0.029	0.023
Plateau modulus ( $G_0$ )(kPa)	14.4	18.5	56.1
Viscosity ( $\eta_0$ ) (kPa s)	18	0.53	1.5

The viscoelastic relaxation time ( $\tau_r$ ) of these gels, the inverse of the frequency at the loss maximum ( $\omega_x^{-1}$ ) (Figure 2.3 (b)), increases strongly with the hydrophobe length; the ~40-fold difference in  $\tau_r$  between 10KC10 and 10KC8 (Table 2.4) shows that two  $\text{CF}_2$  units significantly increase the average residence time of a given  $R_f$  group in a physical junction of the gel (which controls the longest relaxation time).<sup>13-15,18,20-22</sup> Interestingly, 10KC8 and 6KC8 gels at their respective equilibrium states demonstrate similar relaxation times, which indicates that the end-group dominates the relaxation behavior. This is in contrast to single-phase type systems which show strong concentration dependence of  $\tau_r$  until the concentration is sufficiently large that the bridge-loop ratio is  $\alpha(1)$ .<sup>13</sup> This insensitivity to concentration (comparing  $\tau_r$  for 10KC8 and 6KC8) is a consequence of the fact that the equilibrium gel concentrations are high enough that the bridge-loop ratios are already  $\alpha(1)$ . Finally, the zero-shear viscosity ( $\eta_0$ ), which is the product of the plateau modulus and relaxation time, varies over an order of magnitude with modest changes in molecular structure (10KC10 > 6KC8 > 10KC8, Table 4.4).

**Erosion characteristics.** Erosion characteristics of the hydrogels were determined using surface plasmon resonance (SPR). For those hydrogels which exhibit sol-gel coexistence, the transient resonance angle ( $\theta$ ) shows four distinct stages (Figure 2.4): an initial rapid decrease ( $\tau_0$ ); a small gradual increase to an equilibrium value ( $\tau_1$ ); constant  $\theta$  for a prolonged period ( $\tau_2$ ); and finally a decrease to the value corresponding to the bare gold surface in contact with water ( $\tau_3$ ). The initial rapid decrease of  $\theta$  during  $\tau_0$  is due to swelling from the dried state, which reduces the polymer concentration, producing a concomitant decrease in the refractive index. The resonance angle drops even lower than

that of the equilibrium state,  $\theta_{\text{eq}}$ : during the interval  $\tau_1$ , the resonance angle approaches the equilibrium value. Since the resonance angle tracks the polymer concentration in the first  $\sim 1\mu\text{m}$  adjacent to the gold film,  $\theta$  passing through a minimum indicates that transiently the concentration drops below the equilibrium gel concentration then rises back up to  $C_{\text{gel, eq}}$ . This anomalous overswelling is reminiscent of similar phenomena in a variety of systems.<sup>34</sup> Since the thickness of the swollen film ( $\sim 8\mu\text{m}$  in the example shown in Figure 2.4) is much greater than the depth probed by SPR ( $\sim 1\mu\text{m}$ ), the constant resonance angle observed during  $\tau_2$  indicates that the polymer concentration in the gel is constant. The decrease of  $\theta$  during  $\tau_3$  results from the decrease in thickness as the last  $\sim 1\mu\text{m}$  of the gel erodes.

For a given polymer (10KC8), the resonance angle during the interval  $\tau_2$  is independent of the initial thickness of the film, consistent with the polymer concentration being that of the equilibrium gel throughout the period  $\tau_2$  and  $\tau_3$ . The duration of the prolonged plateau  $\tau_2$  grows linearly with film thickness, consistent with surface erosion of the equilibrium gel at a constant erosion rate. The increase in  $\tau_2$  dominates the behavior of the total dissolution time, defined in Figure 2.4, leading to the linear increase in  $t_{\text{dissolution}}$  with film thickness (Figure 2.5). The initial swelling transient ( $\tau_0$  and  $\tau_1$ ) is also sensitive to film thickness: as the initial dry thickness increases from 0.5 to 2  $\mu\text{m}$ , the time for the initial swelling step  $\tau_0$  increases from  $\sim 0.5$  hr to  $\sim 2.5$  hr, and the depth of the undershoot decreases (for the thickest films studied, the  $\tau_1$  interval is no longer well defined, so the trends in  $\tau_1$  with film thickness are not as pronounced). The final transient



in  $\theta(t)$  during the  $\tau_3$  period is independent of the initial thickness, consistent with the interpretation that this final process occurs at the intrinsic erosion rate for the equilibrium gel of a given polymer as the film decreases in thickness from the threshold of sensitivity of SPR to zero thickness.

The dissolution rate of the polymers that exhibit sol-gel coexistence is computed from the linear relationship between dry thickness and dissolution time (e.g., Figure 2.5). For these species, the dissolution rate appears to be controlled mainly by the hydrophobe length: the dissolution rate of 6KC8 is the same order of magnitude as that of 10KC8, while 10KC10 dissolves at least 100 times slower than 10KC8 (the final stage was too slow to be observed within the experimental time).

For comparison, we also examined dissolution of two types of hydrogels that do not show sol-gel coexistence: an associative polymer that exhibits the usual single-phase behavior (20KC10) and hydrogels formed by lyotropic ordering of micelles<sup>35</sup> (5KmPC10, Figure 2.6). In these systems, there is no thermodynamic barrier for dissolution from the bulk, and the driving force for dissolution is the concentration of the polymer matrix ( $\sim 10^1$  wt %), which is much greater than the driving force for dissolution of equilibrium gels (the equilibrium sol concentration for the sol-gel coexisting polymers is only  $\sim 10^{-2}$  wt %). Consistent with the high driving force for dissolution and the continuous change in concentration upon exposure to an open system, the resonance angles of 20KC10 films of initial thickness from 0.1 to 2  $\mu\text{m}$  decrease rapidly to their final values without any constant region, which implies fast and homogeneous erosion of the gels. Since the erosion rate was too fast to quantify by SPR, the erosion rates were instead obtained during the initial linear regime of dissolution of thick gels prepared in vials. As expected,

20KC10 and 5KmPC10 exhibit much faster dissolution rates than species that exhibit sol-gel coexistence ( $\sim 10^2$  times faster than dissolution of 10KC8). The erosion rates of the various samples span five orders of magnitude (Table 2.5).

The erosion kinetics of the systems with C8 fluoroalkyls roughly track their equilibrium sol concentrations; however, it is interesting to note that the relative erosion rate of 10KC10 is much slower than one would expect based on its equilibrium sol concentration. The usual expectation for surface erosion is that it is limited by the mass transfer rate at the surface, often described in terms of a mass transfer coefficient (mostly determined by the flow conditions at the surface) and the equilibrium concentration of the eroding species. In this series of experiments, the flow conditions are held fixed, and the molecular or micellar diffusivities are similar across all systems. Therefore, the mass transfer coefficient can be regarded as constant, and the ratio of the erosion rates is expected to follow the ratio of the equilibrium sol concentrations. This appears to be a good approximation for 10KC8 and 6KC8, within the uncertainty in determining  $C_{\text{sol,eq}}$ . However, the very large difference in the dissolution rates between 10KC10 and 10KC8 cannot be understood in terms of the small difference ( $\sim 4$  times) in their equilibrium sol concentrations. This suggests that a different physical mechanism applies.

If the rate of diffusion of micelles away from the surface exceeds the rate of release of micelles from the surface, the surface concentration may drop below  $C_{\text{sol,eq}}$ . The overall flux would then be determined by the rate of detachment of micelles from the gel. Our rheological data suggests that this could explain the more than two orders of magnitude slower erosion rate for C10 systems than C8 systems: the rheological relaxation time is approximately 40 times slower for 10KC10 than 10KC8 or 6KC8 (Table 2.4). The

rheological relaxation time is related to the average time required for a single chain end to be freed from the aggregate core in which it resides. For a chain to become completely free to leave the gel, both ends must be free, which would be a much more rare event, scaling as  $\sim(\text{viscoelastic time}, \tau_r)^{-2}$ . Release of a micelle from the gel may be even more rare.

**Table 2.5. Dissolution Rates at 25 °C**

Species	10KC10	10KC8	6KC8	20KC10	5K-M-C10
Conc. (wt %)	(6.8 wt %)	(6.5 wt %)	(11.0 wt %)	(10.0 wt %)	(12.8 wt %)
Dissolution rate (mg/cm <sup>2</sup> /hr)	$\ll 10^{-5}$	$1.67 \times 10^{-3}$	$3.33 \times 10^{-4}$	0.168	0.201

Note: For the systems exhibiting sol-gel coexistence, the compositions of the polymer matrix used are the equilibrium gel concentrations. For single-phase (20KC10) and lyotropic (5K-M-C10), the initial concentration was chosen to be high enough that they form a gel (Figure 2.6. (a)). For these fast-dissolving gels, the rates are from the initial linear stage of dissolution from the bulk gel state.

## Discussion

**Comparison to prior studies of R<sub>f</sub>-PEGs.** This study represents the first report of sol-gel coexistence in a fluorocarbon-terminated PEG system. However, in view of our results, it is surprising that previous studies of similar materials did not observe sol-gel phase separation. Menchen et al. reported the insolubility of 8KC8 in water, although it is not clear whether it was precipitated or phase-separated.<sup>15</sup> Neither phase separation nor precipitation was reported for solutions of 6 kD or 10 kD PEG modified with -C<sub>11</sub>H<sub>22</sub>C<sub>8</sub>F<sub>17</sub>.<sup>20,22</sup> The origin of these discrepancies may lie in differences in chemical

structure (the degree of end-capping) or due to differences in experimental methods (differences in methods have been implicated previously as the source of wide differences in the reported aggregation number for a given end group<sup>17</sup>). For example, the absence of a viscosity enhancement for a solution of 6 kD PEG modified with  $-C_{11}H_{22}C_8F_{17}$ <sup>20</sup> might have resulted from the low viscosity of the sol phase in which the coexisting gel may have been suspended. And the absence of phase separation in 10 kD PEG with  $-C_{11}H_{22}C_8F_{17}$  may be due to the low conversion rate of end-capping (<80%).<sup>36</sup>

**Implications for biomedical applications.** For potential applications of bifunctional  $R_f$ -PEGs that demonstrate sol-gel coexistence as a delivery vehicle, it is desirable to have systematic control of gel properties, such as composition and modulus, as well as transport properties such as diffusion coefficient and viscosity. The observed properties of the equilibrium gel phase of  $R_f$ -PEGs that exhibit sol-gel coexistence show that the gel composition, modulus, and viscosity can be adjusted by choice of the PEG midblock length, the end group length, or both. The low concentration in the dilute phase translates into a small driving force for the dissolution of these gels when they are exposed to an open system (e.g., when used as an implant, or as a drug release depot). Also, the addition of salts causes a small increase of the equilibrium gel concentration and decrease of the equilibrium sol concentration. The effect of dissolved salts (Table 2.3) will be present *in vivo* with the small, but beneficial, result of increasing the modulus and reducing the rate of dissolution.

By choice of the lengths of the hydrophilic PEG and hydrophobic end groups, the type and rate of erosion of the hydrogel can be controlled as well. The dissolution characteristics in an open system correlate with the type of phase behavior of the polymer

matrix: sol-gel coexistence provides a constant polymer concentration during the erosion process (Figure 2.8 (c)) in contrast to the continuous decrease in the polymer concentration of the whole matrix for single phase systems (Figure 2.8 (a), (b)). The constant polymer concentration during erosion at sol-gel equilibrium implies that erosion occurs only at the surface, indicating that this hydrogel degrades heterogeneously and that a constant release rate of an embedded nondiffusible target material is achievable. A strong dependence of the erosion rate on the end-group length suggests that the erosion for sol-gel coexisting species is controlled by end group dissociation. The absolute values of dissolution rates of the sol-gel coexisting species are sufficiently slow that these would be appropriate for applications as delivery depots in the body.

**Implications for theory.** The key features to capture regarding systems that can exhibit sol-gel coexistence are the compositions of the equilibrium phases and the transition from single phase to sol-gel coexistence behavior. As mentioned above, two models have been presented to capture the phase behavior of telechelic associating polymers: Semenov's scaling theory,<sup>28</sup> which describes how the aggregation number,  $p$ , and the segments of hydrophilic chain,  $N$ , affect the equilibrium gel concentration, but cannot predict the quantitative composition of the equilibrium phases or the transition from single phase to sol-gel coexistence behavior; and Pham et al.'s approach using the sticky hard-sphere model,<sup>17</sup> which makes quantitative predictions of the composition of the equilibrium phases and the transition from single phase to sol-gel coexistence behavior, but is formulated in terms of a "stickiness parameter ( $1/\tau_s$ )" that must be determined empirically to account for the experimental data. Here we compare the observed phase behavior of the present systems and those previously described in the

literature to the predictions of each of these models, starting with the equilibrium gel concentration, then the equilibrium sol concentration, and, finally, the transition from single phase to sol-gel coexistence behavior.

Equilibrium gel concentration: Experimental results show that the equilibrium gel concentration is more sensitive to PEG length ( $\sim N$ ) than to the aggregation number ( $p$ , mainly determined by the end group length<sup>37,38</sup>), in qualitative accord with the scaling relation predicted by Semenov:  $\phi^* \sim (p^{1/2}/N)^{3\nu-1}$ , where  $\phi^*$  is the average polymer concentration within the equilibrium gel and  $\nu$  is the Flory exponent.<sup>28</sup> For example, pairwise comparisons for similar relative changes in  $p$  vs.  $N$  in Pham et al.<sup>17</sup> show that increasing  $p$  from  $\sim 20$  (35 kD PEG with C16 alkyl ends) to  $\sim 33$  (35 kD PEG with C18 alkyl ends) gives  $\sim 17\%$  increase in  $C_{\text{gel,eq}}$ . (Figure 8 of [17]), while a decrease in PEG length from 35 kD PEG to 20 kD PEG (both with C16 alkyl ends) gave a  $\sim 65\%$  increase in  $C_{\text{gel,eq}}$ . (Figure 8 of [17]). From the present study, a  $\sim 50\%$  increase in  $p$  from 10KC8 to 10KC10 determined by SANS<sup>38</sup> gives no distinct change in  $C_{\text{gel,eq}}$ , while a  $\sim 40\%$  decrease in PEG length from 10KC8 to 6KC8 gives a  $\sim 70\%$  increase in  $C_{\text{gel,eq}}$ . Indeed, the observed behavior suggests that the greater sensitivity of  $C_{\text{gel,eq}}$  to  $N$  than to  $p$  is even more pronounced than indicated by the Semenov scaling expression.

In the context of the model of Pham et al., the  $N$ -dependence of the polymer concentration in the equilibrium gel arises solely from the decrease in polymer concentration within a micelle as  $N$  increases.<sup>17</sup> However, this does not fully account for the observed decrease in  $C_{\text{gel,eq}}$  with increasing  $N$ .<sup>40</sup> The present fluoroalkyl-ended systems also illustrate the significant dependence of the intermicelle attraction on the PEG midblock length. The small difference in gel volume fraction between 10KC8 and

10KC10 ( $\phi \sim 0.61$  and  $\sim 0.59$ , respectively)<sup>41</sup> suggests a weak dependence of the intermicelle attraction on  $p$ , while the significant difference between 10KC8 and 6KC8 ( $\phi \sim 0.59$  and  $\sim 0.70$ , respectively)<sup>41</sup> shows a strong dependence on  $N$  (Figure 2.7 (a)). This argues that the attraction between the micelles depends significantly on both  $p$  and  $N$ . In addition, the observed  $\phi$  of the 6KC8 equilibrium gel is too large to describe using the adhesive hard-sphere phase diagram,<sup>17</sup> presumably because unlike hard spheres, micelles can deform and even overlap.

Equilibrium sol concentration: The dependence of the equilibrium sol concentration on  $N$  and  $p$  reinforces the conclusion that the intermicelle attraction depends on both  $p$  and  $N$ . The most striking indication of this is the much smaller  $C_{\text{sol,eq}}$  for the present systems than for those studied by Pham et al.<sup>17</sup> To account for  $C_{\text{sol,eq}}$  being from two to ten times lower in the present systems than in those of Pham et al., the intermicelle attraction would have to be substantially larger. In their application of the sticky hard-sphere model, this difference in intermicelle attraction would be attributed to a difference in  $p$ . However, there is very little change in intermicelle attraction with  $p$ <sup>38</sup>, and the aggregation numbers for the present fluoroalkyl ended systems are similar to those of the alkyl ended PEG of Pham et al.<sup>39</sup> Therefore, it is difficult to explain the much smaller  $C_{\text{sol,eq}}$  based on  $p$  alone. On the other hand, the present systems show very large changes in phase behavior with PEG length (Table 2.3). Therefore, we believe that the low values of  $C_{\text{sol,eq}}$  in the present systems may predominantly reflect the shorter PEG lengths in this study (which were 10 kD and 6 kD PEG) compared to those in Pham et al. (which have 20 kD and 35 kD PEG).

The relative values of the equilibrium sol and gel volume fractions<sup>41</sup> also support the need to incorporate physical interactions not incorporated within the sticky hard-sphere model. Pham et al. found for one system (35 kD PEG with C16 alkyl ends) good agreement between the stickiness parameter ( $\tau_s$ ) inferred from three different characteristics: the second virial coefficient (from dynamic light scattering at  $C < C_{\text{sol,eq.}}$ ),  $\phi_{\text{sol,eq.}}$  and  $\phi_{\text{gel,eq.}}$ . However, for 35 kD PEG with C18 alkyl ends, the  $\tau_s$  inferred from light scattering ( $\tau_s \sim 0.07$ ) was substantially lower than the two different values of  $\tau_s$  inferred from  $\phi_{\text{sol,eq.}}$  and  $\phi_{\text{gel,eq.}}$ <sup>17</sup> (Figure 2.7 (a)). The discrepancies between the values of  $\tau_s$  inferred from  $\phi_{\text{sol,eq.}}$  vs.  $\phi_{\text{gel,eq.}}$  are even more pronounced in our systems (10KC10, 10KC8 and 6KC8 on Figure 2.7 (a)).<sup>42</sup> Indeed, for 6KC8,  $\phi_{\text{gel,eq.}}$  is simply too large to be explained within the context of the sticky hard-sphere model (Figure 2.7 (a)).

Transition from single phase to sol-gel coexistence behavior: Three fluoroalkyl terminated PEGs have been described that exhibit single-phase behavior that is particularly instructive to compare to the systems that exhibit sol-gel equilibrium: the 35KC8 studied by Winnik and coworkers<sup>14,15</sup> and the 20KC10 and 20KC8 of the present study. All of these systems show that PEG length plays a very large role, since pairwise comparisons can be made to systems with the same hydrophobe (35KC8 and 20KC8 vs. 10KC8, and 20KC10 vs. 10KC10). Considering the insensitivity of the intermicelle attraction to  $p$ ,<sup>17</sup> the change in phase behavior on increasing PEG from 10 kD to 20 kD (Figure 2.7 (a)) also indicates that the intermicelle attraction is very sensitive to  $N$ .

Regarding the effect of end group at fixed  $N$  and similar  $p$ , for 35 kD PEG, Winnik et al. found that 35KC8 showed single phase behavior, while Pham et al. found that 35 kD PEG with C16 or C18 alkyl ends showed sol-gel coexistence. If the aggregation number



for 35KC8 is indeed similar to that for 10KC8 ( $p \sim 30^{39}$ ), it is larger than that for the 35 kD PEG with C16 alkyl groups and similar to  $p$  for 35 kD PEG with C18 alkyl ends.<sup>17</sup> Therefore, one would expect the 35KC8 to have intermicelle attraction as strong as 35 kD PEG with C18 alkyl ends and to exhibit sol-gel coexistence (Figure 2.7 (a)), which is not the case. Similarly, comparing 20KC10 to 20 kD PEG with C16 alkyl ends show the surprising result that 20KC10 exhibits single phase behavior in spite of having larger  $p$  ( $\sim 50^{39}$ ) than that of the 20 kD PEG with C16 alkyl ends ( $p \sim 20$ , based on 35kD PEG with C16), which exhibits sol-gel coexistence. These comparisons show effects of  $p$  contrary to the physics of both the Semenov model and the model of Pham et al., while holding PEG length fixed. This discrepancy suggests that the type of hydrophobe plays an important role that is not captured by current models (fluoroalkyl ended systems show weaker intermicelle attraction than their alkyl ended counterparts). Perhaps this reflects a difference in corona structure due to the difference in core structure: it is believed that fluoroalkyl groups behave as short rods that aggregate laterally such that the PEG chains must emerge from the faces of the fluoroalkyl aggregate core, while alkyl groups form liquid-like, spherical cores that do not as tightly constrain the lateral spacing of the PEG chains.

Unexplained effects of  $N$  and hydrophobe type: Current physical models of the interaction between micelles lead to interaction potentials that are independent of  $N$  because the softer repulsion with increasing  $N$  is offset by the increasing area over which the repulsion acts when micelles come into contact, which is valid whether the chains in the corona are stretched or not.<sup>17,28,43</sup> Consequently, the intermicelle interaction potential used by both Semenov and Pham et al. is determined exclusively by the aggregation

number of the hydrophobic core. In contrast, the phase behaviors of the present systems, (20KC10 vs. 10KC10) and (10KC8 vs. 6KC8), and the previously reported data<sup>14,15,17</sup> consistently reveal that the intermicelle interaction potential is also affected by the size of the micelle (determined by the PEG midblock length).

The substantial effect of PEG length on the phase behavior could qualitatively be explained by a change of shape of the intermicelle interaction potential. It is known that small changes in inter-particle potential  $\Phi(r)$  can cause profound shifts in the phase boundary.<sup>44,45</sup> In the context of micelles, a change in  $\Phi(r)$  might result from a cross-over from having strong chain stretching to weak chain stretching as  $N$  increases. This is reasonable, given that the outermost blob size  $\xi_0$  was half the micelle radius  $R$  for 35 kD PEG with C18 alkyl ends ( $p \sim 30$ ),<sup>17</sup> indicating that this relatively long PEG was not substantially stretched; however, as PEG length decreases,  $\xi_0/R$  is expected to decrease in the cross-over regime between unstretched and stretched brushes, making the intermicelle potential steeper. Thus, the observed phase behavior may indicate that for approximately fixed aggregation number (set by the hydrophobe), the change in the character of the corona (e.g., degree of stretching) may cause the position of the gas-liquid phase boundary to shift (Figure 2.7 (b)).

The peculiarities in the phase behavior of PEG itself might cause one to question whether the explanation of the observed  $N$  dependence could be PEG-specific. For example, PEG displays an unusual dependence of solvent quality as a function of PEG concentration. Increasing the PEG concentration produces significantly poorer solvent conditions.<sup>46</sup> Accordingly, with increasing molecular weight of the PEG, and thus increasing blob size for the outermost corona, the solvent quality improves. Therefore,

bringing micelles together for larger PEG midblocks might cost more free energy (due to increasing PEG-PEG contacts when the outer corona is in a good solvent condition) than bringing micelles together for shorter PEG midblocks (since they were in a poorer solvent condition, having increased PEG-PEG contacts costs less). However, in the concentration range relevant here (“outer blob” concentrations of 2 to 6 wt %), this effect seems to be too small to explain the large change in the interaction potential suggested by the observed phase behavior.<sup>46,47</sup>

In search of some physical explanation for the observed effects of hydrophobe type and of PEG length on the position and nature of the sol-gel coexistence curve and the character of the resulting gels, one could consider the interfacial energy of the hydrophobic core and how its effect is progressively shielded with increasing  $N$ . One might speculate that increasing PEG length might screen the hydrophobic core more effectively, so the micelle would be more soluble (weaker intermicelle attraction). However, since the PEG chains are stretched near the core of all the micelles reported in the literature, it seems that the identity of the core would be well shielded in all existing systems. Therefore, we do not know how important this effect would be. Thus, understanding the observed effects of PEG length and hydrophobe type appears to be an unsolved problem.

## Conclusions

The phase behavior, rheology and erosion kinetics of bifunctional  $R_f$ -PEGs provide a unified picture and show that the material properties of this class of hydrogels can be systematically tuned over a wide range. By judicious choice of the lengths of the PEG

and fluoroalkyl end groups, different phase behavior — from single-phase behavior, to sol-gel coexistence (phase separation), to essentially insoluble precipitate — are obtained. For those polymers that exhibit sol-gel coexistence, the swelling ratio and modulus of the gel phase are determined by the PEG midblock length; the relaxation time and erosion kinetics are dominated by the hydrophobe length, and the viscosity and equilibrium sol concentration depend on both PEG midblock and hydrophobe length.

The accessibility of sol-gel coexistence behavior has a number of important implications for potential applications of PEG hydrogels formed by aggregation of hydrophobes. By providing hydrogels that exhibit surface erosion at slow enough rates to be useful, these materials are candidates for applications in controlled release of therapeutic proteins and in tissue engineering. Quantitative theoretical description of the phase behavior remains elusive, particularly the effects of PEG length, hydrophobe type, and the soft (deformable and compressible) nature of micelles.

## **Acknowledgements**

We acknowledge Diethelm Johannsmann at Max Planck Institute for Polymer Research in Mainz, Germany, for the supply of experimental setup of surface plasmon resonance.

## References

- [1] Deluca, P. P.; Mehta, R. C.; Hausberger, A.G.; Thanoo, B. C. In *Polymeric Delivery Systems*; ACS: Washington, DC, **1993**, pp 53-79
- [2] Holland, S. J.; Tighe, B. J.; Gould, P. L. *J. Controlled Release* **1986**, *4*, 155
- [3] Sawhney, A. S.; Hubbell, J. A. *J. Biomed. Mater. Res.* **1990**, *24*, 1397
- [4] Domb, A. J.; Gallardo, C. F.; Langer, R. *Macromolecules* **1989**, *22*, 3200
- [5] Heller, J.; Perhale, D. W. H.; Helwing, R. F.; Fritzing, B. K. *Polym Eng. Sci.* **1981**, *21*, 727
- [6] Sawhney, A. S.; Pathak, C. P.; Hubbell, J. A. *Macromolecules* **1993**, *26*, 581
- [7] Sawhney, A. S.; Pathak, C. P.; van Rensburg, J. J.; Dunn, R. C.; Hubbell, J. A. *J. Biomed. Mater. Res.* **1994**, *28*, 831
- [8] Zaho, X.; Harris, J. M. *J. Pharmaceutical Sci.* **1998**, *87*, 1450
- [9] Harris, J. M., *Poly(ethylene glycol) chemistry. Biotechnical and Niomedical Applications*, Ed., Pletinum: New Yrok, **1992**
- [10] Han, D. K.; Hubbell, J. A. *Macromolecules* **1996**, *29*, 5233
- [11] West, J. L.; Hubbell, J. A. *Macromolecules* **1999**, *32*, 241
- [12] Rubinstein, M.; Dobrynin, A. V. *Trends Polym. Sci.* **1997**, *5(6)*, 181
- [13] Annable, T.; Buscall, R.; Ettelaie, R. *J. Rheo.* **1993**, *37(4)*, 695
- [14] Menchen, S.; Johnson, B.; Winnik, M.A.; Xu, B. *Chem. Mater.* **1996**, *8*, 2205
- [15] Menchen, S.; Johnson, B.; Winnik, M.A.; Xu, B. *Electrophoresis* **1996**, *17*, 1451
- [16] Pham, Q. T.; Russel, W. B.; Lau, W. *J. Rheo.* **1998**, *42(1)*, 159
- [17] Pham, Q. T.; Russel, W. B.; Thibeault, J. C.; Lau, W. *Macromolecules* **1999**, *32(9)*, 2996

- [18] Pham, Q. T.; Russel, W. B.; Thibeault, J. C.; Lau, W. *Macromolecules* **1999**, *32(15)*, 5139
- [19] Francois, J.; Maitre, S.; Rawiso, M.; Sarazin, D.; Beinert, G.; Isel, F. *Colloids Surf. A* **1996**, *112*, 251
- [20] Xu, B.; Li, L.; Yekta, A.; Masoumi, A.; Kanagalingam, S.; Winnik, M. A.; Zhang, K.; Macdonald, P.M.; Menchen, S. *Langmuir* **1997**, *13(9)*, 2447
- [21] Cathebras, N.; Collet, A.; Viguiet, M.; Berret, J. *Macromolecules* **1998**, *31*, 1305
- [22] Serero, Y.; Aznar, R.; Porte, G.; Berret, J.-F.; Calvet, D.; Collet, A.; Viguiet, M. *Phys. Rev. Lett.* **1998**, *81(25)*, 56584
- [23] Jenkins, R. D.; Silebi, C. A.; El-Asser, M. A. *Polymer Mat. Sci. Eng.* **1989**, 629
- [24] Kaczmarek, J. P.; Glass, J. E. *Macromolecules* **1993**, *26*, 5149.
- [25] Lundberg, D. J.; Brown, R. G.; Glass, J. E.; Eley, R.R. *Langmuir* **1994**, *10*, 3027
- [26] Tam, K. C.; Jenkins, R. D.; Winnik, M. A.; Bassett, D. R. *Macromolecules* **1998**, *31*, 4149
- [27] de Gennes, P.G. *Scaling Concepts in Polymer Physics*, Cornell University Press, **1979**
- [28] Semenov, A.N.; Joanny, J.F.; Khokhlove, A.R. *Macromolecules* **1995**, *28*, 1066
- [29] Zhang, H.; Pan, J.; Hogen-Esch, T.E. *Macromolecules* **1998**, *31*, 2815
- [30] Childs, C. E. *Microchemical Journal* **1975**, *20*, 190
- [31] Aust, E. F.; Ito, S.; Sawodny, M.; Knoll, W. *Trends Polym. Sci.* **1994**, *2(9)*, 313
- [32] Bailey, Jr., F. E.; Callard, R. W. *J. Appl. Polym. Sci.* **1959**, *1(1)*, 56
- [33] To examine carefully whether 10KC8 and 6KC8 also follow the single relaxation behavior, we need to obtain the data in the frequency window above the cross-over

frequency,  $\omega_x$ . Unfortunately, in the accessible range of frequency (up to 100 rad/sec), we cannot go much beyond  $\omega_x$  for C8 fluoroalkyl-ended PEGs.

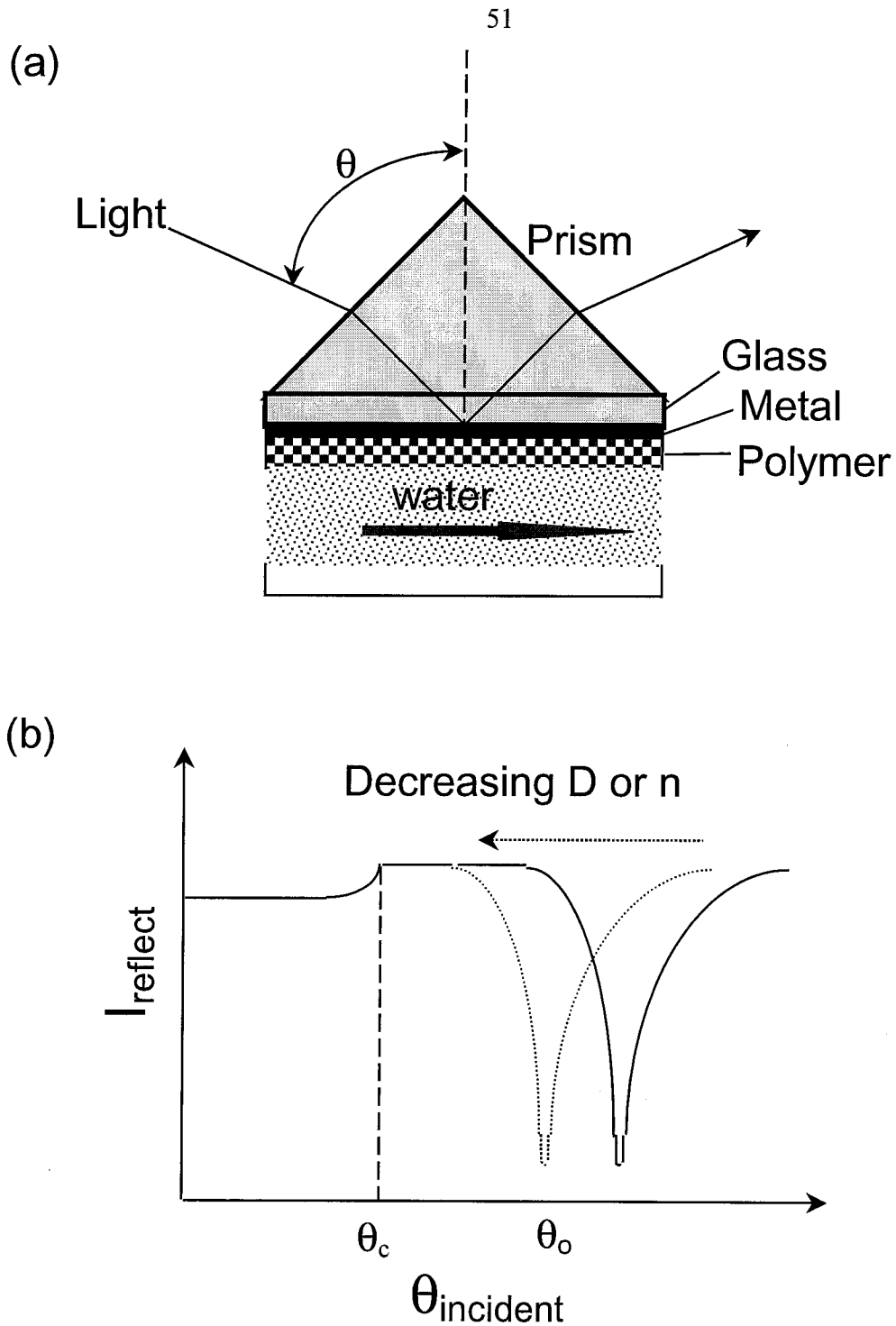
- [34] a) Vrentas, J.S.; Duda, J.L.; Hou, A.-C. *J. Appl. Poly. Sci.* **1984**, *29*, 399 b) Scranton, A.B.; Klier, J.; Peppas, N.A. *Polymer* **1990**, *31*, 1288 c) Franson, N.M.; Peppas, N.A. *J. Appl. Poly. Sci.* **1983**, *28*, 1299 d) Titow, W.V.; Braden, M.; Currell, B.R.; Loneragan, R.J. *J. Appl. Poly. Sci.* **1974**, *18*, 867 e) Kim, D.; Caruthers, J.M.; Peppas, N.A. *Macromolecules* **1993**, *26*, 1841
- [35] Jeong, B.; Bae, Y. H.; Lee, D. S.; Kim, S. W. *Nature* **1997**, *338*, 860
- [36] Private communication with Berret, J.-F.
- [37] Alami, E.; Almgren, M.; Brown, W., Francois, J. *Macromolecules* **1996**, *29*, 2229
- [38] The weak effect of  $\tau_s$  is evident first in the relatively small decrease in  $\tau_s$  from  $\sim 0.091$  to  $\sim 0.067$  as  $p$  increases from  $\sim 20$  to  $\sim 33$ [17], and second in the small change in  $C_{sol,eq}$  as  $p$  increases from  $\sim 30$  (10KC8) to  $\sim 30$  (10KC8); see Table 3 [39].
- [39] Tae, G.; Kornfield, J.A.; Hubbell, J.A.; Lal, J. submitted.
- [40] It is challenging to make quantitative comparisons to the predicted phase behavior. First, from measured mass concentrations one must compute the corresponding volume fraction; however, the uncertainty in the determination of the micelle volume is large, particularly when using  $[\eta]$  for PEG at 25 °C[41]. Next, independent determination of the “stickiness parameter” from dynamic light scattering is only applicable to polymers of high enough solubility and has substantial uncertainty. In evaluating the relative change in  $C_{gel,eq}$  reported in Fig 8 of [17] as PEG length increases from 20 kD to 35 kD, if one uses the reported

insensitivity of  $\tau$  to  $p$  [17], and the insensitivity of  $p$  to PEG length for fixed hydrophobe [38], and using the reported effect of PEG length on  $[\eta]$  [41], it is only possible to explain approximately two-thirds of the observed change in  $C_{\text{gel,eq}}$ . However, considering the sensitivity of equilibrium sol and gel volume fractions to the “stickiness parameter” in the sticky hard-sphere phase diagram, and the uncertainty in experimental determination of the stickiness parameter from light scattering and of the mass/volume of micelles from intrinsic viscosity, it is difficult to make a quantitative evaluation.

[41] The volume fractions were estimated using  $[\eta]C/2.5$  as used in reference [17]. The  $[\eta]$  values were estimated using the relation for pure PEG of  $[\eta] = 4.33 \times 10^{-4} \times (M_w)^{0.679}$  (dl/g) (Kawaguchi et al. *Polymer* **1997**, *38*, 2885), based on the result that there is no noticeable difference between  $[\eta]$  of hydrophobically modified PEG and unmodified PEG in reference [17]. However, there are a number of caveats regarding this method. First,  $[\eta]$  is the volume per mass at infinite dilution, but significant overlap among micelles is postulated when they are phase-separated; the outermost blob size (anticipated overlap width) was about half the radius of the micelle for the systems in reference [17]. Second, there are various ranges of reported  $[\eta]$  for PEG as discussed in reference [17]. Considering the sensitivity of the inferred “stickiness parameter” to the volume fractions of the equilibrium sol and gel in the sticky hard-sphere phase diagram, a small change in  $[\eta]$  will cause the significant change in “stickiness parameter” inferred from measured mass fractions of each phase.



- [42] Estimation of “stickiness parameters” were not possible for our system due to the very low  $C_{\text{sol,eq}}$ .
- [43] Daoud, M.; Cotton, J.P. *J. Physique* **1982**, *43*, 531
- [44] Hagen, M.H.J; Frenkek, D. *J. Chem. Phys.* **1994**, *101*, 4093
- [45] Bellier-Castella, L., Xu, H., Baus, M. *J. Chem. Phys.* **2000**, *113*, 8837
- [46] Bae, Y.C.; Shim, J.J.; Soane, D.S.; Prausnitz, J.M. *J. Appl. Polym. Sci.* **1993**, *47*, 1193
- [47] Venohr, H.; Fraaije, V.; Strunk, H.; Borchard, W. *Eur. Polym. J.* **1998**, *34*, 723



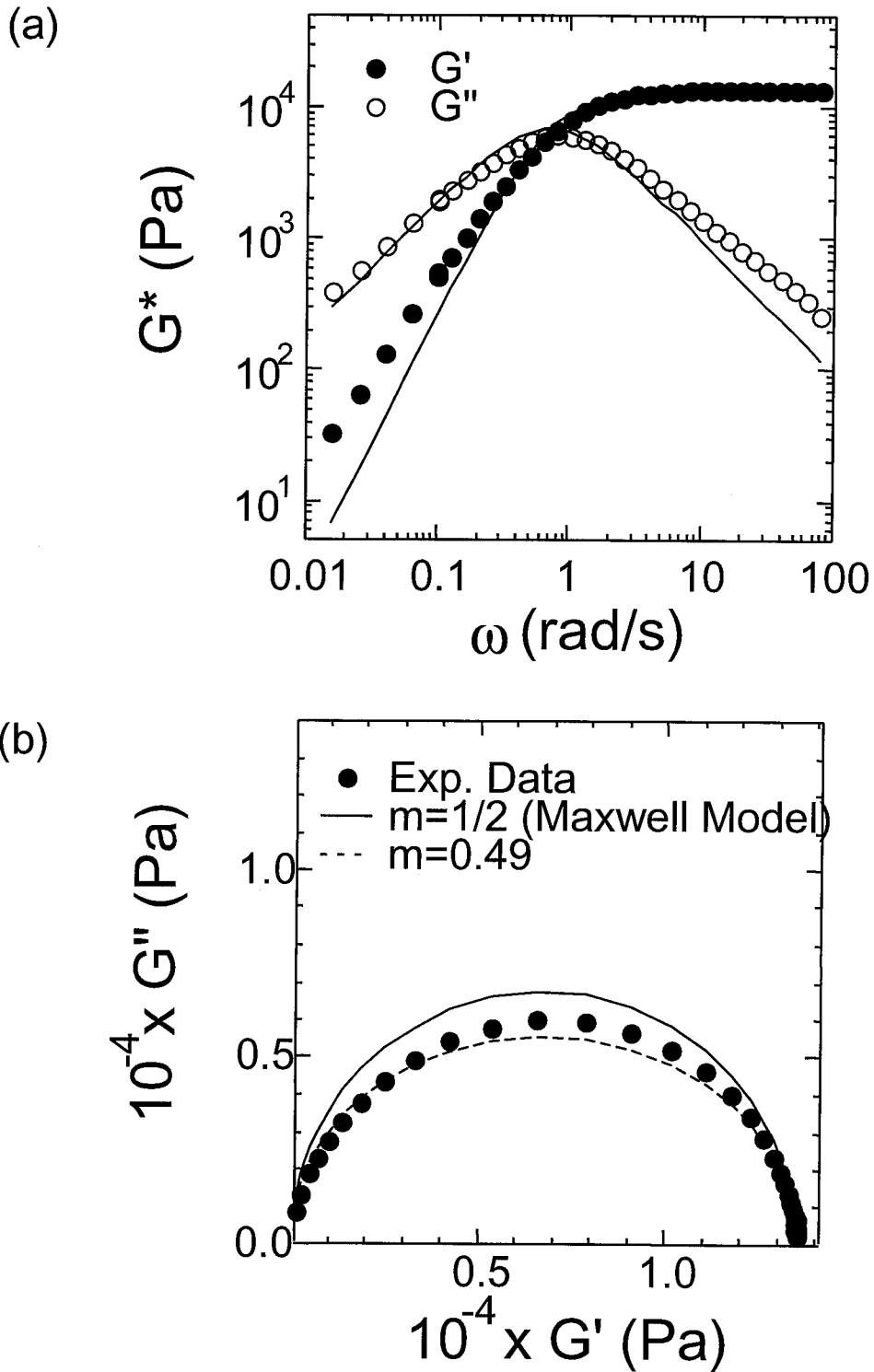
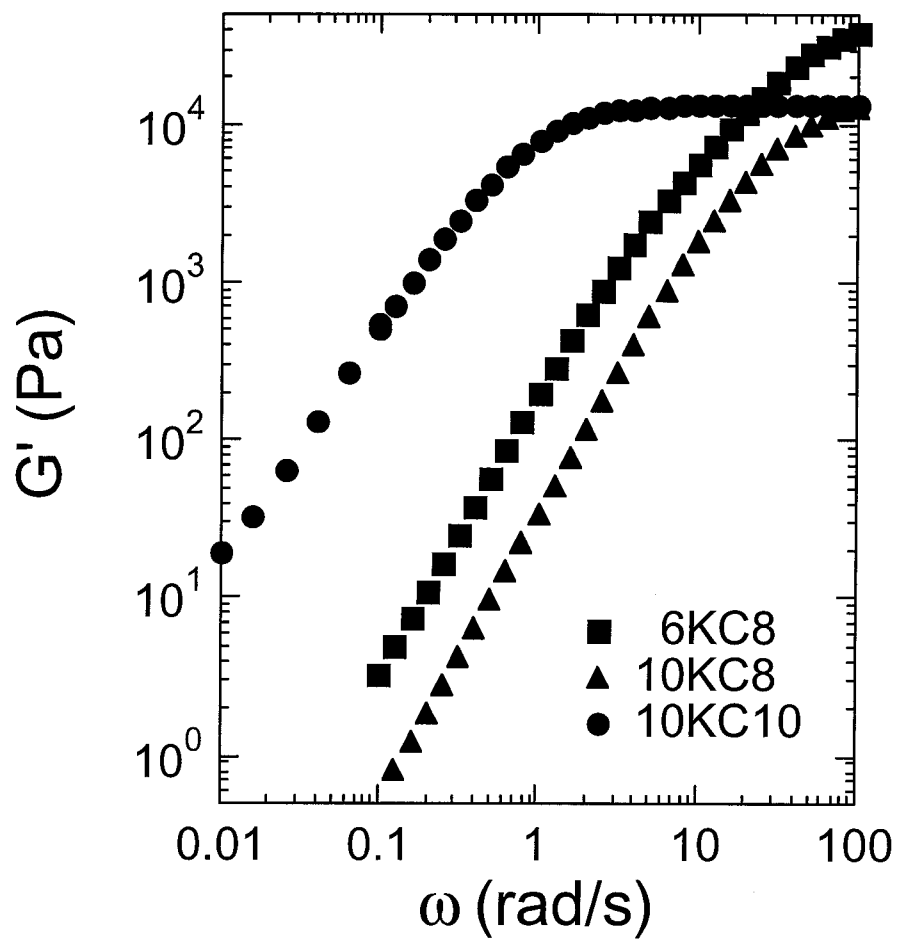


Figure 2.2 The systems that exhibit sol-gel coexistence show nearly single relaxation behavior of the equilibrium gel, illustrated here by 10KC10: (a) dynamic moduli, (b) Cole-Cole plot. Solid curve for a single Maxwell element. Dashed curve is for  $G''(\omega) = [G'(\omega)G_0 - G'(\omega)^2]^{-m}$  with  $m = 0.49$ . ( $T = 25^\circ\text{C}$ ).

(a)



(b)

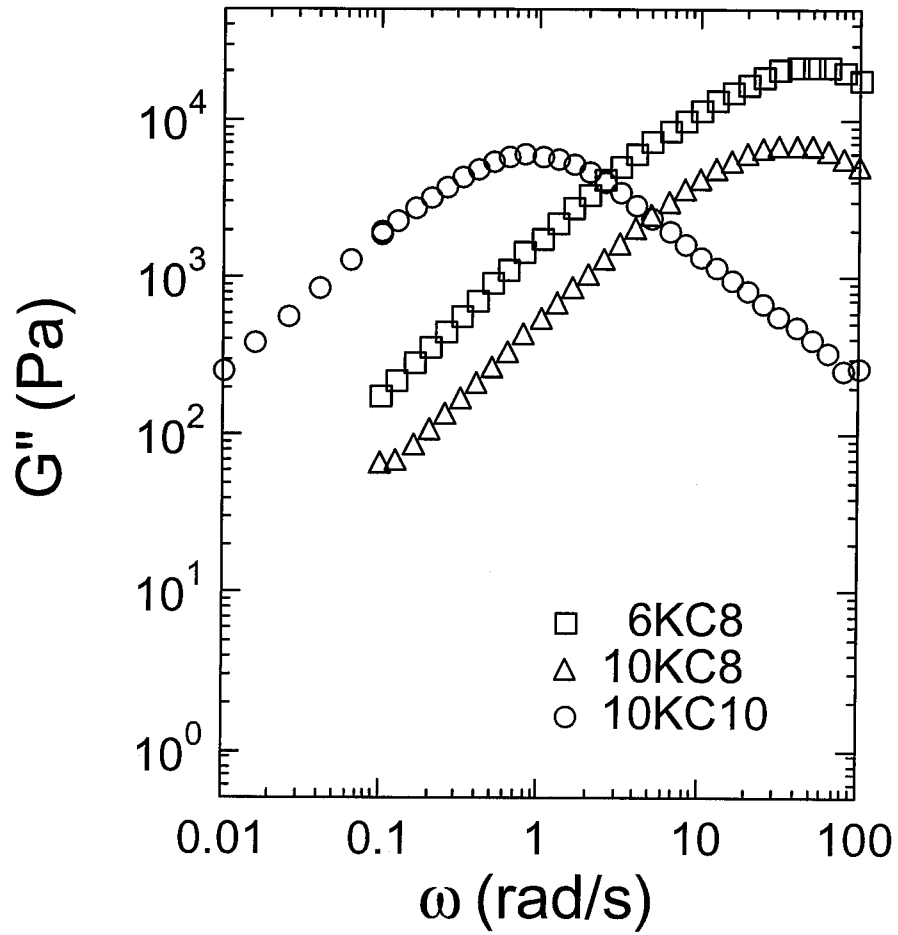


Figure 2.3 Dynamic moduli of gel phases of sol-gel coexisting species at equilibrium compositions ( $C_{\text{gel,eq}}$ ): (a) storage moduli, (b) loss moduli. ( $T = 25^\circ\text{C}$ ).

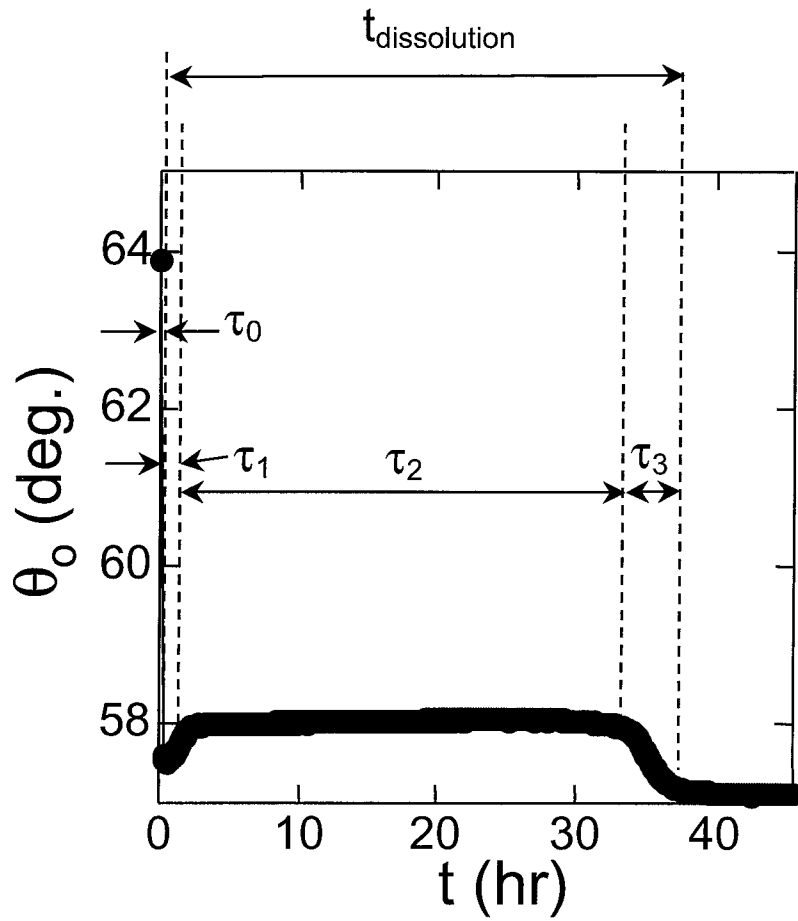


Figure 2.4 Change of surface plasmon resonance angle with time for 10KC8 film of initial dry film thickness  $0.55 \mu\text{m}$ .

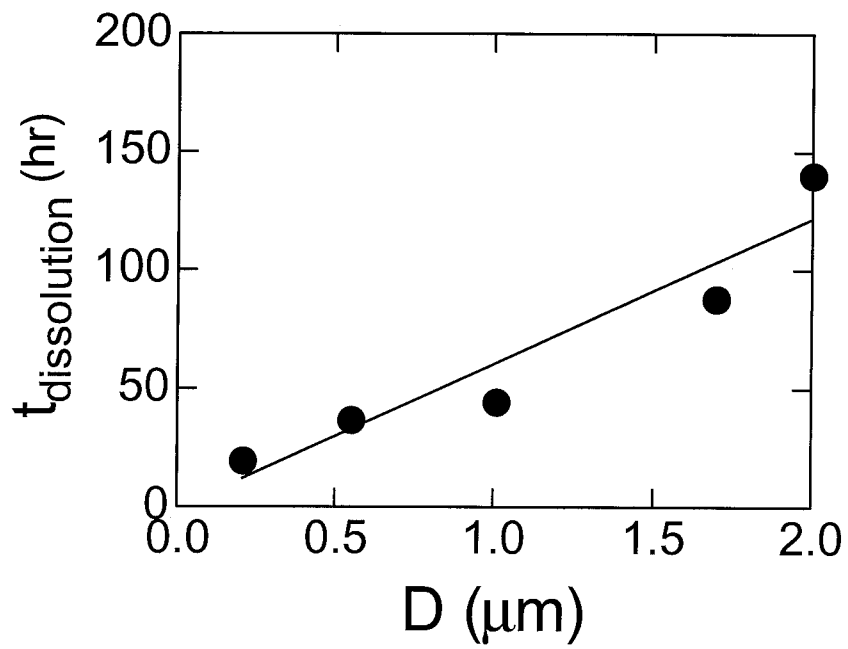


Figure 2.5 Dissolution time as a function of the initial dry thickness of 10KC8 gels.

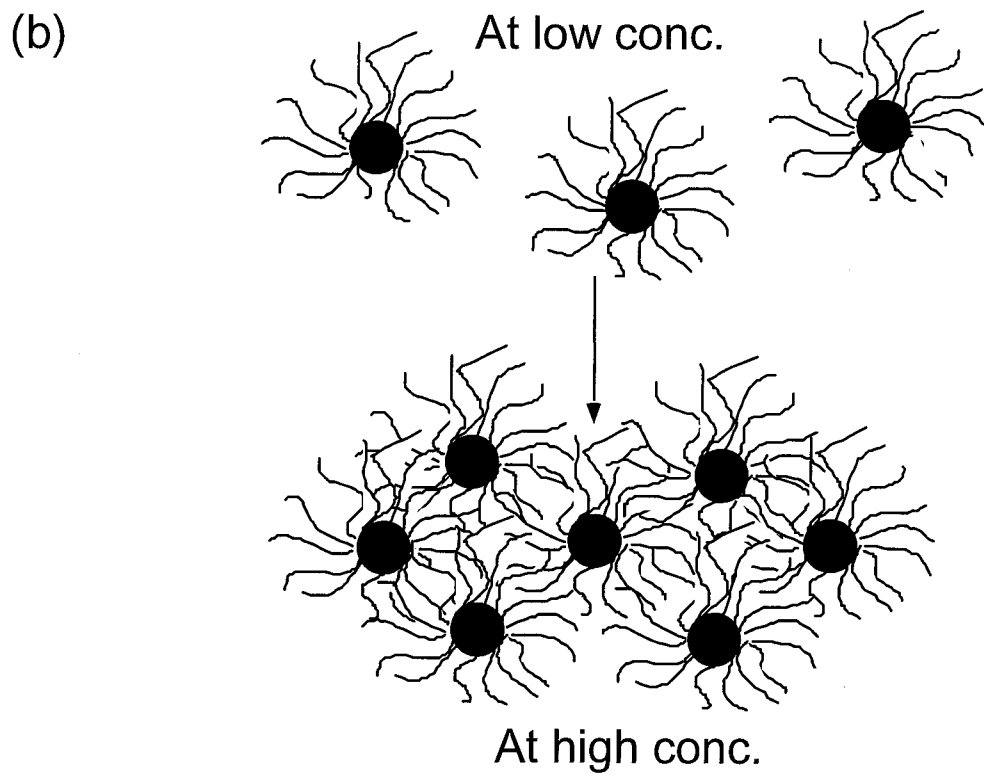
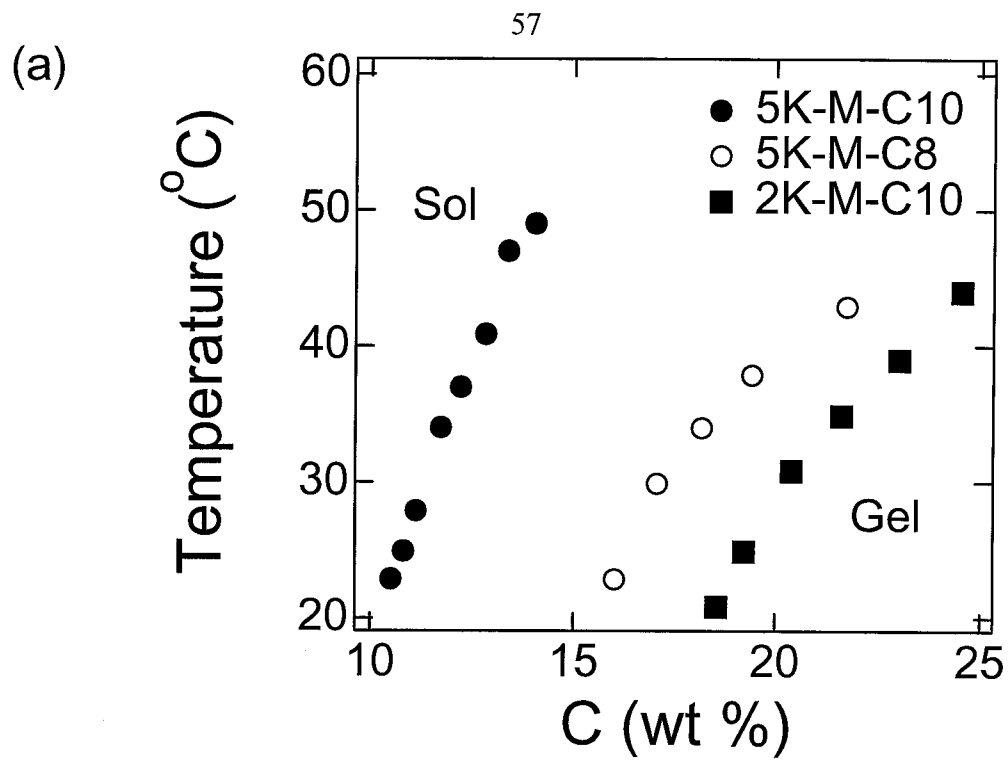


Figure 2.6 Lyotropic phase transition of one-end modified PEG solutions: (a) phase diagram, (b) schematic representation.



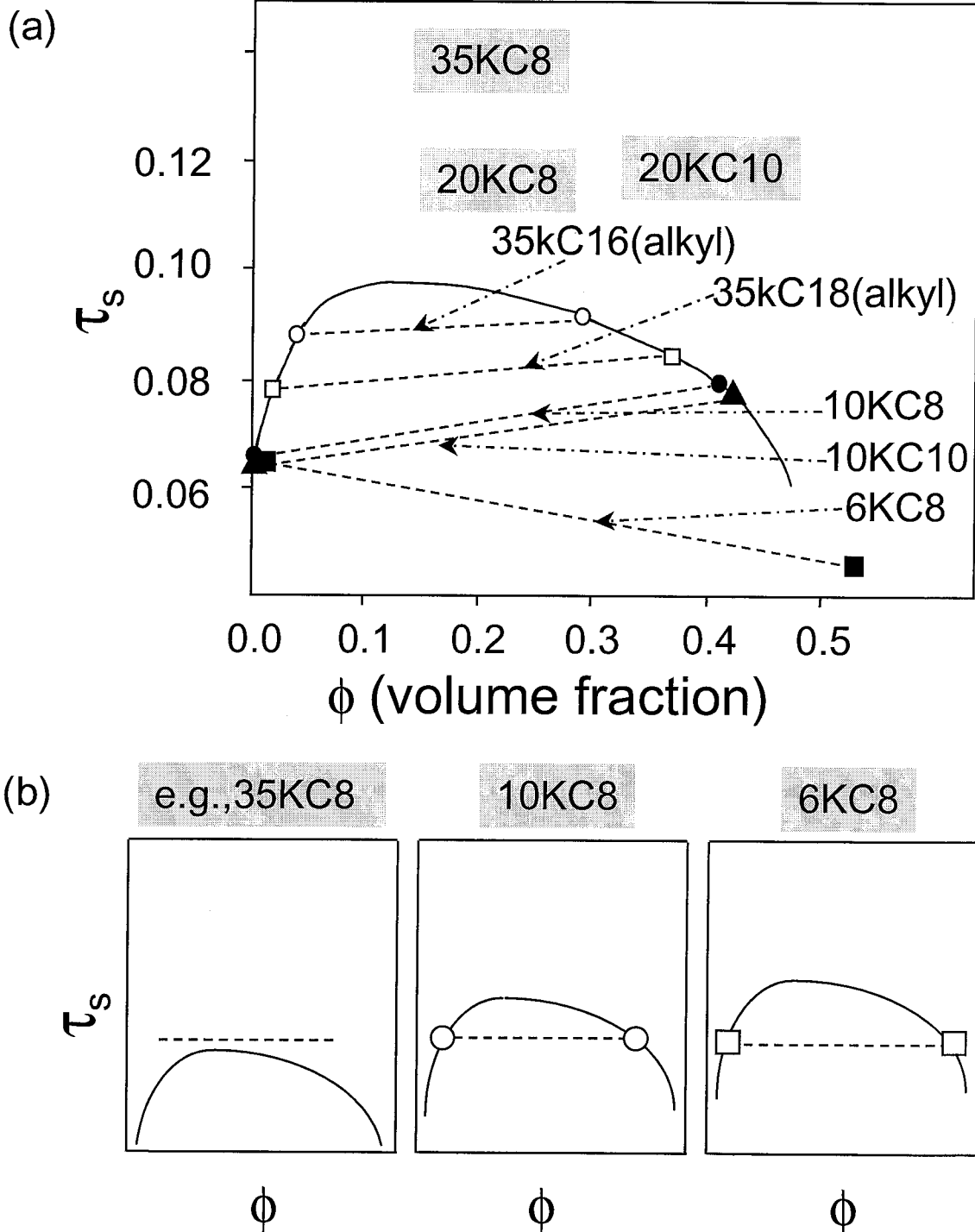


Figure 2.7 Phase diagram of the end-group modified PEG systems (a) sticky hard-sphere phase diagram in terms of  $\tau_s \sim (\text{stickiness parameter})^{-1}$ , adapted from Figure 11 of [17], (b) possible explanation of the change in phase behavior with  $N$  in terms of a shift in the phase boundary due to changes in the intermicelle potential with PEG length (see text).

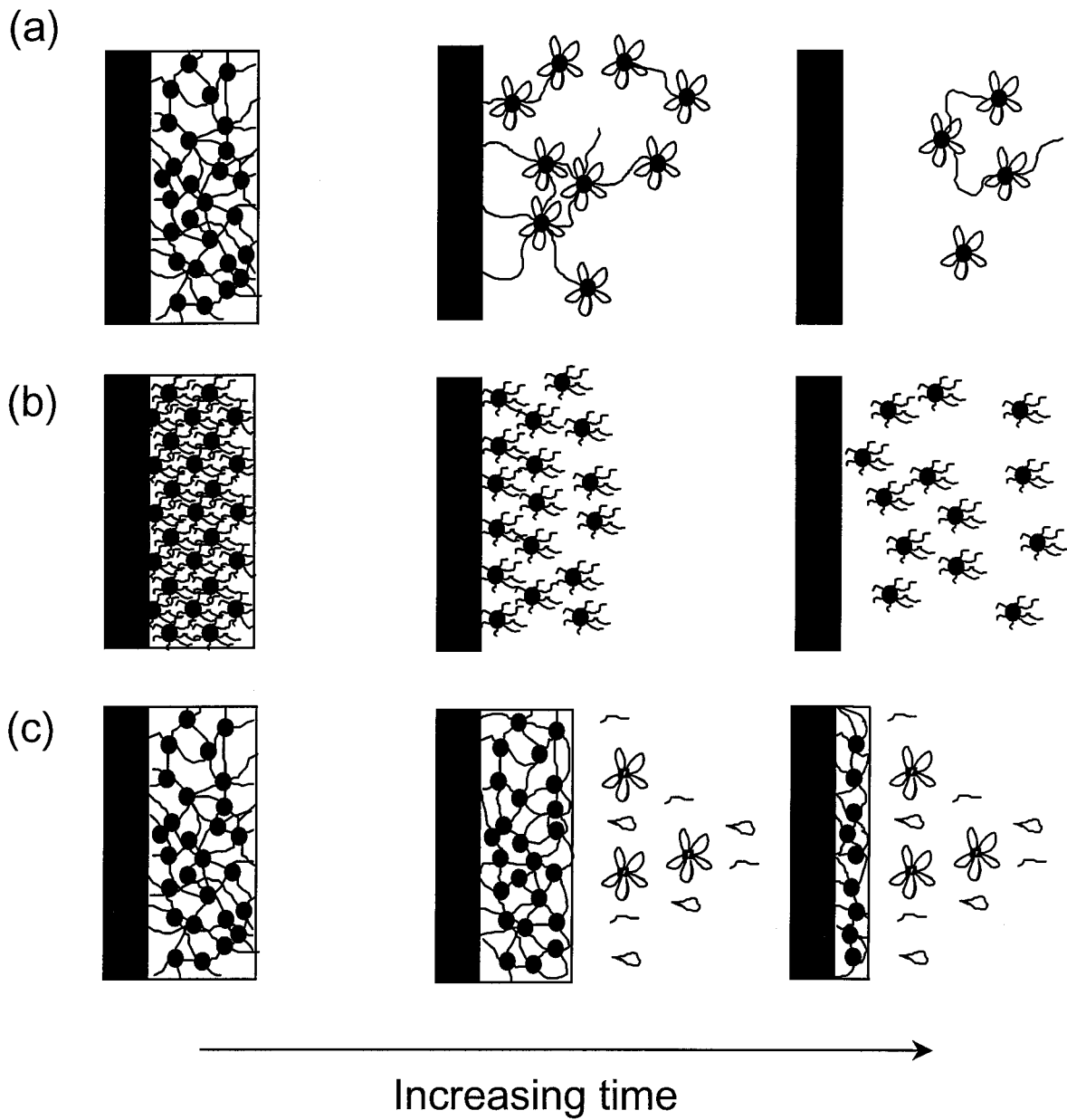


Figure 2.8 Schematic representation of dissolution of the polymer gel in an open environment: (a) single phase species (e.g., 20KC10), (b) lyotropic cubic phase gel (e.g., 5K-M-C10), (c) sol-gel coexisting species.

## Chapter 3. Ordering Transitions of R<sub>f</sub>-PEGs: Rheology and SANS

### Abstract

Aqueous solutions of associative polymers consisting of poly(ethylene glycol) (PEG) (6k or 10k g/mol) terminated at both ends with hydrophobic fluoroalkyl segments,  $-(\text{CH}_2)_2\text{C}_n\text{F}_{2n+1}$  ( $n = 6, 8$  or  $10$ ), exhibit ordering transitions with increasing concentration. The hydrophobic cores of the micelle-like aggregates order into a body-centered-cubic (BCC) structure, as observed by small angle neutron scattering (SANS). The aggregation number of the hydrophobic core  $N_{ag}$  is determined by the length of the hydrophobic end group, and is insensitive to polymer concentration or temperature. Ordering is enhanced by reducing PEG length for a given end group (hence, similar  $N_{ag}$ ), or by increasing end group length (larger  $N_{ag}$ ) for a given PEG length. This micelle packing effect is manifested in changes in the viscoelastic properties. Specifically, the single-relaxation behavior in the dynamic moduli changes upon ordering as a new low frequency elastic plateau appears; and in creep a linear response changes to yielding behavior.

## Introduction

Poly(ethylene glycol)s (PEGs) modified with hydrophobes at both ends have been investigated widely as model associative polymers.<sup>1-19</sup> Most of the systems studied so far do not exhibit phase separation, but form a single phase over the entire concentration range.<sup>4-13,19</sup> The physical state of this non-phase separating associative polymer solution can be qualitatively understood in terms of the change in aggregation with concentration: the size of the connected clusters of associative polymers starts to grow continuously as the concentration increases, and finally forms an infinite cluster. However, a few cases of phase separation (i.e., sol-gel coexistence) have been reported for PEGs modified with alkyl groups.<sup>14-17</sup> We also observed phase separation phenomena for the PEGs (10k or 6k g/mol) modified with fluoroalkyl ends ( $C_nF_{2n+1}CH_2CH_2-$ ,  $n = 6, 8, 10$ ).<sup>20</sup> This phase separation was predicted by Semenov et al. as a gas-solid like transition, composed of a close packed phase of micelles and a dilute phase of micelles and free chains.<sup>21</sup> Alternatively, Pham et al. advanced a view in which the phase separation is a state of a liquid and a gas of micelles.<sup>15</sup>

Considering the micelle-like state of the associative polymer, the solution can display a lyotropic ordering transition. The lyotropic ordering transition of soft colloidal suspensions has been well studied for cases of purely repulsive interactions using model systems (diblock copolymers in a selective solvent for one block<sup>22</sup> or star-polymers in solution<sup>23</sup>). The diblock copolymer micellar solution normally orders into a body-centered-cubic (BCC) structure. However, a face-centered-cubic (FCC) structure forms when the corona is sufficiently thin compared to the size of the core.<sup>22</sup> Similarly, star-polymer solutions order into a BCC structure when the number of arms is modest (~30 -

~60), whereas it orders into a FCC structure when this number becomes higher.<sup>23</sup> For both cases, the soft colloids prefer a BCC structure in their lyotropic ordering, but this tendency shifts toward a FCC structure when the colloids become more rigid.

Telechelic associating polymer solutions combine the usual osmotic repulsion with attraction due to bridging among micelles. Lyotropic ordering has been reported for some telechelic cases. Cubic order was reported for the gel phase of systems with short PEG chains (2k and 4k g/mol) with  $C_{12}H_{25}$  ends,<sup>17</sup> possibly a BCC or a simple cubic (SC) structure. An ordered phase was also observed in a system with relatively long PEG and fluorocarbon ends (10k with  $C_8F_{17}C_{11}H_{22}$ ), which was assigned as a FCC structure.<sup>19</sup> In contrast, disordered, liquid-like phases were reported for systems with longer PEG (35k or 20k g/mol PEG with alkyl groups), even though they displayed phase separation.<sup>15,16</sup>

The rheological properties of associative polymer systems have been studied mainly by using PEG modified with alkyl groups that do not show phase separation.<sup>10-13</sup> It was found that they are almost perfect Maxwell (single relaxation time) fluids. Annable et al.<sup>10</sup> proposed a relaxation mechanism by breakage of the junction between micelles. The plateau modulus results from the bridges between micelles plus superbridges among them, excluding the entanglement effect among chains, based on the single relaxation behavior observed. The flow curve (viscosity vs. shear rate) consists of three regimes: a shear-rate-independent region at low shear rates, a modestly shear thickening region at moderate shear rates, and a shear thinning region at high shear rates. The concentrated phases of alkyl-ended systems that exhibit sol-gel coexistence (35k g/mol PEG with C16 and C18 hydrocarbon end groups) show essentially the same rheological characteristics as the single-phase species.<sup>16</sup>

Motivated by the stronger hydrophobicity of fluoroalkyl groups, PEGs modified with fluorocarbon ends have also been examined. Prior studies reported only materials that exhibit a single phase. Winnik and coworkers explored samples of long PEG chains (35k g/mol) modified with fluorocarbon end block (C8) and found essentially the same characteristics as the hydrocarbon systems, except for the disappearance of shear thickening.<sup>4-6</sup> Cathebras et al. also found that PEG (6, 10, and 20 kg/mol) modified with C<sub>8</sub>F<sub>17</sub>C<sub>11</sub>H<sub>22</sub> ends showed single-relaxation characteristics.<sup>18</sup> So far studies have found that the rheology of fluoroalkyl ended PEGs are similar to their alkyl ended counterparts, except for the surprising observation that short PEG (6k g/mol) with C<sub>8</sub>F<sub>17</sub>C<sub>11</sub>H<sub>22</sub> ends gave no viscosity enhancement.<sup>18</sup> However, the aggregation state of fluoroalkyls has not been as extensively investigated as that of alkyls. Aggregation numbers for hydrocarbon ends have been measured by several research groups and range between 20-80 (summarized in Table 2 of ref. [15]), but for fluorocarbon end groups, there are only three reports with disparate findings. For comparable PEG lengths (5k monofunctional, 10k telechelic), dimeric association was reported<sup>24,25</sup> for a C6 fluoroalkyl (C<sub>6</sub>F<sub>13</sub>C<sub>2</sub>H<sub>4</sub>-), whereas a large aggregation number (~100) was found<sup>19</sup> for a C8 fluoroalkyl (C<sub>8</sub>F<sub>17</sub>C<sub>11</sub>H<sub>22</sub>-). For a much longer PEG length (35k), aggregation numbers of 20 for C6 and 30 for C8 end groups were observed.<sup>6</sup>

Here we are particularly interested in the ordering transition and the resulting rheological responses of associating polymers with fluorocarbon ends that exhibit separation into coexisting sol and gel phases.<sup>20</sup> While considerable rheological data have been gathered for associating polymers in the single phase regime, little information is available for phase separating systems with fluorocarbon ends. We describe the

rheological properties of a range of materials that include systems that show phase separation. We examine their ordering transitions by SANS, and correlate their rheological properties with their fluid structure. By spanning a wide range of PEG lengths and fluoroalkyl lengths, we make the connection between molecular structure and lyotropic ordering, rheological responses, and the aggregation state of the hydrophobes (aggregation number of the fluoroalkyl ends).

## Experimental Section

**Synthesis of PEGs with fluorocarbon end-groups ( $R_f$ -PEGs).** Poly (ethylene glycol) (PEG) of nominal molecular weights 6k, 10k and 20k g/mol were end-group modified with fluorocarbon ends ( $-C_qF_{2q+1}CH_2CH_2$ ,  $q = 6, 8, \text{ or } 10$ ) using di-isocyanate linkage. Syntheses and characterizations were done as described previously.<sup>20</sup> The samples prepared for this study are described in Table 2.1, where  $pKCq$  is a polymer with a PEG midblock that is  $p$  kg/mol and with  $q$ -carbon fluoroalkyl end groups,  $C_qF_{2q+1}CH_2CH_2$ . Similarly,  $pKmCq$  is a monofunctional  $R_f$ -PEG prepared using  $p$  kg/mol PEG methyl ether, therefore having a  $q$ -carbon fluoroalkyl hydrophobe only at one end (Table 2.2).

**Rheological measurements.** In a vial, weighed amounts of dried bifunctional PEG- $R_f$ 's were dissolved in deionized water and mechanically shaken. The mixing time was adjusted so that the solution reached equilibrium, as inferred from the disappearance of any visible turbidity. The prepared samples were centrifuged before loading to remove entrapped bubbles. A stress-controlled rheometer (SR 5000, Rheometric Scientific) equipped with a solvent trap was used with a cone-and-plate geometry (0.1 radian cone

angle and 25 mm diameter) for rheological measurements. Evaporation from the sample restricts measurement temperature and time. With the appropriate solvent trap, drying of the sample was negligible for 12 hr at 25 °C, but at higher temperatures, the drying effect was noticeable after a few hr. Drying is also unavoidable during the loading of the sample on the rheometer, which takes 5-10 min. So, the actual concentration of the sample might be slightly higher than indicated. All data shown in the figures are at 25°C, unless otherwise indicated; and the reference temperature for time-temperature superposition is also 25 °C. Sample loading is achieved by lowering the upper part of sample holder (cone) slowly after placing the sample at the center of the bottom plate. Then, the sample is trimmed to match the diameter of the cone. The sample is allowed to re-equilibrate after loading. Prior to rheological testing, the approach to equilibrium is monitored using small strain dynamic shear (~2% at 1 rad/s), applied until no appreciable change of modulus is observed (typically 2 hr or less).

**SANS measurements.** Samples were dissolved in D<sub>2</sub>O (over a period of several days at 37 °C) at various concentrations and loaded into closed quartz sample holders of 2 mm thickness. Each sample was annealed at 45 °C (typically for 12 hr), then reequilibrated to ambient temperature (> 1 hr) before loading into the temperature-controlled stage. Measurements were performed in time of flight mode in the SAD (small angle diffractometer) beamline at the Intense Pulsed Neutron Source (IPNS) in Argonne National Laboratory (Argonne, IL, USA) with  $0.005\text{\AA} < q < 0.7\text{\AA}$ . At each experimental temperature, the sample was allowed to equilibrate for 1 hr. and held isothermal during acquisition. The acquisition times were 30 min. for most samples and 5 hr for the dilute (0.5 wt %) samples of monofunctional R<sub>f</sub>-PEGs.



## Results

**Phase behavior.**<sup>20</sup> The phase behavior of bifunctional R<sub>f</sub>-PEGs is governed by the relative length of the PEG midblock and the fluoroalkyl end groups (Table 2.3). 6KC10 does not exist as a homogeneous phase in water; rather it exists only as a slightly swollen precipitate. At the other extreme, 20KC10 and 20KC8 exist as homogeneous solutions over the whole range of concentration. Polymers that lie in between in terms of the relative length of PEG to R<sub>f</sub> (for example, 6KC6, 6KC8, 10KC8 and 10KC10) show phase separation into a gel coexisting with a sol.

The equilibrium gel phase concentration ( $C_{\text{gel,eq}}$ ) varies inversely with PEG midblock length and is insensitive to R<sub>f</sub>-length (Table 2.3). The phase boundary is almost temperature-invariant, but some increase of the gel phase concentration was observed for 10KC8 above 60 °C. These characteristics agree with previously reported hydrocarbon-ended phase separating systems.<sup>15</sup> The sol phase concentrations are very small for all samples (< 0.1 wt %), and unlike the gel composition, the end group length as well as the PEG length affects the equilibrium sol concentration.

**Linear viscoelastic properties of non-phase separating species.** The single phase systems, e.g., 20KC10, show single relaxation behavior over most of the observed frequency range for all concentrations in the range tested (from 5 to 17 wt %) (Figure 3.1). With increasing concentration (up to 17 wt %), the plateau modulus increases quadratically and the relaxation time increases linearly up to 17 wt % (Figure 3.2).<sup>16</sup> In steady shear, the flow curve shows only the plateau and shear thinning regimes (shear thickening is not found).<sup>6</sup> These observations agree with the general characteristics of

previously examined fluorocarbon ended systems.<sup>4-6,18</sup> However, as concentration increases (>10 wt %), an upturn of  $G''$  at high frequency (Figure 1) is observed. This upturn has been observed previously in single-phase type hydrocarbon-modified PEG.<sup>7</sup> To further investigate this phenomenon, higher concentration (25 wt %) samples were tested. Although these experiments were complicated by the very long equilibration times required at such high concentration (the samples were still noticeably turbid after several weeks), the upturn was observed in both  $G''$  and  $G'$  in the high frequency regime for this concentration.

**Linear viscoelastic properties of gels for sol-gel coexisting species.** At their equilibrium gel concentrations, these systems are described by a single relaxation behavior, like the single-phase systems.<sup>4-6,10,16,20</sup> The end-group largely determines the relaxation time: increasing the  $R_f$  length from C8 to C10 produces a large change (~40 fold) in the relaxation time, in contrast to the similar relaxation times for 10KC8 and 6KC8 gels at their respective  $C_{gel, eq.}$ .<sup>20</sup> The PEG midblock determines the modulus of the gel phase; a similar value in the plateau modulus is observed for 10KC10 and 10KC8 (~ $10^4$  Pa, Figure 2.3) at their  $C_{gel, eq.}$ , reflecting the similar density of physical junctions in these gels, evident from the similar values of their swelling ratios (Table 2.3). A higher value of the plateau modulus was observed for 6KC8 at  $C_{gel, eq.}$  (Figure 3), indicating that a higher density of physical junctions is present, which also agrees with its smaller swelling ratio as compared to 10KC10 and 10KC8 (Table 2.3).

However, with increasing concentration, a new plateau appears in the low frequency regime. For 10KC8, this new plateau develops gradually with increasing concentration from 8 to 12%; above 11 wt %,  $G'$  and  $G''$  do not cross in the frequency window tested

(Figure 3.3). The plateau is not observed immediately after loading the sample in the rheometer. During loading a significant deformation is exerted on the sample, after which the equilibrium state gradually recovers (Figure 3.4). Initially, terminal behavior is observed, followed by the development of the low frequency plateau. For 10KC8 at 12 wt % concentration, this change is almost complete in 4 hr, observed with ~2% strain at 1 rad/s. This new plateau extends below 0.01 rad/s, and  $G'$  and  $G''$  seem to cross around 0.001 rad/s at 25 °C for 12 wt % solution of 10KC8 (Figure 3.5), which is about 4 or 5 orders of magnitude smaller compared to the case of single relaxation mode (Figure 3.3). Therefore, stress relaxation will occur much more slowly than in the case of single relaxation behavior.

As the temperature increases, the tendency to form the new plateau is reduced. Thus, time-temperature superposition fails (Figure 3.5). For 10KC10, this new plateau occurs at somewhat lower concentration than that of 10KC8. Above 10 wt %,  $G'$  and  $G''$  no longer cross over each other. In the case of 6KC8, this change is more pronounced. For a specimen with 89% substitution of the ends (6KC8 in Table 2.1), the new plateau modulus is observed at 12 wt %, close to  $C_{gel,eq.}$ , at relatively low temperature (<9 °C). Another  $R_f$ -PEG prepared with 6k g/mol PEG and C8  $R_f$  ends with a higher conversion (~95% substitution) shows this new plateau at 12 wt% even at 25 °C.

**Comparison of  $R_f$ -PEG to bare PEG.** Solutions of PEG homopolymers of 6k, 10k, and 20k g/mol in the concentration range tested above show negligible viscoelasticity compared to the fluoroalkyl-modified samples. So the observed viscoelastic response results from the association of the hydrophobic groups.

**Creep behavior.** Qualitatively different creep behavior was observed for the single-relaxation time samples vs. those with the extended, low-frequency plateau (Figure 3.6). In response to a constant applied stress, the single phase system 20KC10 behaves like a Maxwell fluid: the strain grows nearly linearly (Figure 3.6 (a)) and the compliance  $J(t) = \gamma(t)/\sigma$  was independent of stress from 10 to 100 Pa. Furthermore,  $J(t)$  is very reproducible, even when successive experiments are performed with a short time in between (a few min.). The compliance rate decreases as the concentration increases. These characteristics accord well with linear response, in view of the dynamic moduli of 20KC10 (Figures 3.1 and 3.2). The solutions of sol-gel coexisting species near  $C_{gel,eq}$  (the single-relaxation time samples) also show a linear growth of strain from the beginning of the creep experiment.

In contrast, for the solutions of sol-gel coexisting systems that show the new low frequency plateau in  $G'$ , the strain increases non-linearly, showing a transition from a gradual (e.g., roughly  $J(t) \sim t^n$  with  $n \sim 0.13$  for 10KC8) creep initially to viscous flow at long time (10KC8 in Figure 3.6 (a)). Decreasing PEG length (cf. 6KC8 and 10KC8 in Figure 3.6 (a)) makes the ordered state stiffer and shifts the transition to viscous flow to higher stress and longer time (500 Pa is not large enough for 6KC8 to show viscous flow behavior in 30 min, Figure 3.6 (a)). Increasing fluoroalkyl length (cf. 10KC8 in Figure 3.6 (a) to 10KC10 in Figure 3.6 (b)) also makes the gel stiffer and delays the transition to viscous flow. The initial very slow creep is insensitive to the applied stress (Figure 3.6 (b)); however, the time at which the viscous flow regime emerges and the magnitude of the viscosity both decrease with increasing stress. The distinctive shape of  $J(t)$  for

10KC10—initial creep, then an elastic plateau, then viscous flow—is reminiscent of the behavior of certain ordered micellar solutions.<sup>26</sup>

The ordered fluids also show a significant memory of their flow history. Following a given creep experiment (reaching strain  $>5\%$ ), a subsequent creep experiment leads to a different  $J(t)$  as a function of the resting time allowed between the two experiments. Just as the low frequency modulus required a substantial time to recover after loading the sample in the rheometer (Figure 3.4), the initial, elastic-like response in creep requires time to recover. The initial very-slow creep is absent when stress is applied right after the completion of a preceding creep experiment with large strain ( $> 10\%$ ). The timescale for fully recovering the initial creep response is similar to that required to recover the low frequency plateau after loading (several hr).<sup>27</sup> Thus, the formation of the new elastic plateau in the dynamic moduli is correlated with the “yielding behavior” of the samples in creep tests.

**Lyotropic ordering of the gel phase.** To examine whether micelle packing is responsible for the development of the new plateau, SANS measurements were performed. The scattering pattern originating from the ordering of the hydrophobic cores of the micelles is observed as a primary peak. This peak becomes more distinct and shifts to higher wave vector,  $q$ , at higher concentrations (Figure 3.7). The sharper peak suggests improved long-range order, and the increase in  $q$  indicates a decrease in the lattice spacing as the concentration increases. The emergence of the low frequency plateau in the storage modulus correlates with the formation of the ordered structure; the increase in the low frequency modulus correlates with stronger ordering (cf. Figures 3.3 and 3.8).

Increasing temperature decreases the degree of ordering (Figure 3.8). However, the peak position does not change with temperature, which implies that the aggregation number of the hydrophobic cores does not change in the temperature range tested (25 to 49 °C). Thus, the decrease in the elastic plateau at low frequency with increasing temperature (Figure 3.5) can be understood in terms of softening of the ordered lattice.

At the same concentration, very different ordering is observed for different PEG lengths (20KC10 vs. 10KC10 in Figure 3.9). Systems having shorter PEG chains order more distinctively compared to system having longer PEG chains. In addition, for the same PEG midblock, somewhat better ordering is observed for systems with longer end-group lengths (10KC10 vs. 10KC8 in Figure 3.9).

**Aggregation number of the hydrophobic core.** To estimate the aggregation number of the hydrophobic cores from the SANS data, it is necessary to know what ordered structure is formed (BCC, FCC or SC). The distinct primary peak alone is not sufficient to distinguish what kind of cubic structure is formed. However, 15 wt % solution of 10KC10 reveals small secondary and tertiary peaks at  $\sqrt{2}$  and  $\sqrt{3}$  positions relative to the primary peak (Figure 3.10). This excludes the possibility of a FCC structure. The simple cubic (SC) structure is considered very unlikely, since a variety of experimental and theoretical studies of colloidal crystallization have found only FCC and/or BCC structures.<sup>22-23</sup> Assuming a BCC structure, the aggregation numbers can be calculated from the corresponding scattering data (Table 3.1). In addition, the aggregation numbers were also estimated from the extrapolated absolute intensities at  $q \rightarrow 0$  ( $I(q \rightarrow 0)$ ) of dilute (0.5 wt %) solutions of monofunctional  $R_f$ -PEGs. Using the correlation that  $I(q \rightarrow 0) = n(\phi)(\Delta\rho)^2 v^2$ , where  $n(\phi)$  is the number density of particles,  $(\Delta\rho)$  is the excess scattering

length density of the R<sub>f</sub>-PEGs respect to D<sub>2</sub>O, and  $v$  is the dry volume of an aggregate,<sup>19</sup> the aggregation numbers were estimated from these  $I(q \rightarrow 0)$  values. The results for dilute micelles coincide well with the aggregation numbers inferred from ordered gels based on a BCC structure assignment (Table 3.1). Therefore, we conclude that the present systems order into a BCC structure.

**Table 3.1. Aggregation Number of R<sub>f</sub>-PEG Solutions**

Species	Conc. (wt %)	Aggregation Number <sup>a</sup>
6KC8	15	32±4
10KC8	8	32±4
10KC8	12	32±4
10KC8	17	34±4
10KC10	12	50±6
10KC10	15	45±6
20KC10	12	51±9
5KmPC8	0.5	28±4
5KmPC10	0.5	44±5

<sup>a</sup> Determined from SANS (see text).

All aggregation numbers in Table 3.1 were calculated using the position of the primary peak and the BCC structure assignment. The observed aggregation numbers are relatively high. Neither concentration (8 to 17 wt % for 10KC8 and 0.5 wt % for 5KmPC8; 12 to 15 wt % for 10KC10 and 0.5 wt % for 5KmPC10) nor temperature (25 to 49 °C for 10KC8 in Figure 3.8) affects the aggregation number. Aggregation number is

not affected (within experimental uncertainty) by substantial changes in PEG length (C8 with 6k or 10k here, or 35k in ref 6; C10 with 10k or 20k) or topology (dangling ends *vs.* loops: 5KmPC8 *vs.* 10KC8; 5KmPC10 *vs.* 10KC10). Thus, the hydrophobe length governs the aggregation number.

## Discussion

Here we provide an integrated view of the rheological and structural properties of these associating polymers, and their implications for theory. The rheology of the single-phase systems reflects the progression of network topology with concentration established for associative thickeners; however, the aggregation numbers actually observed are much higher than the values inferred based on the Annable model. In contrast, micelle-micelle packing governs the structure and rheology of the systems that exhibit sol-gel equilibrium. Micelle-micelle repulsion drives ordering at concentrations above but near their equilibrium gel concentration and enhances the elastic moduli of their disordered gels. Proximity of the ordering concentration to  $C_{\text{gel,eq}}$  also explains the very weak concentration dependence of the end-group relaxation mode.

**Characteristics of single-phase species.** We expect fluoroalkyl ended PEGs that have a continuous transition from a solution to a gel to be described by the model that Annable<sup>10</sup> developed for alkyl ended PEGs. The key features of the model are accounting for the continuous change in network topology with increasing concentration: at low concentration the polymers exist in isolated flower-like micelles, as concentration increases these form clusters that grow until one spans the whole system, forming a very soft gel. This initial gel has bridging strands that may be chains of flowerlike micelles,



“superbridges”; with further increase in concentration, the average length of these superbridges decreases until it drops to the length of a single bridging strand between adjacent micelle cores. This physical picture explains the increase in the plateau modulus (Figure 3.2 (a)) and relaxation time (Figure 3.2 (b)) of 20KC10 with concentration.

Although the Annable model describes the general qualitative behavior of single-phase systems (whether hydrocarbon or fluorocarbon ended), it does not describe them quantitatively. The aggregation numbers deduced by fitting the model to experimental results are relatively small (3 or 4) compared to the observed aggregation numbers (between 20-40 for C16 alkyl-ended systems<sup>15</sup> and ~50 for 20KC10 from our SANS observations). If the observed aggregation numbers are used, the model predicts too rapid an increase in both the relaxation time and modulus as a function of concentration, reaching their saturated values at much lower concentration than is actually observed. Therefore, it appears that there is some additional physics that causes the system to prefer super-bridges over direct bridges. We proposed that the excluded volume repulsion between the micelles, which is not included in Annable’s model, may suppress direct bridging. If this effect were included, then the length of super-bridges would decrease more gradually with increasing concentration than is predicted by the current model, providing better accord with the observed behavior.

The observed dynamic moduli also show a high frequency response that is not captured by the model (Figure 1 for fluoroalkyl-ended and ref. [7] for alkyl ended PEG), which focusses on the viscoelasticity due to the aggregated structures. These high frequency contributions can be attributed to relaxation modes of the PEG chains (Rouse or entanglement),<sup>28</sup> which are beyond the scope of the Annable model.

**Ordering transition.** The most distinct rheological characteristic of the present sol-gel coexisting species—the appearance of a new elastic plateau in the low frequency regime—has not been reported before for associative polymer solutions. The densely packed micelle structure, verified by the ordering observed using SANS, explains this new plateau. Relaxation times related to the movement of whole micelles are much longer than the time scale of the end group dissociation mode. Therefore, the ordering transition shifts the terminal regime to much lower frequencies, and results in a long recovery time after loading and yielding behavior in creep.

The observed effects of temperature and molecular structure are consistent with this physical picture. Due to the LCST behavior of PEG in water, the micelle corona becomes thinner with increasing temperature. At fixed concentration, the average distance between micelle cores remains the same. Thus, with increasing temperature the average repulsion between micelles decreases, which causes a decrease in long-range order. The weaker ordering with increasing temperature (Figure 3.8) correlates with the decrease in the low-frequency modulus (Figure 3.5), supporting the hypothesis that the elasticity of the ordered lattice is responsible for the low frequency plateau. With decreasing length of the PEG midblock for a given end group length (hence, fixed aggregation number of the hydrophobic core), the corona is thinner and more dense; the ordering transition shifts to higher weight concentration (similar volume concentration of micelles) and displays stronger long-range order, which correlates with higher low-frequency modulus and greater resistance to creep. With increasing fluoroalkyl length for a fixed PEG length and concentration, the degree of ordering increases, as does the low-frequency modulus and the resistance to creep. These effects are consistent with the increase in aggregation

number with increasing fluoroalkyl length (Table 3.1), since increasing the aggregation number of the micelle (or the number of the arms of a star-polymer) makes the corona more rigid.<sup>23</sup>

Given that ordering occurs at concentrations just above  $C_{\text{gel, eq.}}$ , the phase separation observed in the present systems appears to be closer to a gas-solid-like transition as predicted by Semenov et al.<sup>21</sup> than a gas-liquid transition observed for a longer PEG (35k) with hydrocarbon tails.<sup>16</sup>

**Plateau modulus.** The theories of rubber elasticity<sup>29</sup> and transient networks have been adapted<sup>10</sup> to explain the modulus of the associating polymer system, which says that

$$G_0 = g\nu\kappa T = g\rho RT/M_{e0}$$

where  $G_0$  is the pseudo equilibrium modulus of the material,  $\nu$  is the number of chains per unit volume,  $\rho$  is the density of the material,  $M_e$  is the apparent molecular weight between crosslinks, and  $g$  is the correction factor to account for network defects. This correction factor is close to 1 and varies weakly with the functionality of the crosslinks.<sup>29</sup> Inter-chain looping or entanglement tends to increase  $g$ , whereas dangling bonds and other network defects tend to decrease  $g$ . For an associating polymer solution that is described by the Maxwell model,  $G_0$  corresponds to the plateau value of  $G'$  at high frequency,<sup>30</sup> assuming that only the entropic elasticity of the chains contributes to the modulus. So,  $G_0/n\kappa T$  is an estimate for the fraction of elastically effective chains, where  $n$  is the number of polymer chains per unit volume (based on the known concentration and molecular weight). For hydrocarbon-ended systems, this value increases linearly at low concentrations and saturates to  $\sim 1$  at high concentrations.<sup>10, 16</sup> For 20KC10, a single phase system (Figure 3.12 (a)), this was also the case. This linear increase of  $G_0/n\kappa T$  (or

quadratic increase of  $G_0$ , Figure 3.2) with concentration has been observed previously in a number of single-phase alkyl-ended PEG systems.<sup>10-13</sup> Two explanations have been offered: the change in superbridge length with concentration<sup>10</sup> or pairwise colloidal interactions.<sup>16</sup>

Interestingly, a much higher concentration is required to reach saturation of  $G_0/nkT$  for 20KC10 (no roll-off is evident even at 17 wt %) than for previously reported hydrocarbon-ended systems (roll-off is evident at concentrations below 10 wt % for either 35k or 20k PEG with C16 alkyl ends<sup>10,16</sup>). This difference cannot be explained by a difference in aggregation number, since they are similar ( $\sim 50$  for 20KC10 compared to  $\sim 40$  for C16 alkyl ended 35k PEG, and greater  $N_{ag}$  shifts saturation to lower concentration in Anable's model). Also, at a given concentration (wt %), comparable fluoroalkyl systems show lower  $G_0/nkT$  than their alkyl ended counterparts. This pair of observations is consistent with fluoroalkyl ended systems having a stronger inter-micelle repulsive interaction than their alkyl ended counterparts (with similar  $N_{ag}$  and PEG length). An increase in the repulsive part of the intermicelle interaction would disfavor direct bridging in favor of superbridging. Therefore, at the same concentration, the length of superbridges would be longer and the modulus would be lower; the concentration required to drive the system completely to direct bridging would be higher. A related difference between the phase behavior of fluoroalkyl ended PEG relative to alkyl ended PEG has been noted previously: pairs of systems have been identified that have comparable  $N_{ag}$  and PEG length, in which the fluoroalkyl ended system exhibits single phase behavior and their alkyl ended analogue shows sol-gel equilibrium. This difference implies that the intermicelle attraction is weaker in the fluoroalkyl ended system. Since

the entropic attractive term is regulated by  $N_{ag}$ , this suggests that the intermicelle repulsion accounts for the difference (greater for fluoroalkyl ended PEGs).

In contrast to the small values of  $G_o/nkT$  ( $<1$ ) for single phase systems, large values of  $G_o/nkT$  ( $>1$ ) are found for the phase separating species, even near  $C_{gel,eq}$ . (Figure 3.12 (a)). When compared at a given concentration above their ordering transitions, 10KC10, 10KC8 and 6KC8 all exhibit similar  $G_o/nkT$  at high-frequency (at 17 wt %,  $G_o/nkT \sim 1.8$ ). As previously predicted by Semenov and inferred from observations of  $G_o/nkT > 1$  in an alkyl ended PEG, the high values of  $G_o/nkT$  indicate that micelle packing gives a significant contribution to the elasticity of these gels. However, the intermicelle repulsion appears to be much stronger in the present fluoroalkyl ended PEGs, which show a high value of  $G_o/nkT$  from the equilibrium gel compositions onwards and reach values substantially greater than 1, contrary to the alkyl ended system (35k PEG with C18 alkyl ends) that only exhibited  $G_o/nkT > 1$  at concentrations much greater ( $\sim 2x$ ) than  $C_{gel,eq}$ .<sup>16</sup> This difference may be a consequence of the different PEG lengths used: In addition, the larger values of  $G_o/nkT$  in the present systems may reflect the differences between fluoroalkyl ended and alkyl ended systems discussed above: fluoroalkyl ended systems appear to have stronger intermicelle repulsion than their alkyl ended counterparts.

**End-group dissociation mode.** The reciprocal of the critical frequency at which  $G''$  shows a maximum is a relaxation time attributed to the end-group dissociation mode,  $\tau_{e.d}$ .<sup>31</sup> When the end-group dissociation is the predominant relaxation mechanism,  $\tau_{e.d}$  is the single relaxation time and the fluid is well approximated by a Maxwell fluid (e.g., 20KC10 at all concentrations investigated). The value of  $\tau_{e.d}$  is dominated by the end-group length regardless of the phase behavior (Figure 3.12 (b)); for single-phase type

systems,  $\tau_{e,d}$  increases linearly with concentration over our experimental range (e.g., up to 17 wt % for 20KC10). For species showing phase separation, the effect of concentration on  $\tau_{e,d}$  is much weaker than for single-phase systems. This reduced dependency of  $\tau_{e,d}$  on concentration for the phase-separating species implies that the topology of the network does not change much in this concentration range.

## Conclusions

Previously, the phase transition of long PEG (35k) modified with hydrocarbon systems was described as a gas-liquid transition,<sup>15,16</sup> so the gel phase is a disordered but highly associated micellar liquid, even far above the equilibrium gel concentration. However, the phase transition of our fluorocarbon systems is closer to a gas-solid transition, as predicted by Semenov.<sup>21</sup> This was concluded from the evidence of distinct micelle packing effects at concentrations slightly above  $C_{gel,eq}$ : (1) the ordering of the hydrophobic cores as observed by SANS, (2) the formation of a new low-frequency plateau, (3) yielding behavior in creep, and (4) relatively high values of  $G_0/n\kappa T$  (above 1).

## Acknowledgements

We acknowledge Jyotsana Lal at Argonne National Lab. in Argonne, Illinois, USA, for the help in small angle neutron scattering experiments.

## References

- [1] Glass, J.E, Ed. "Hydrophilic Polymers: Performance with Environmental Acceptability," ACS Advances in Chemistry Series 248, Washington, DC, **1996**
- [2] Schulz, D.N.; Glass, J.E. Ed. "Polymers as Rheology Modifiers," ACS Symposium Series 462; Washington, DC, **1989**
- [3] Rubinstein, M.; Dobrynin, A.V. *Trends Polym. Sci.* **1997**, June, *5(6)*, 181
- [4] Menchen, S.; Johnson, B.; Winnik, M.A.; Xu, B. *Chem.Mater.* **1996**, *8*, 2205
- [5] Menchen, S.; Johnson, B.; Winnik, M.A.; Xu, B. *Electrophoresis* **1996**, *17*, 1451
- [6] Xu, B.; Li, L.; Yekta, A.; Masoumi, A.; Kanagalingam, S.; Winnik, M.A.; Zhang, K.; Macdonald, P.M.; Menchen, S. *Langmuir* **1997**, *13(9)*, 2447
- [7] Xu, B.; Yekta, A.; Li, L.; Maosumi, Z.; Winnik, M.A. *Colloids and Surfaces A* **1996**, *112*, 239
- [8] Yekta, A.; Xu, B.; Duhamel, J.; Adiwidjaja, H.; Winnik, M.A. *Macromolecules* **1995**, *28*, 956
- [9] Tam, K.C.; Jenkins, R.D.; Winnik, M.A.; Bassett, D.R. *Macromoleculs* **1998**, *31*, 4149
- [10] Annable, T.; Buscall, R.; Ettelaie, R. *J.Rheo.* **1993**, *37(4)*, 695
- [11] Jenkins, R.D.; Silebi, C.A.; El-Asser, M.A. *Polymer Mat.Sci.Eng.* **1989**, 629
- [12] Kaczmariski, J.P.; Glass, J.E. *Macromolecules* **1993**, *26*, 5149
- [13] Lundberg, D.J.; Brown, R.G.; Glass, J.E.; Eley, R.R. *Langmuir* **1994**, *10*, 3027
- [14] Pham, Q.T.; Russel, W.B.; Lau, W. *J.Rheo.* **1998**, *42(1)*, 159
- [15] Pham, Q.T.; Russel, W.B.; Thibeault, J.C.; Lau, W. *Macromolecules* **1999**, *32(9)*, 2996

- [16] Pham, Q.T.; Russel, W.B.; Thibeault, J.C.; Lau, W. *Macromolecules* **1999**, *32*(15), 5139
- [17] Francois, J.; Maitre, S.; Rawiso, M.; Sarazin, D.; Beinert, G.; Isel, F. *Colloids Surf. A* **1996**, *112*, 251
- [18] Cathebras, N.; Collet, A.; Viguier, M.; Berret, J. *Macromolecules* **1998**, *31*, 1305
- [19] Serero, Y.; Aznar, R.; Porte, G.; Berret, J.-F.; Calvet, D.; Collet, A.; Viguier, M. *Phys. Rev. Lett.* **1998**, *81*(25), 5584
- [20] See Chapter 2: Tae, G.; Kornfield, J.A.; Hubbell, J.A.; HogenEsch, T.E.; Johannsmann, D. in *Macromolecules* **2001**, *34*, 6409
- [21] Semenov, A.N.; Joanny, J.F.; Khokhlove, A.R. *Macromolecules* **1995**, *28*, 1066
- [22] McConnel, G.A.; Gast, A.P.; Huang, J.S.; Smith, S.D. *Phys. Rev. Lett.* **1993**, *71*(13), 2102
- [23] Watzlawek, M.; Likos, C.N.; Lowen, H. *Phys. Rev. Lett.* **1999**, *82*(26), 5289
- [24] Zhang, H.; HogenEsch, T.E. *Langmuir* **1998**, *14*, 4977
- [25] Zhang, H.S.; Pan, J.; HogenEsch, T.E. *Macromolecules* **1998**, *31*, 2815
- [26] Paulin, S.E.; Ackerson, J.; Wolfe, M.S. *Phys. Rev. E* **1997**, *55*, 5812
- [27] The results shown in Figure 7 represent those for ~4 hr of recovery from prior flow history; different results might be obtained if even longer annealing were allowed between experiments.
- [28] Groot, R.D.; Agterof, W.G.M. *Macromolecules* **1995**, *28*, 6284
- [29] Treloar, L.R.G. "The physics of rubber elasticity," 3<sup>rd</sup> Ed. Oxford, London, UK, **1975**
- [30] Roovers, J. *Macromolecules* **1991**, *24*, 5985



- [31] Zhang, K.W.; Xu, B.; Winnik, M.A.; Macdonald, P.M. *J. PHYS. CHEM.* **1996**, *100*, 9834

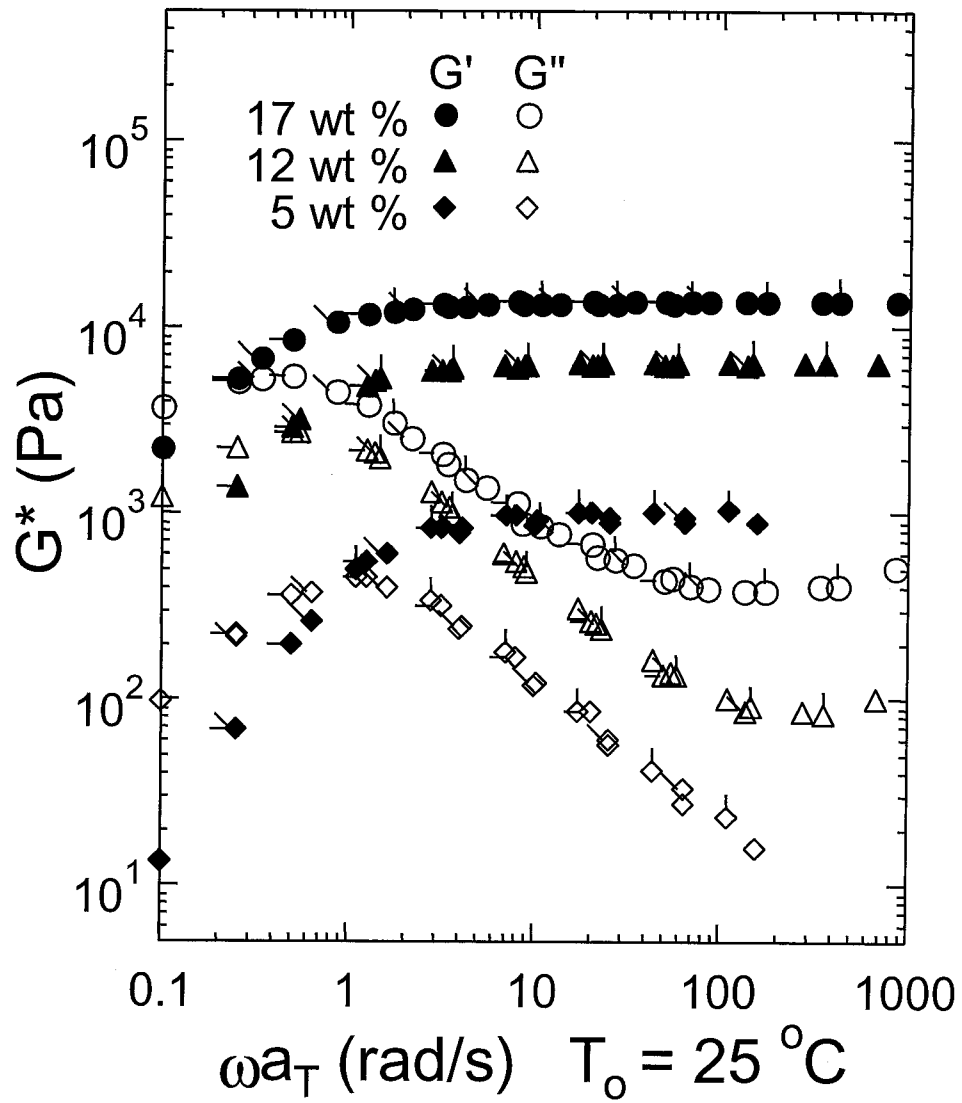
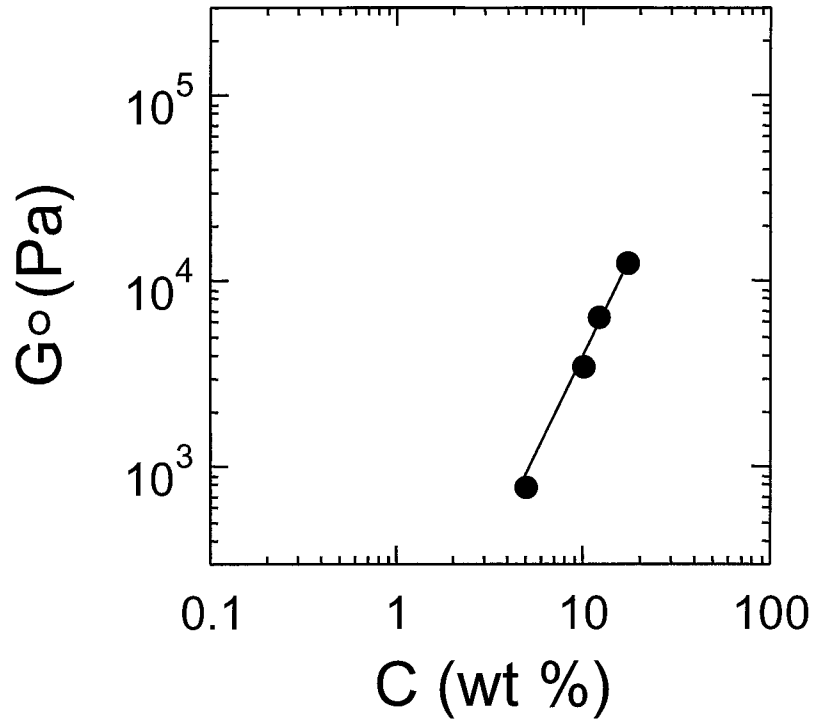


Figure 3.1 Dynamic moduli of 20KC10 solutions (skip marks denote temperature of the measurements:  $\blacklozenge$  25 °C,  $\circ$  17 °C,  $\blacklozenge$  9 °C, and  $\bullet$  1 °C).

(a)



(b)

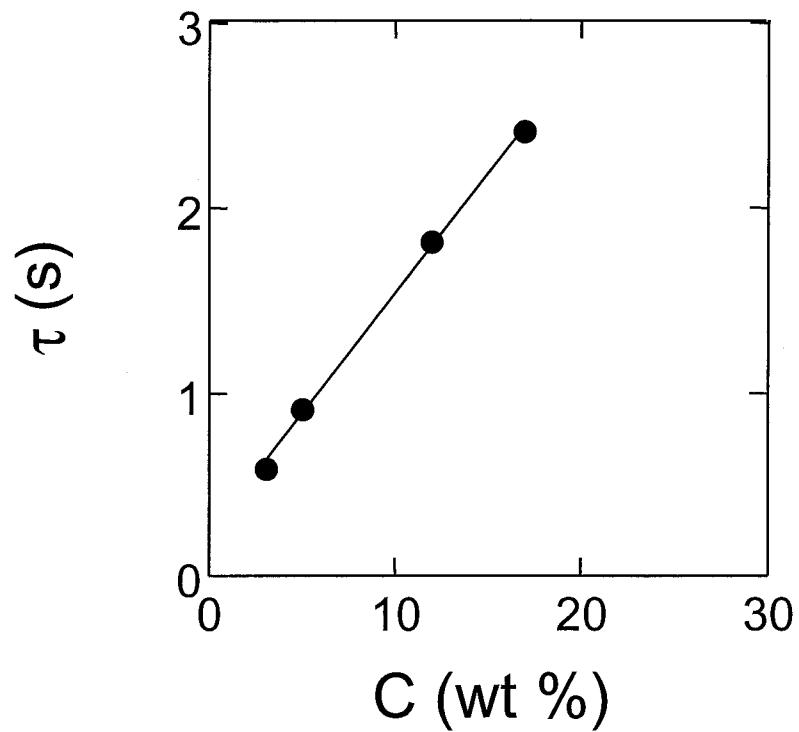
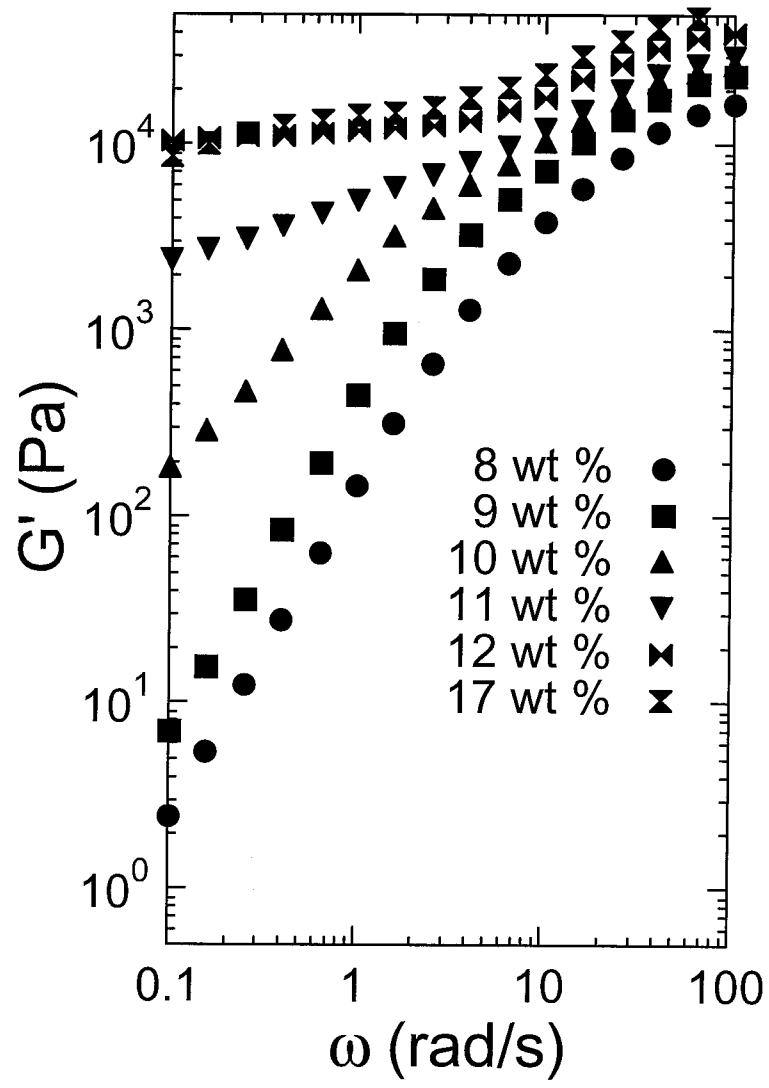


Figure 3.2 Concentration dependence of material properties of 20KC10 solutions: (a) high-frequency plateau modulus, and (b) relaxation time end-group dissociation mode.

(a)



(b)

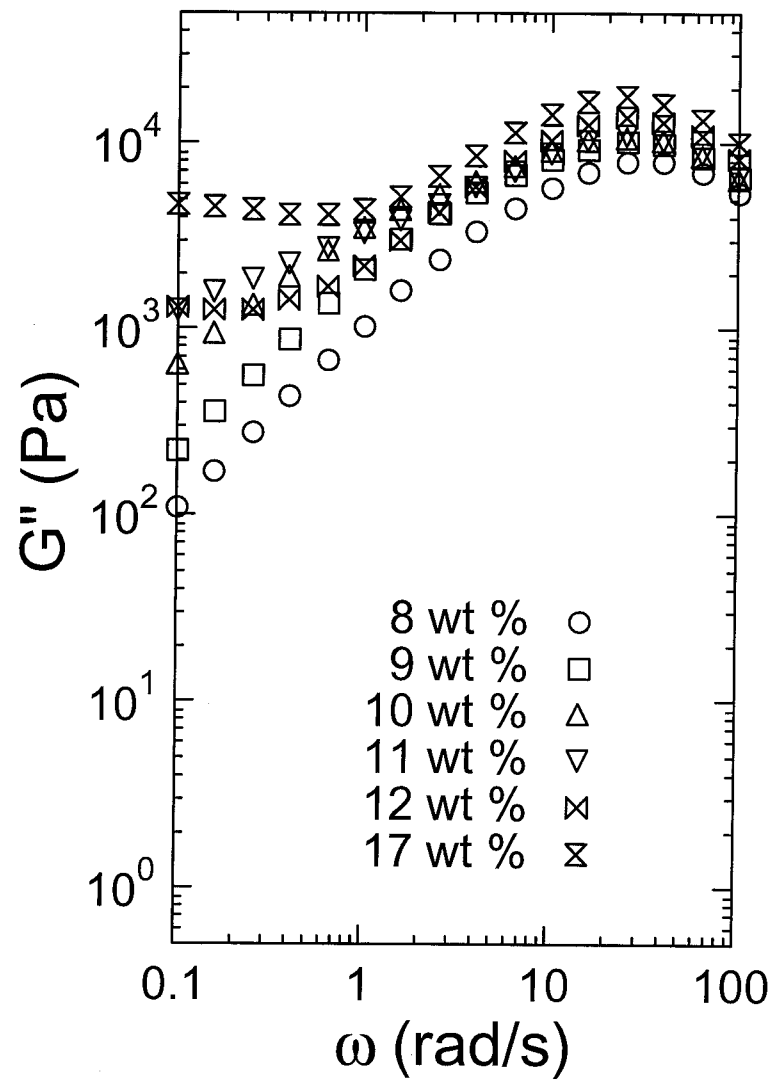
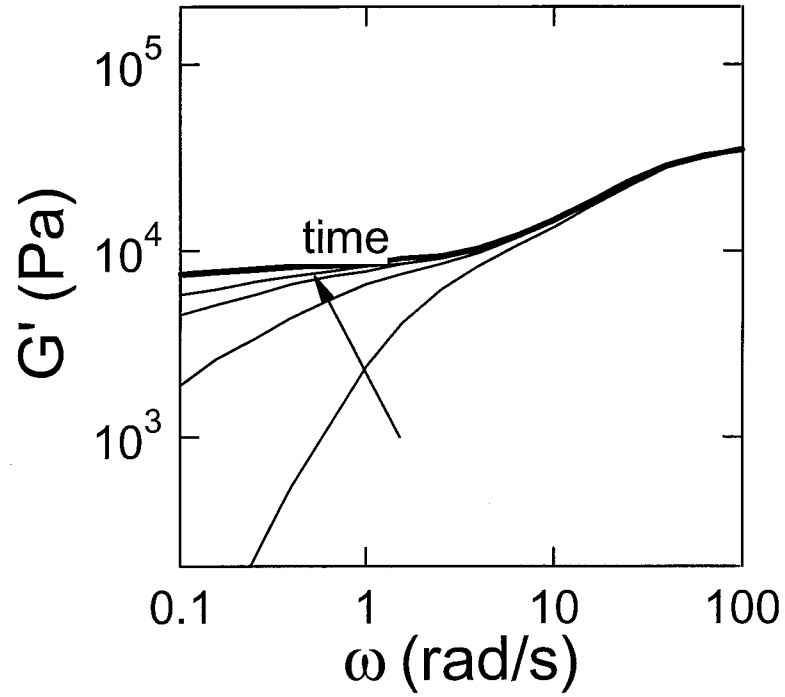


Figure 3.3 Dynamic moduli of 10KC8 solutions at  $C > C_{gel,eq}$ . at 25 °C: (a) storage modulus, and (b) loss modulus.

(a)



(b)

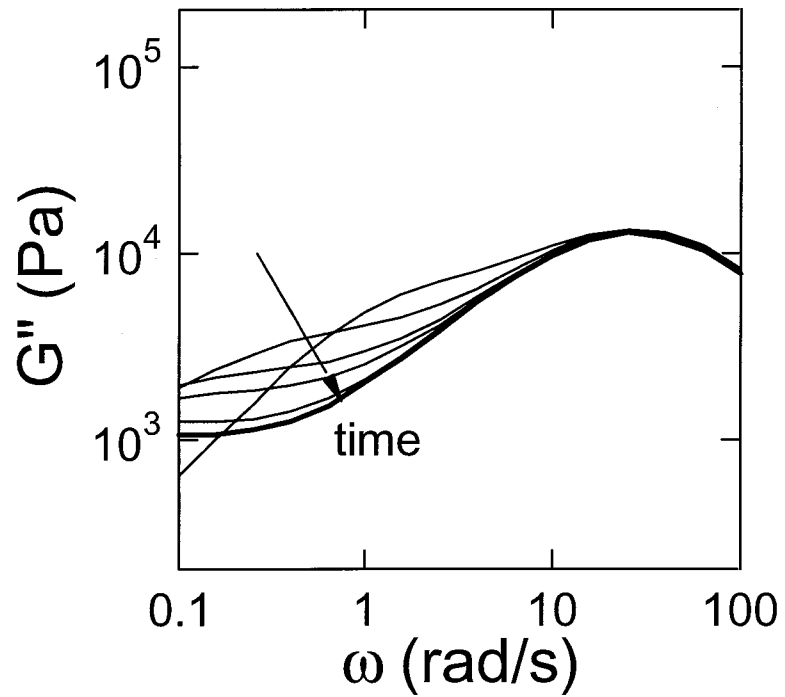


Figure 3.4 Development of the low-frequency plateau with time after loading (see text), illustrated by 10KC8 at 12 wt % and at 25 °C: (a) storage modulus, (b) loss modulus. Dotted curve recorded immediately after loading; successive curves recorded at 1 hr intervals.

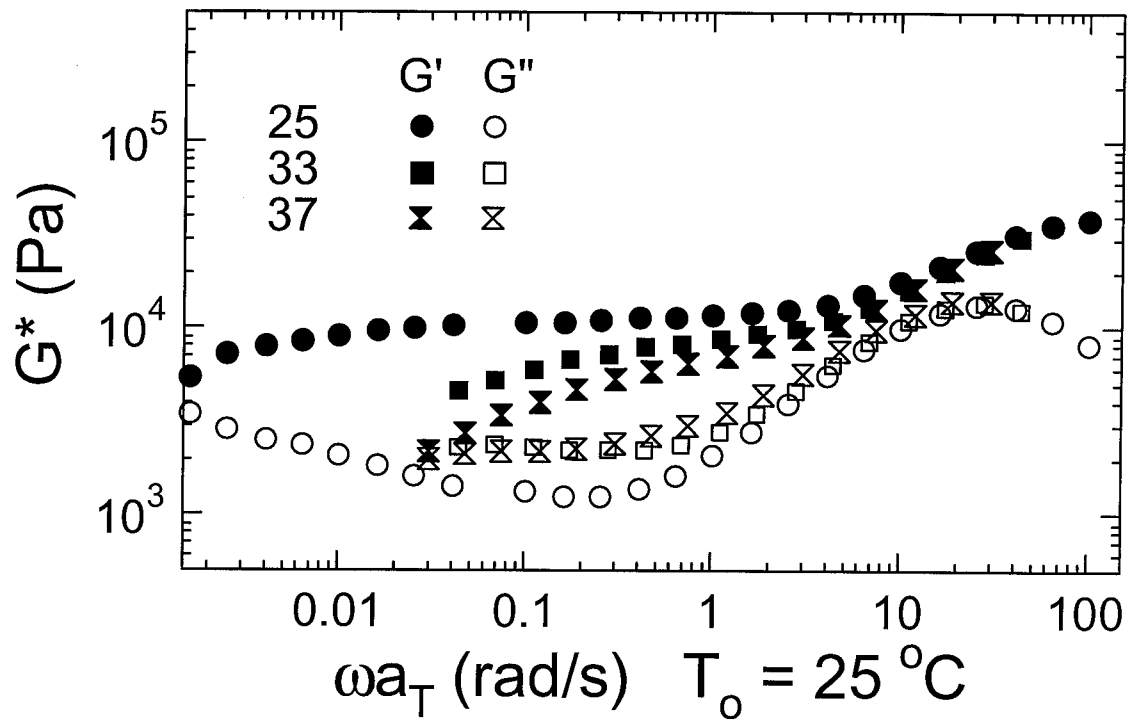
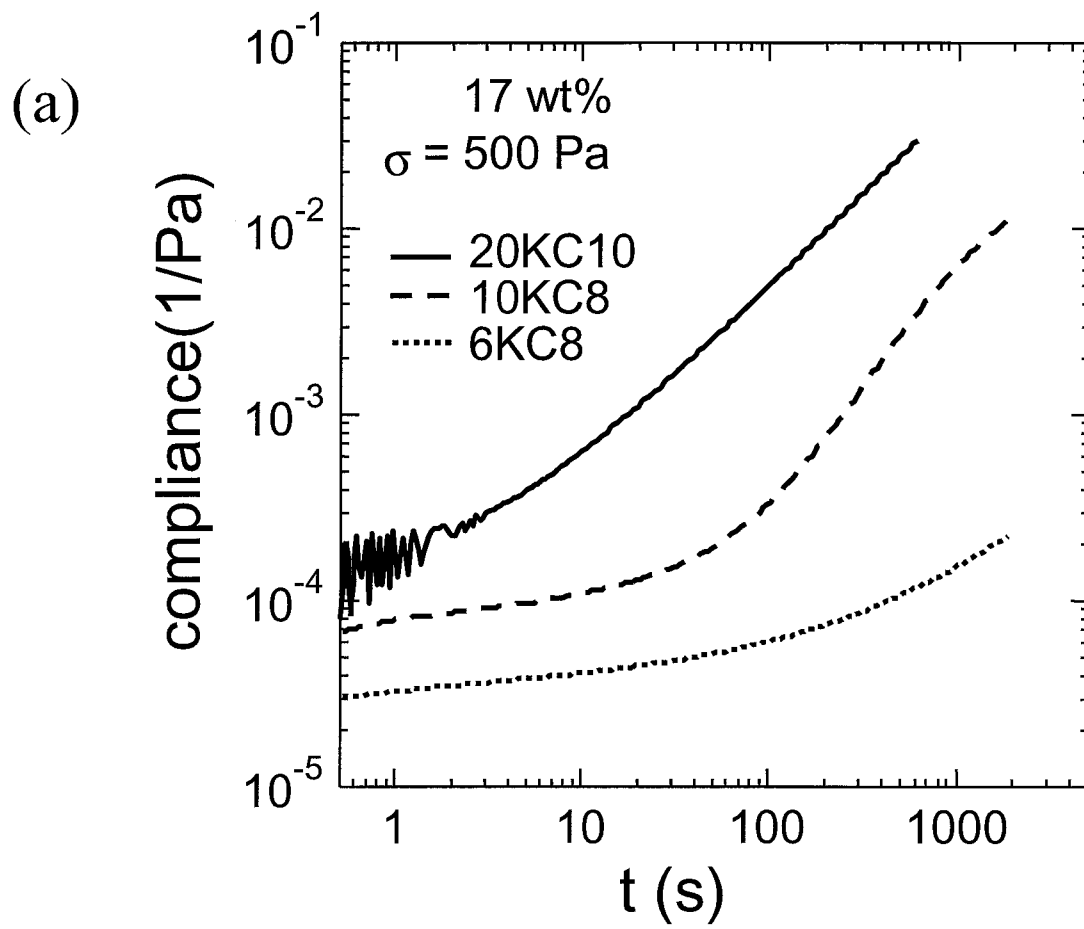


Figure 3.5 Dynamic moduli of 10KC8 12 wt % solution at various temperatures, shifted so that their end-group dissociation modes superimpose.





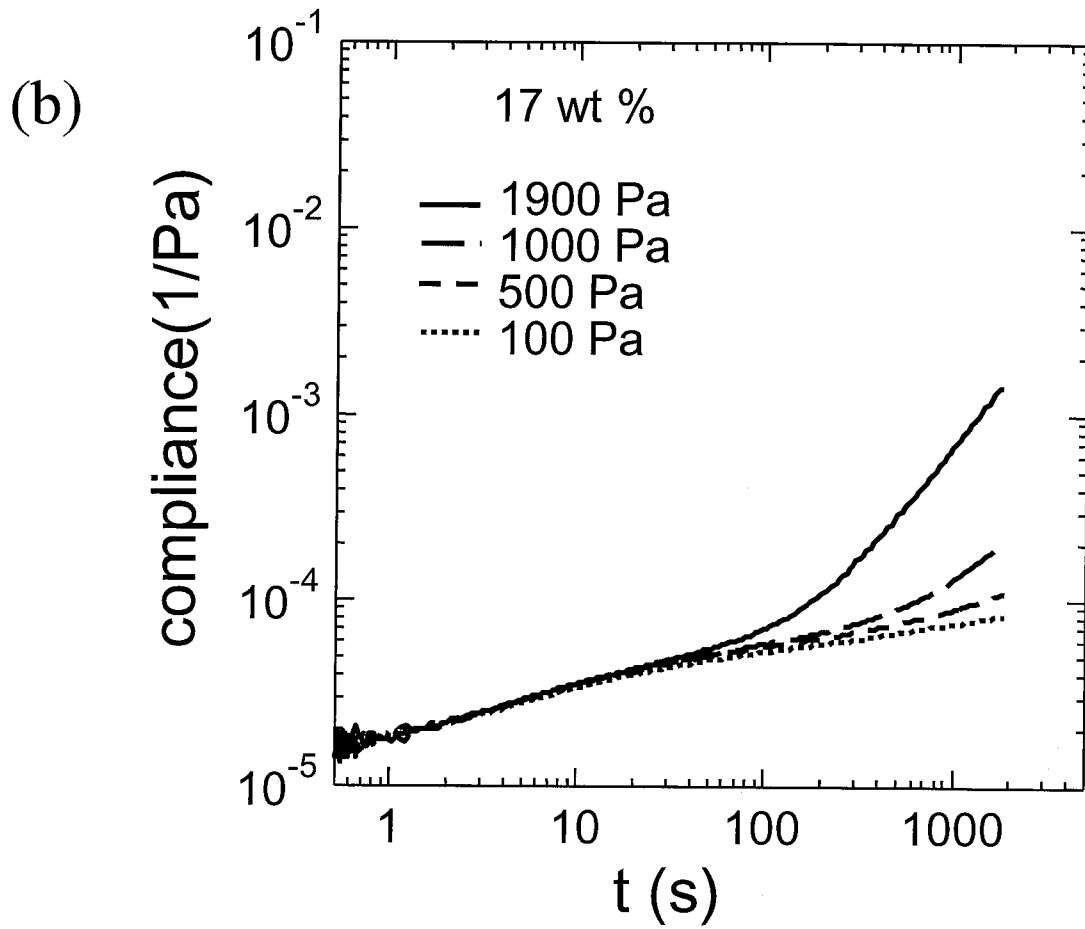


Figure 3.6 Creep responses (a) as a function of molecular structure for fixed concentration (17 wt %,  $\sigma = 500$  Pa), and (b) as a function of applied shear stress (for 10KC10 17 wt%).

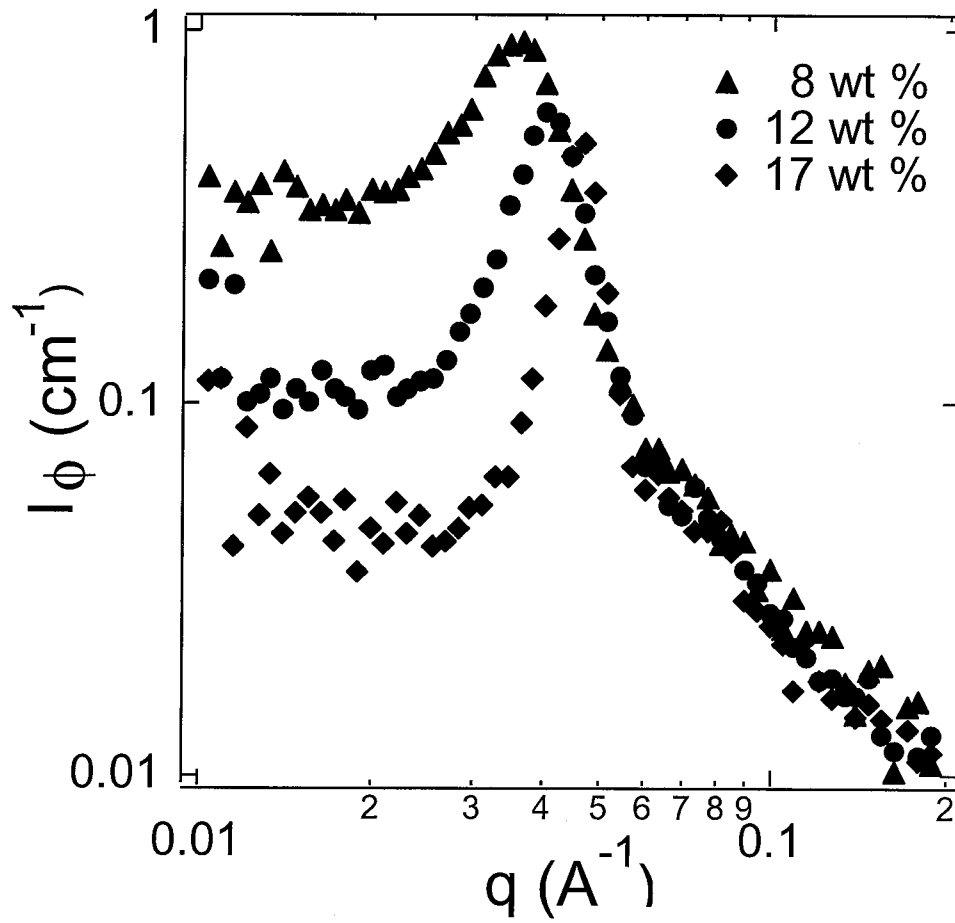


Figure 3.7 SANS pattern of 10KC8 solutions as a function of concentration at 25 °C.

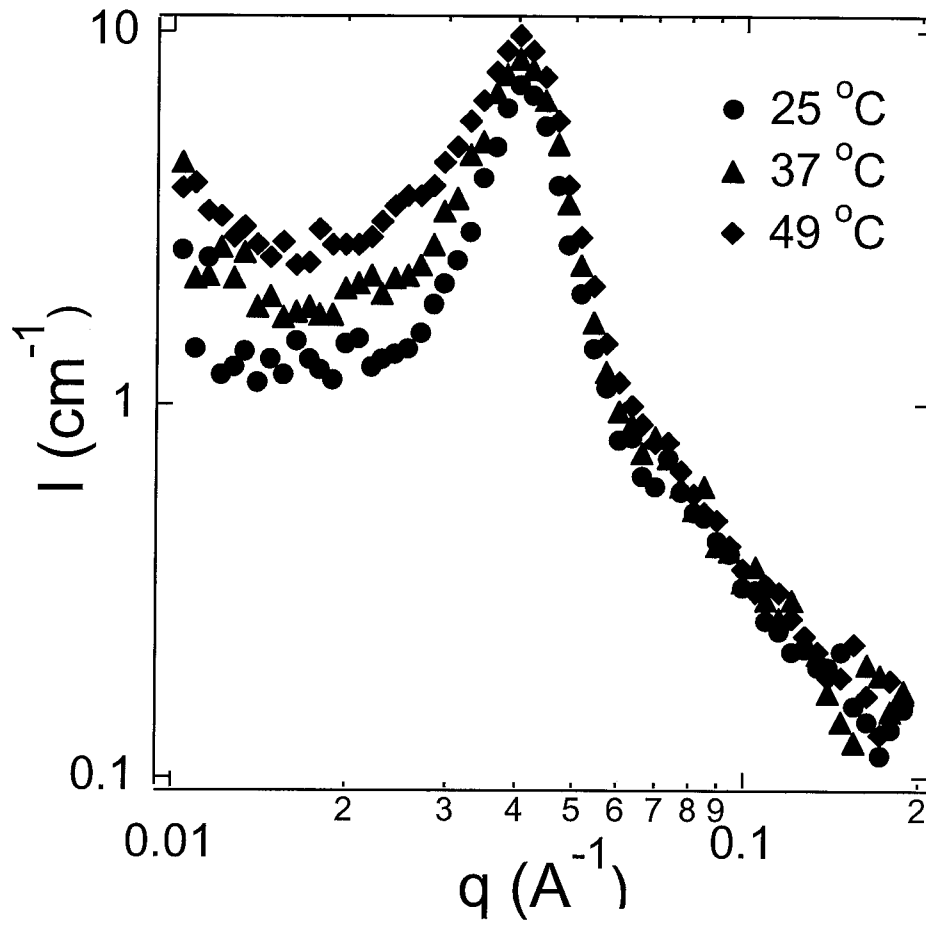


Figure 3.8 SANS pattern of 10KC8 12 wt % as a function of temperature.

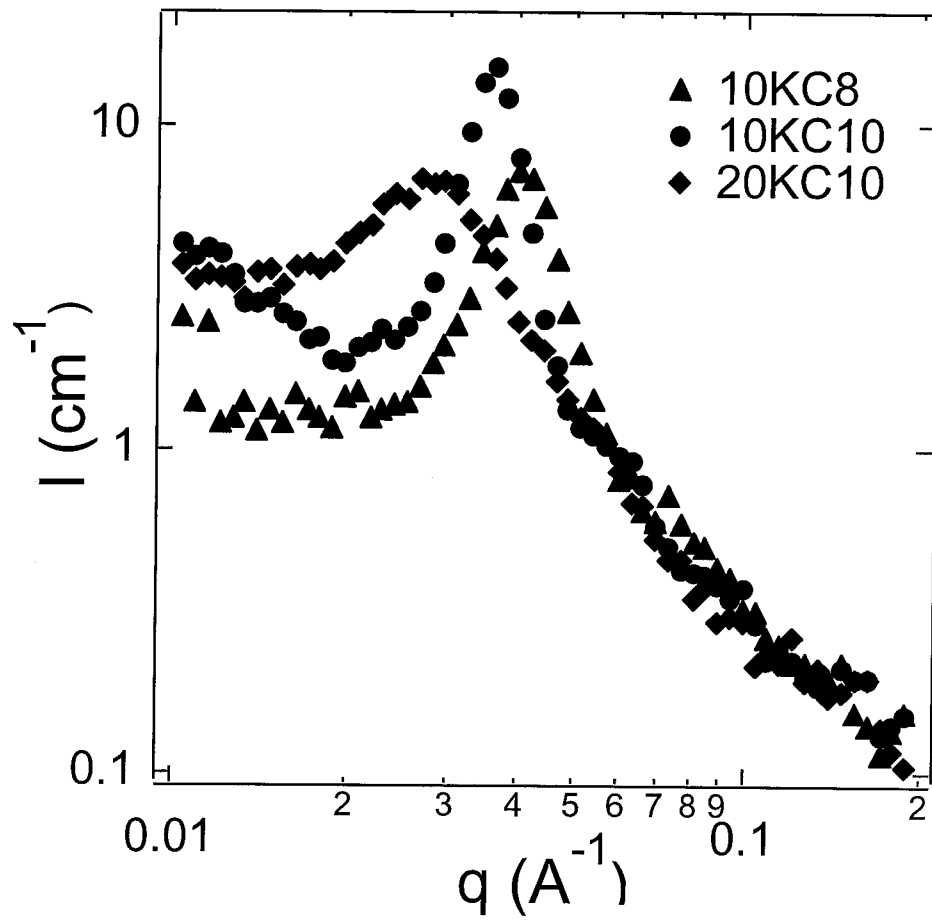


Figure 3.9 Comparison of SANS patterns for various species at fixed concentration (12 wt % at 25 °C).

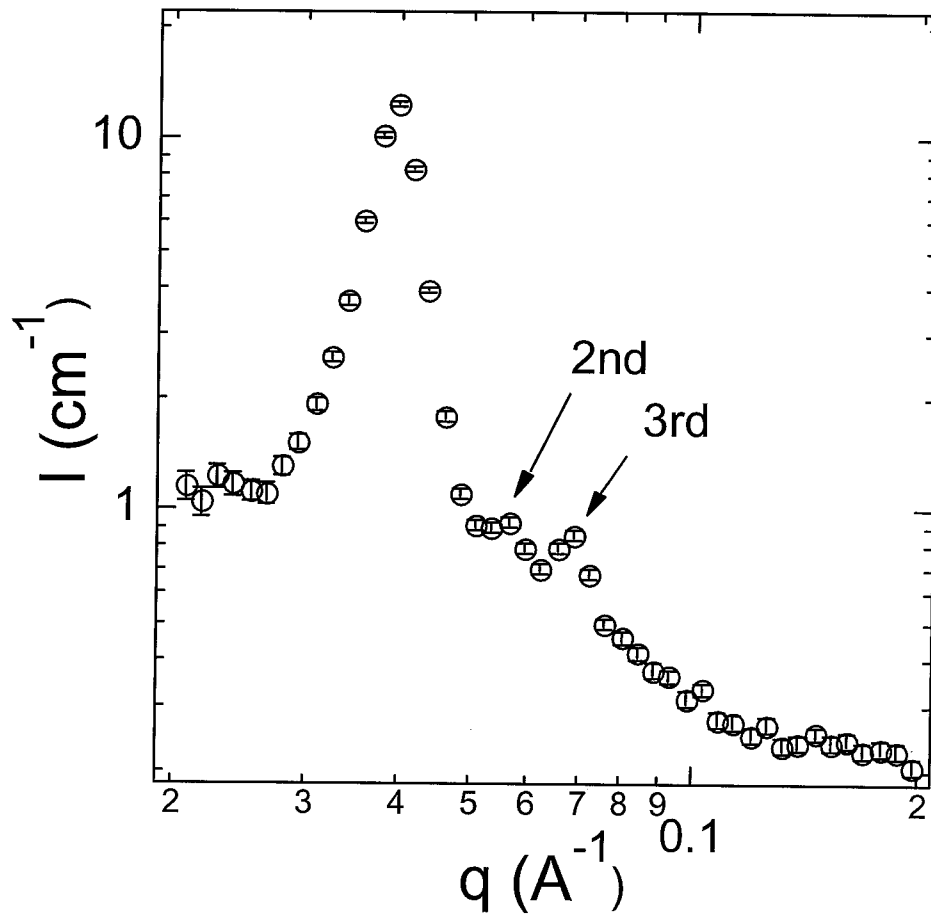


Figure 3.10 SANS pattern of 10KC10 15 wt % solution at 25 °C.

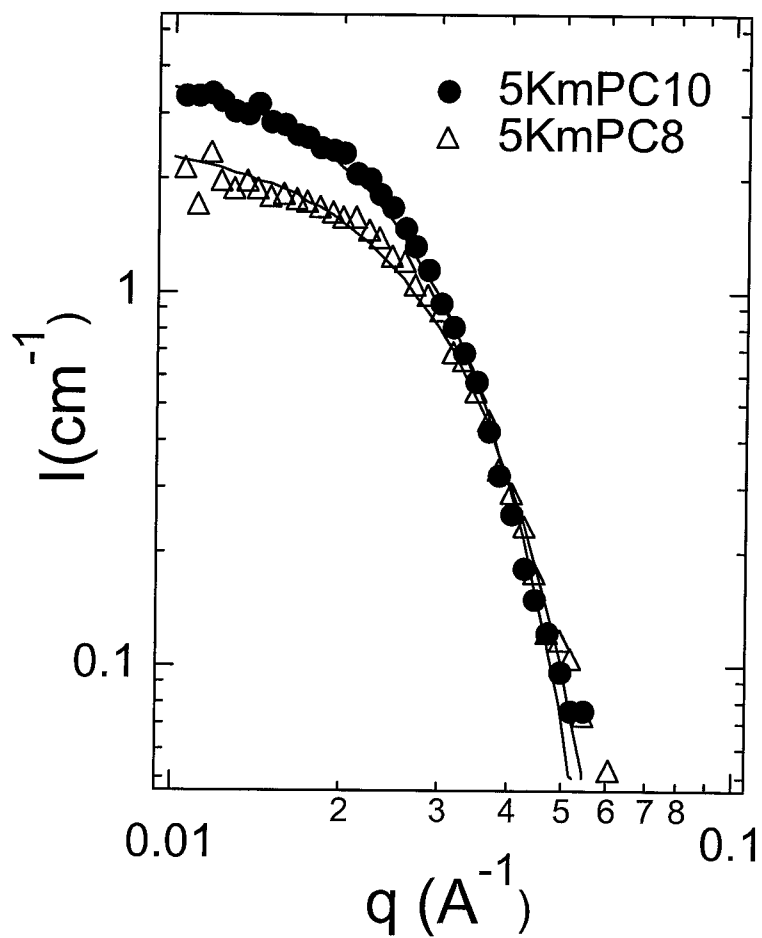
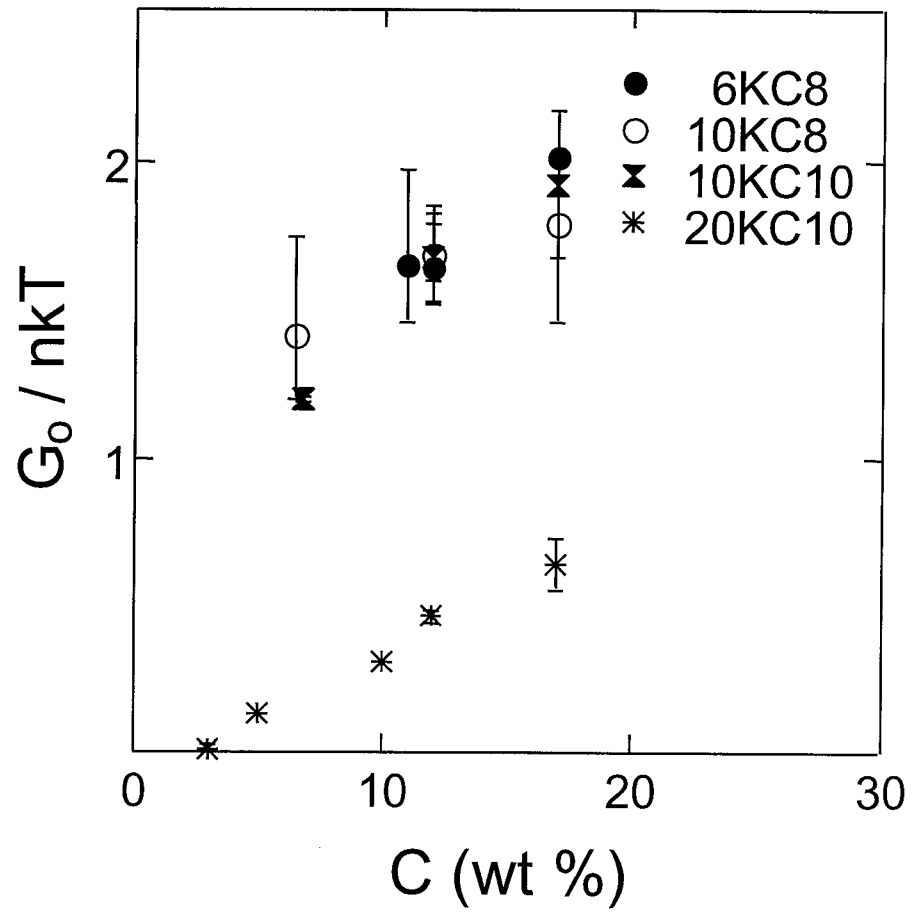


Figure 3.11. SANS pattern of dilute (0.5 wt %) monofunctional  $R_f$ -PEG solutions. Curves show the best fit with the Guinier relation,  $I = I(q \rightarrow 0) \exp(-q^2 R_G^2/3)$ . For 5KmPC10,  $I(q \rightarrow 0) \approx 4.1 \text{ cm}^{-1}$ , corresponding to  $R_G \approx 70 \text{ \AA}$ . For 5KmPC8,  $I(q \rightarrow 0) \approx 2.6 \text{ cm}^{-1}$ , and  $R_G \approx 63 \text{ \AA}$ .

(a)



(b)

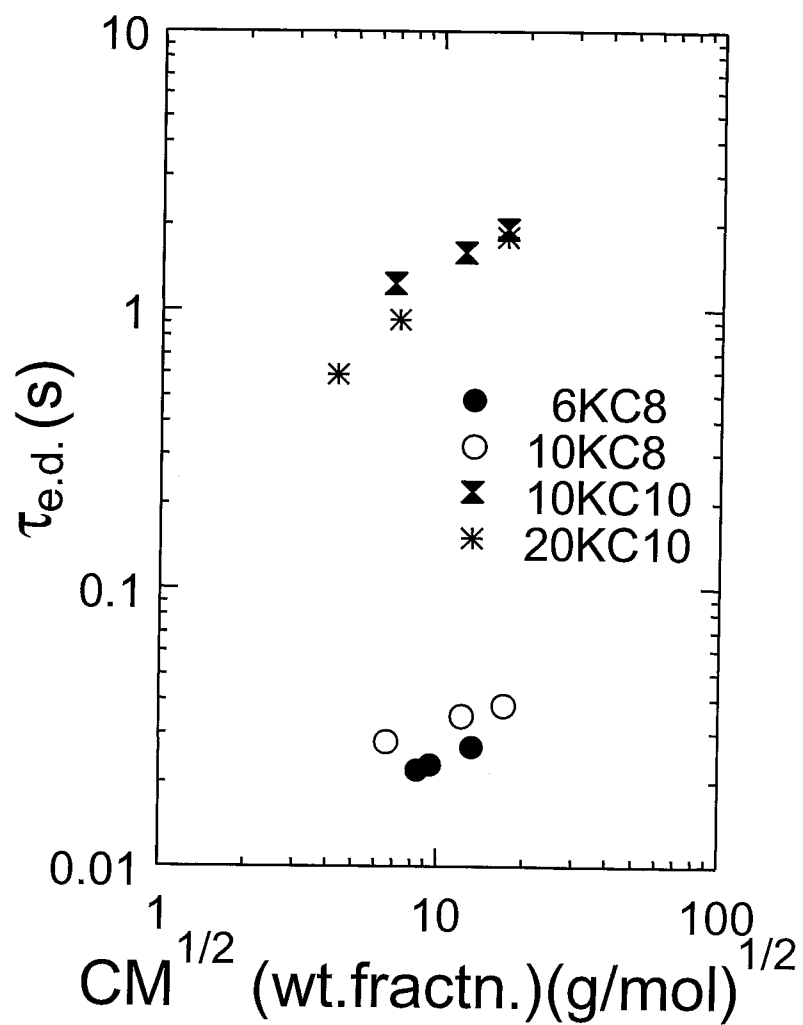


Figure 3.12 Concentration dependence of the (a) “effective fraction,”  $G_0/nkT$ , and (b) relaxation time of the end-group dissociation mode,  $\tau_{e.d.}$ , where  $C$  is concentration (weight fraction) and  $M$  is molecular weight.



## Chapter 4. *In situ* Transformation and Protein

### Release from Injectable Formulation

#### Abstract

A new class of materials is introduced, capable of *in situ* transition from an injectable liquid to a viscoelastic hydrogel using self-assembly of associating polymers; this material is useful for a variety of biomedical applications, including sustained protein release. Poly(ethylene glycol)s modified with fluorocarbon end groups are shown to form hydrogels by hydrophobic interaction of the end groups. The hydrogel state can be transformed into an injectable state by the addition of a toxicologically acceptable organic solvent, such as N-methyl pyrrolidone, and this solution can be restored to a gel state quickly after injection by diffusion of the organic solvent into the surrounding environment. *In vitro* characterization of sustained release of human growth hormone (hGH) using this injectable depot shows that hGH remains stable inside the hydrogel formed, and demonstrate more than 2 weeks of prolonged release of hGH complexed with Zn<sup>2+</sup> ions without protein aggregation or initial burst.

## Introduction

It is of special interest in medicine to develop materials that permit transformations from a sol state to a gel state using means that are sufficiently gentle that they can be carried out *in situ*. From the perspective of material administration to the body, *in situ* formation of a hydrogel from a liquid precursor placed at the implantation site permits conformal matching of the final hydrogel implant to the complex tissue shapes found in the body, as well as the delivery of a large implant through a small hole through the surface of the body via minimally invasive surgery.<sup>1</sup> From the perspective of delivery of biological therapeutics, such transformations, if they are sufficiently chemically and physically gentle, can be used to deliver protein or DNA drugs, as well as living cells for cell-based therapeutics. As such, an '*in situ*' transformation refers to hydrogel formation in the presence of biological structures, whether proteins, cells and tissues in the body or proteins, DNA and cells within the administered liquid.

Several methods have been previously explored to accomplish *in situ* transformation from sols to gels: Photopolymerization of macromeric gel precursors by UV or visible light irradiation<sup>2,3</sup> has been evaluated; while this method is very powerful, it requires complex instrumentation for provision of optical irradiation inside the body. Thermal phase transitions in block co-polymers have been exploited from the soluble state at one temperature to the gel state at the temperature of injection or mixing with the biological therapeutic;<sup>4,5</sup> while this method is very simple, the gels that result may be of weak mechanical strength,<sup>4</sup> the injection temperature can be high, which might be harmful to the tissue,<sup>5</sup> and the gels can demonstrate unacceptably fast degradation rates in open systems.<sup>4,5</sup> Precipitation of polymer solutions from organic solvents by mixing in water,

typically provided at the injection site, has also been explored;<sup>6</sup> while this method can make use of commercially available polymers, such as poly(D,L-lactic-*co*-glycolic acid) (PLGA), high concentrations of the organic solvent are required. Finally, chemical reactions have been exploited between two reactive precursors in solution, which then react with each other in multifunctional manner to form a cross-linked network;<sup>7</sup> while this method can lead to very fast transitions, side reactions with chemical features on biological molecules can occur,<sup>8</sup> and the number of highly selective reaction pairs is rather limited.<sup>9</sup>

An important application of *in situ* forming materials systems lies in the sustained release of therapeutic proteins, which generally have very short half-lives *in vivo* due to clearance and, to a lesser extent, degradation. Recombinant human growth hormone (rhGH), used to treat short stature caused by growth hormone deficiency, is one of the clinical targets for advanced sustained release systems. rhGH has been developed as an injectable sustained release dosage form by encapsulation within PLGA using a double emulsion method, obtaining microspheres that can be injected as a suspension.<sup>10</sup> Incorporation within PLGA matrices has also been obtained by adaptation of a cryogenic spraying process to encapsulate rhGH within PLGA, instead of the double emulsion method, to prevent the water-organic interface during the process. Zn<sup>2+</sup> are also incorporated within the microsphere to induce Zn<sup>2+</sup>-rhGH complexation, which reduces the irreversible aggregation of rhGH as it diffuses from the PLGA spheres.<sup>11</sup> Sustained release of the incorporated protein is obtained by diffusion of the protein through complex pore structure in the PLGA matrix and is accompanied by degradation of PLGA microspheres. In these approaches, it is possible to manipulate the pore structure by

controlling the rate of polymer precipitation and solvent exchange, obtaining smaller pores and slower release with more slow precipitation and exchange.<sup>12</sup> In spite of efficient encapsulation, this method met with limited success, related to the release of a large fraction of the rhGH in an initial burst.<sup>11,13</sup> In clinical studies, children treated with a sustained release form of Zn<sup>2+</sup>-rhGH in PLGA microspheres were observed to grow at a lower rate than those treated with daily injections, and moreover the incidence of anti-hGH antibody formation was higher.<sup>14</sup> As an alternative to the PLGA-based sustained release systems developed so far, hydrogel forms could be used, such as a poly(ethylene glycol) (PEG)-based hydrogel. It is well known that conjugation of PEG to proteins increases their stability and reduces their immunogenicity due to steric effects.<sup>8</sup> Also, PEG-rich gels would be expected to show a reduced inflammatory response relative to that which can occur near the PLGA-based release matrices.<sup>15,16</sup> As such, given that immunological interactions may be particularly important, PEG-based matrices represent promising candidates as carriers for protein release.<sup>17</sup> However, PEG-based hydrogels for protein release developed so far are not injectable as monolithic depots; they must be injected as particulate suspensions, and the maximum needle size permitting painless injection limits one to rather small particles, which may impact release characteristics. In this context, we wished to explore materials that could be administered as sols, with *in situ* transformation to a monolithic gel.

In this paper, we describe a new method that permits *in situ* transformation to form a hydrogel by applying the following concepts. 1) Physical association, specifically hydrophobic interaction of associating polymers, is used to form a desired hydrogel. 2) An injectable state is achieved by disruption of association among the hydrophobic end

groups by adding a small amount of a toxicologically acceptable organic solvent. Finally, 3) restoration to the gel state is achieved by removal of the added organic solvent by diffusion after delivery into a desired site. The example of incorporation and sustained release of hGH is presented.

## Experimental Section

**Synthesis of end-group modified PEGs ( $R_f$ -PEGs).** PEGs of nominal molecular weight 6k, and 10k g/mol were end-group modified with fluorocarbon ends ( $-C_mF_{2m+1}CH_2CH_2$ ,  $m = 8$ , or 10) using a diisocyanate linkage. Synthesis and characterization was performed as described elsewhere.<sup>18</sup> The samples prepared for this study are described in Table 1, where nKCm is a polymer with a PEG midblock that is n kg/mol and with m-carbon fluoroalkyl end groups,  $C_mF_{2m+1}CH_2CH_2$ . Monofunctional  $R_f$ -PEGs were also prepared similarly using monomethoxy PEG to be used for the *in situ* forming method. They are named as nK-M-Cm, where the middle -M- is used to distinguish from two-end modified  $R_f$ -PEGs.<sup>18</sup>

**Mechanical properties.** The restoration kinetics of the hydrogel was measured by preparing a thin layer (~1.5 mm) of  $R_f$ -PEG (50% by weight) solution in NMP in a vial and immersion of the vial into a water reservoir at 37 °C. The vial was kept for a specified time at this condition, removed from the reservoir, and the supernatant was decanted. The hydrogel that remained at the bottom of the vial was loaded into a rheometer (SR 5000, Rheometric Scientific, Piscataway, NJ) and characterized.

***In situ* transition experiments.**  $\beta$ -CD,  $\alpha$ -amylase from aspergillus oryzae (crude powder), and amyloglucosidase from aspergillus niger (solution in 1M glucose) were

purchased from Sigma (St. Louis, MO), and N-methyl pyrrolidone (NMP) was purchased from Fluka (Milwaukee, WI).

**Protein release experiments.** Release experiments used two types of gel formulation, namely an injectable and a pre-formed formulation. The injectable formulation was prepared by dissolving polymer in NMP, followed by adding protein particles to make a suspension with the composition of 10:10:1 of polymer:NMP:protein by weight. Release experiments were performed by injecting a given amount of the injectable formulation into a vial of phosphate buffered saline (PBS) at 37 °C using a 500  $\mu$ L syringe from Hamilton (Reno, NV) (typically,  $\sim$ 60  $\mu$ L of the injectable formulation was injected into a vial of 1.33 cm<sup>2</sup> area containing 4 ml of PBS buffer with 0.1 wt % sodium azide). The injectable formulation makes a gel quickly at the bottom of the vial. The pre-made gel was formed by making a thin film of polymer and protein at the bottom of a vial by dissolving the polymer in dichloromethane and evaporating the solvent, then adding PBS to the vial and incubating at 37 °C to get a concentrated gel state (40 wt % polymer gel). An excess amount of buffer was added to the vial to start release experiment. In all cases, the released protein amount was obtained by measuring the total protein concentration of the sampled buffer solution using a protein concentration assay kit from Bio-Rad (Hercules, CA), refreshing the buffer solution at an interval of 1 hr at the beginning, and up to 2 days at the later stages of the experiment. Aqueous size exclusion columns (SEC) and a photodiode array detector of the Waters HPLC system (Milford, MA) were used to analyze the released hGH from the hydrogel. 1 mL/min. of 10 mM phosphate buffer with 30 mM of NaCl was used as a mobile phase, and absorption at either 220 or 280 nm was used to detect the protein.

## Results and Discussion

**Hydrogel with controlled, surface erosion characteristics.**<sup>18</sup> We demonstrate that hydrogels with controlled, surface erosion characteristics can be obtained using PEGs modified at both ends with fluorocarbon end groups ( $R_f$ -PEGs).  $R_f$ -PEGs can form networks in aqueous environments by hydrophobic interactions between the end groups. Our studies demonstrate that the phase behavior of  $R_f$ -PEGs in solution is governed by the relative length of the PEG midblock to the fluoroalkyl end groups: if the PEG's relative length is too short, the material does not exist as a homogeneous phase in water, but rather exists only as a slightly swollen precipitate. On the other hand, if the relative length is too large, the material exists as a homogeneous solution over the whole range of concentration. Polymers that lie in between in terms of the relative length of PEG to  $R_f$  show phase separation into a gel coexisting with a sol. This is demonstrated in the present system in Table 4.1, where  $nKC_m$  is a polymer with a PEG midblock that is  $n$  kg/mol and with  $m$ -carbon fluoroalkyl end groups (i.e.,  $C_mF_{2m+1}CH_2CH_2$ ).

The erosion characteristics of these gel phases were characterized in open systems, i.e., placed suddenly into non-equilibrium conditions in a large volume of polymer-free water, were determined using surface plasmon resonance (SPR). These studies demonstrated that heterogeneous erosion occurs from the surface of the gel (Chapter 2), and that the erosion rate is determined primarily by the length of hydrophobe end group. Further, these experiments showed that the dissolution rates for these gels are sufficiently slow to be used as a delivery carrier in open systems (Table 4.1), e.g., as injectable drug

release depots. Moreover, the experiments demonstrated that the equilibrium gel phase concentration ( $C_{gel,eq.}$ ), the inverse of swelling ratio of the gel, and the modulus of the gel phase ( $G_0$ ) are dominated by the length of the PEG midblock, whereas the viscoelastic relaxation time ( $\tau_r$ ) of these gels is dominated by the hydrophobe length. Accordingly, the zero-shear viscosity ( $\eta_0$ ), which is the product of the plateau modulus and relaxation time, varies over an order of magnitude with modest changes in molecular structure (Table 4.1). As such, it is apparent that the erosion rate and mechanical properties of these hydrogels can be controlled by modulating molecular structure of the Rf-PEGs.

**Table 4.1. Rf-PEGs with Controlled, Surface Erosion Characteristics  
(Properties at 25 °C)**

Sample	10KC10	10KC8	6KC8
PEG-block	10 kg/mol	10 kg/mol	6 kg/mol
End Group <sup>a</sup>	-C <sub>10</sub> F <sub>21</sub>	-C <sub>8</sub> F <sub>17</sub>	-C <sub>8</sub> F <sub>17</sub>
$C_{gel,eq.}$ <sup>b</sup> in PBS (wt %)	8.1±0.7	7.8±0.2	12.5±0.3
$C_{sol,eq.}$ <sup>c</sup> in PBS (wt %)	0.011±0.003	0.055±0.002	0.017±0.001
Relaxation time ( $\tau_r$ )(s)	1.2	0.029	0.023
Plateau modulus ( $G_0$ )(kPa)	14.4	18.5	56.1
Viscosity ( $\eta_0$ )(kPa s)	18	0.53	1.5
Dissolution rate (mg/cm <sup>2</sup> /nr)	$\ll 10^{-5}$	$1.67 \times 10^{-3}$	$3.33 \times 10^{-4}$

<sup>a</sup> Full end group is -IPDU-(CH<sub>2</sub>)<sub>2</sub>-C<sub>n</sub>F<sub>2n+1</sub>, where IPUD is



<sup>b</sup> Equilibrium gel phase concentration

<sup>c</sup> Equilibrium sol phase concentration

***In situ* transition using cyclodextrin complexation.** To apply the present hydrogel system as an *in situ* forming system, it is necessary to change the hydrogel into an



injectable state by disrupting the hydrophobic interaction among the end groups. Disruption of associative interactions can be achieved by the inclusion complexation of cyclodextrins (CDs) with fluoroalkyl end-groups. Complex formation between  $\alpha$ ,  $\beta$ , and  $\gamma$ -CD and perfluorocarbon surfactants shows that  $\beta$ -CD has the largest association constants among them for a given hydrophilic head. Based on this association, the addition of  $\beta$ -CD to solutions of PEG one end-group modified with perfluorinated groups reduces their viscosity.<sup>19</sup> If the complexation of  $\beta$ -CD to the fluoroalkyl end-groups of two-end modified PEG is sufficient to hide the hydrophobicity of the end groups, the gel phase will not be formed. Mixing a saturated aqueous solution of  $\beta$ -CD and the gel phase of 10KC10 caused the disappearance of the gel-phase. Also, adding one-fold excess  $\beta$ -CD in molar ratio of end groups to 10KC10 and applying water followed by shaking resulted in low viscosity solutions, so  $\beta$ -CD can apparently effectively prevent the strong association among end groups. The solution was not clear, especially for the higher concentration of solutes, and the apparent viscosity was much higher than the same concentration of unmodified pure PEG solution, so it seems that there are weak or local associations among the CD-complexed polymers. Nevertheless, the addition of cyclodextrin is enough to make the gel state injectable.

To restore the gel structure after injecting into delivery site, CD must be removed from the fluoroalkyl group. One way to achieve CD removal is adding the enzymes that degrade CD. There are several sources of enzymes that can degrade cyclodextrin. Most of them are from microbial sources, but enzymes from saliva and pancreas can effectively degrade  $\gamma$ -CD and to a lesser extent  $\beta$ -CD.<sup>20</sup>  $\alpha$ -amylase from *aspergillus oryzae* can degrade  $\beta$ -CD,<sup>21</sup> although it is a relatively poor cyclodextrinase. Two enzymes were

tested: For  $\alpha$ -amylase from *aspergillus oryzae*, 0.008g of the enzyme was added to 0.55g of the homogeneous complex solution of 10KC8 and  $\beta$ -CD (7.73 wt % for 10KC8, and 3.35 wt % for  $\beta$ -CD). After shaking to mix, the sample was kept at 37 °C. It started to become viscous upon mixing, and after 20 min., it showed a gel-like structure. For amyloglucosidase from *aspergillus niger*, 0.065g of the enzyme solution was added to 0.513 g of the precursor solution (7.59 wt % for 10KC8, and 3.27 wt % for  $\beta$ -CD). After 30 min., it started to be viscous, and after 70 min., it became insoluble.

Another way to achieve CD removal is to add other molecules that bind CD strongly so that CD is effectively transferred from the fluoroalkyl end-groups to the molecules added. One-end modified  $R_f$ -PEG solution is injectable below the critical micelle-packing transition concentration (Chapter 2). Furthermore, one-end modified  $R_f$ -PEG having small molecular weight of PEG will have a higher affinity to CD than that with two-end modified  $R_f$ -PEG having large molecular weight of PEG.<sup>22</sup> With 10KC10 as a gel forming agent, 5K-M-C10 and 2K-M-C10 (where M denotes that only one-end is modified with fluoroalkyl group) were explored as CD-transfer inducing agents. First, 5 wt % solution of 10KC10, coupled with CDs and 10.2 wt % solution of 5K-M-C10 solution, were mixed in equal amounts, and the mixture showed a marked enhancement of viscosity, but did not form a gel state (where the gel state was determined by whether there was a noticeable flow when the vial containing it is inverted). Second, using 2K-M-C10 the mixing ratios were varied from 1:1 to 1:3 (10KC10:2K-M-C10, in molar concentration), keeping the total concentrations of them the same, 6.3 wt %. Among these mixtures, the 1:2 ratio gave the most gel-like state, which was maintained up to 37 °C. A 1:2 molar ratio mixture of 10KC10-CD complex solution (0.073 g/ml,

polymer/water) and 18.2 wt % of 2K-M-C10 solution resulted in reversion to gel structure. For 10KC8, a 1:1 molar ratio was enough to induce the gel phase since CD will transfer more easily from C8 end group to the C10 end group.

Even though two methods of removing CD from fluoroalkyl end-groups tested can restore the gel structure eventually, they have limitations for the practical application; for the method of using cyclodextrinase, the enzymes that function effectively for  $\beta$ -CD are all from microbial source, so it is likely that they will induce the immune-response at the second trial for the same person or animal. For the method of adding one-end modified R<sub>f</sub>-PEG, gelation occurs very slowly (over several hr), probably from the mass-transfer limitation. Thus, unless employing a micro-mixer that can mix efficiently two laminar flows in micro-scale, this method will not be acceptable. Therefore, we pursue another effective way to induce sol-gel transition for the R<sub>f</sub>-PEG hydrogel in the following section.

***In situ* transition using organic solvents.** Alternatively, disruption of associative interactions can be achieved by altering the characteristics of the solvent. For example, this can be accomplished by dissolving the gel-forming polymer in a water mixture with a bio-tolerable and water-miscible organic solvent, such as N-methyl pyrrolidone (NMP), or in the organic solvent neat. A dramatic reduction (exponential decrease with NMP concentration) in the viscosity of the system was observed by the addition of various amounts of NMP to the gel phase of R<sub>f</sub>-PEGs (Figure 4.1), so it can effectively weaken the association among end-groups. Furthermore, contact of this flowable solution (in the non-associated state) of the polymer in the NMP or NMP-water mixture with an aqueous environment permits the diffusion of the NMP from the polymer solution, and the

corresponding replacement by water thus converts the material into the associative state. When a 10KC8 solution in NMP (50 wt %) was placed within a reservoir of water (the thickness of the initial sample was ca. 1.5 mm.), the steady viscosity of the sample increased dramatically by more than two orders of magnitude in 10 min. (Figure 4.2). As such, effective restoration of the gel structure is achievable by injecting into aqueous environment.

**The sustained release of hGH from the injection formulation.** The issues of the sustained release systems for proteins are 1) the stability of the protein inside and at the interface of the carrier, i.e., whether they are released as a desired state or in a modified, denatured or aggregated state, 2) the sustained release of the protein, i.e., to what extent the release of the protein is delayed by the carrier material, and 3) the controlled release of the protein, i.e., to what extent the characteristics of the carrier can controllably modulate the release rate and eliminate initial burst. An initial release experiment conducted *in vitro* with bovine serum albumin (BSA) revealed that 6KC8 shows the slower release rate than 10KC8 or 10KC10, due to the smaller midblock length of the polymer that leads to a smaller effective mesh size of the corresponding hydrogel (Figure 4.3). Based on this initial result, to achieve a release profile of clinically useful duration, the release of hGH was characterized from a 6KC8 hydrogel, using the scheme described in Figure 4.4. Two types of gel formulation were used, one being an injectable formulation, obtained by suspension of hGH particles in an R<sub>f</sub>-PEG solution in NMP, and the other being a pre-formed gel, containing hGH but no NMP.

Results of *in vitro* release experiments demonstrated several useful characteristics. First, hGH inside the hydrogel did not undergo irreversible aggregation but remained

stable, as characterized by analyzing the hGH released from the pre-made gel state of 6KC8 using HPLC at different time points. For all samples, the first peak appearing (the highest molecular weight) was detected at the same elution time that corresponds to the monomeric form of hGH. Second, hGH release was compared for the two different gel preparation methods; one, i.e., the pre-made gel with no NMP and the injectable formulation that includes the organic solvent, NMP. In both cases, the release was achieved mainly by diffusion (linear plots for the released amount of protein vs.  $t^{1/2}$ , Figure 4.5 (a)) with no initial burst. Compared to the release from the pre-made gel state, hGH release from the injectable formulation showed a much slower release rate. HPLC analysis revealed a broad range of molecular weight for the hGH released from the injection formulation, in contrast to the single peak from the pre-made gels (Figure 4.5 (b)). As such, aggregation of hGH appears to have occurred in the injectable formulation, probably during the initial stage of gelation when hGH was exposed to the water-NMP mixture before NMP was diffused out from the hydrogel. This aggregation would lead to the slower release rate than that from the pre-made gels, because sustained release is accomplished by the diffusion of hGH through the hydrogel.

Since hGH remains stable once inside the hydrogel, if hGH can tolerate the environment of NMP-water mixture during the initial gelation process for the injection formulation, then the formation of the irreversible aggregation would be prevented. This undesired irreversible aggregation of hGH, observed by us in preparation of the injectable formulation, was also reported in reference to encapsulation of hGH within PLGA,<sup>13</sup> but this aggregation was successfully avoided by adding  $Zn^{2+}$  ions to form the more stable  $Zn^{2+}$ -hGH complex.<sup>11</sup> Employing the same concept, we pretreated hGH with  $Zn^{2+}$  ions

before it was added to the polymer-NMP solution. As shown in Figure 4.6 (b), hGH released after pretreatment with  $\text{Zn}^{2+}$  was released exclusively in the monomeric form, and no aggregation was found. Thus, the  $\text{Zn}^{2+}$  complexation could effectively prevent the irreversible aggregation of hGH for the injectable formulation. Sustained release of hGH was obtained for durations as long as two weeks, and still with no initial burst (Figure 4.6 (a)).

The release profiles of three proteins (hGH, BSA, and  $\gamma$ -globulin) from the injectable formulation (Figure 4.7) showed that for all cases the sustained release is achieved at least in part by diffusion (the larger protein was released more slowly) with little initial burst, which implies the effective transition into a gel state by the injection into a buffered saline solution. Similarly, when this material in the NMP or NMP-water mixture is injected into a tissue site, then the NMP is allowed to exchange with the aqueous component of the body fluids, permitting restoration of the gel state. Macromolecular drugs, including proteins, RNA, and DNA, can be incorporated into the polymer formulations and delivered into a desired site. Due to its low toxicity, NMP is a preferred solvent that can be used *in vivo*, but other solvents that are used in pharmaceutical formulations and can disrupt the association among hydrophobic end groups, including ethyl acetate, may also be useful. Considering the surface erosion of the gel matrix, the release rate of embedded protein inside the hydrogel is expected to be determined by the erosion rate of the gel for proteins that are larger than the effective mesh size of the gel. However, the diffusion-controlled release profiles for all cases imply that, in the range of the tested proteins and polymers, the proteins are not sufficiently large (or alternatively the mesh size of the gel is not sufficiently small) to be entrapped inside the gel matrix. If

such behavior were desired, PEGs of MW less than 6 kg/mol would be applicable, or perhaps branched PEGs or gels formed by blends of PEG-R<sub>f</sub>s. It is also likely that protein solubility plays a role in controlling protein release rate. The hGH was added to the hydrogel materials as a precipitate, and the PEG matrix may act to slow the rate of dissolution, also resulting in sustained release.<sup>9,23</sup> Although not the topic of this paper, it is imaginable that small hydrophobic drugs could be incorporated and released in a sustained manner by association with the hydrophobic end groups of PEG-R<sub>f</sub>, such that partitioning into the hydrophobic core regions that serve as physicochemical crosslinks within the hydrogel.

Although the topic of sustained release of proteins has been investigated for a number of years, the problem has not yet been addressed in a clinically acceptable manner. One can observe this in the high burst and relatively lower clinical efficacy of currently approved sustained release hGH formulations.<sup>14</sup> Given the well established and favorable toxicology profile of both PEG and NMP,<sup>6,8</sup> one could readily imagine administration of a sustained release formulation as we describe in this paper, either by injection of pre-formed gel particles or by injection of the formulation in the non-associated state in the presence of small amounts of NMP.

## Conclusions

*In situ* transformation of R<sub>f</sub>-PEG hydrogel can be achieved by altering the characteristics of the solvent. R<sub>f</sub>-PEG is transformed into an injectable state by the addition of N-methyl pyrrolidone, and this solution is restored to a gel state quickly after injection by diffusion of the organic solvent into the surrounding environment. *In vitro*

characterization of sustained release of human growth hormone (hGH) using this injectable depot shows that hGH remains stable inside the hydrogel formed, and demonstrate more than 2 weeks of prolonged release of hGH complexed with  $Zn^{2+}$  ions, dominated by the diffusion of hGH through the hydrogel, without protein aggregation or initial burst.

## **Acknowledgements**

We acknowledge National Hormone & Pituitary Program of National Institute of Diabetes and Digestive and Kidney Diseases (NIDDK) and A.F. Parlow for the supply of human growth hormone.



**References**

- [1] Hubbell, J.A. *MRS Bulletin* **1996**, Nov. 33
- [2] Sawhney, A.S.; Pathak, C.P.; Van, R.J.; Dunn, R.C.; Hubbell, J.A. *J.Biomed. Mater. Res.* **1994**, 28, 831
- [3] Hill-West, J.L.; Chowdhury, S.M.; Slepian, M.J.; Hubbell, J.A. *Proc. Natl. Acad. Sci. USA* **1994**, 91, 5967
- [4] Malmstan, M.; Lindman, B. *Macromolecules* **1992**, 25, 540.
- [5] Jeong, B.; Bae, Y.H.; Lee, D.S.; Kim, S.W. *Nature* **1997**, 338, 860
- [6] Dunn, R.L.; English, J.P.; Cowsar, D.R.; Vanderbilt, D.D. *US Patent 5,278,202*, **1994**
- [7] Rosenblatt, J.; Rhee, W.; Berg, R. *Fifth World Biomaterials Congress (Toronto, Canada)* **1996**, 344
- [8] Harris, J.M. "Polyethylene Glycol Chemistry. Biotechnical and Biomedical Application," Plenum, New York, **1992**
- [9] Elbert, D.L.; Pratt, A.B.; Lutolf, M.P.; Halstenberg, S.; Hubbell, J.A. *J. Controlled Rel.* **2001**, 76, 11
- [10] Cleland, J.L.; Jones, A.J. S. *Pharm. Res.* **1996**, 13, 1464
- [11] Johnson, O.L.; Cleland, J.L.; Lee, H.J.; Charnis, M.; Duenas, E.; Jaworowicz, W.; Shepard, D.; Shahzamani, A.; Jones, A.J.S.; Putney, S.D. *Nature Medicine* **1996**, 2, 795
- [12] Brodbeck, K.J.; Pushpala, S.; McHugh, A.J. *Pharm. Res.* **1999**, 16, 1825
- [13] Kim, H.K.; Park, T.G. *Biotech. Bioeng.* **1999**, 65, 659

- [14] Reiter, E.O.; Attie, K.M.; Moshang, T.; Silverman, B.L.; Kemp, S.F.; Neuwirth, R.B.; Ford, K.M.; Saenger, P. *J. Clin. Endo. Metabolism*. In press.
- [15] Visscher, G.E.; Pearson, J.E.; Fong, J.W.; Argentieri, G.J.; Robison, R.L.; Maulding, H.V. *J. Biomed. Mater. Res.* **1988**, *22*, 733
- [16] Ignatius, A.A.; Claes, L.E. *Biomaterials* **1996**, *17*, 831
- [17] Zhao, X.; Harris, J.M. *J. Pharmaceut. Sci.* **1998**, *87*, 1450
- [18] Tae, G.; Kornfield, J.A.; Hubbell, J.A.; Hogen-Esch, T.E.; Johannsmann, D. *Macromolecules* **2001**, *34*, 6409
- [19] Zhang, H.; Hogen-Esch, T.E.; Boschet, F.; Margaillan, A. *Langmuir* **1998**, *14*, 4972
- [20] Saha, B.C.; Zeikus, J.G. *starch/stärke* **1992**, *44*, 312
- [21] Jordal, I.; Kandra, L.; Harangi, J.; Nanasi, P.; Szejtli, J. *Starch/Starke* **1984**, *36*, 104
- [22] Amiel, C.; Seville, B. *J. Inclusion Phen. & Mol. Recog.* **1996**, *25*, 61
- [23] Stevenson, C.L.; Hageman, M. *J. Pharm. Res.* **1995**, *12*, 1671

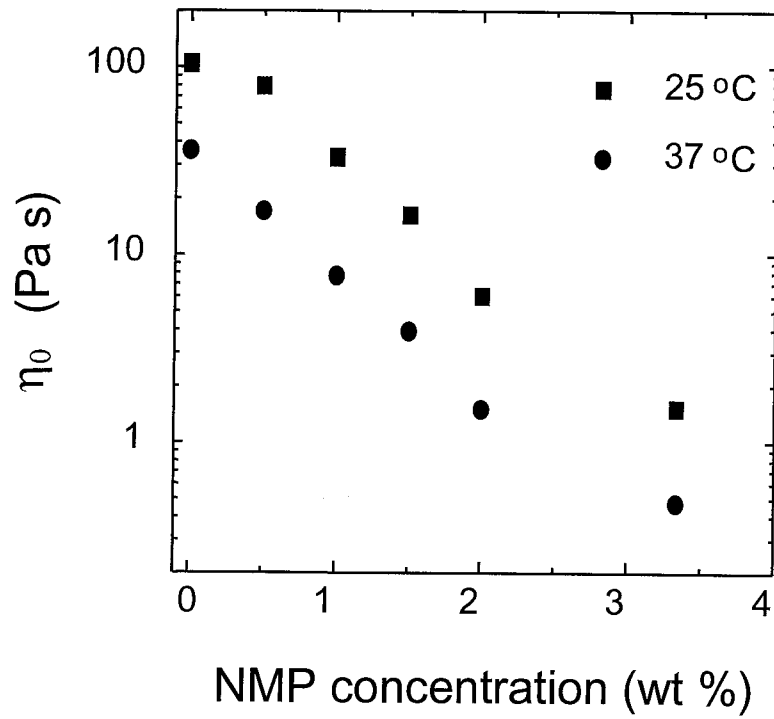


Figure 4.1 Decrease in viscosity of 10KC8 in aqueous solution, induced by addition of NMP to disrupt association.

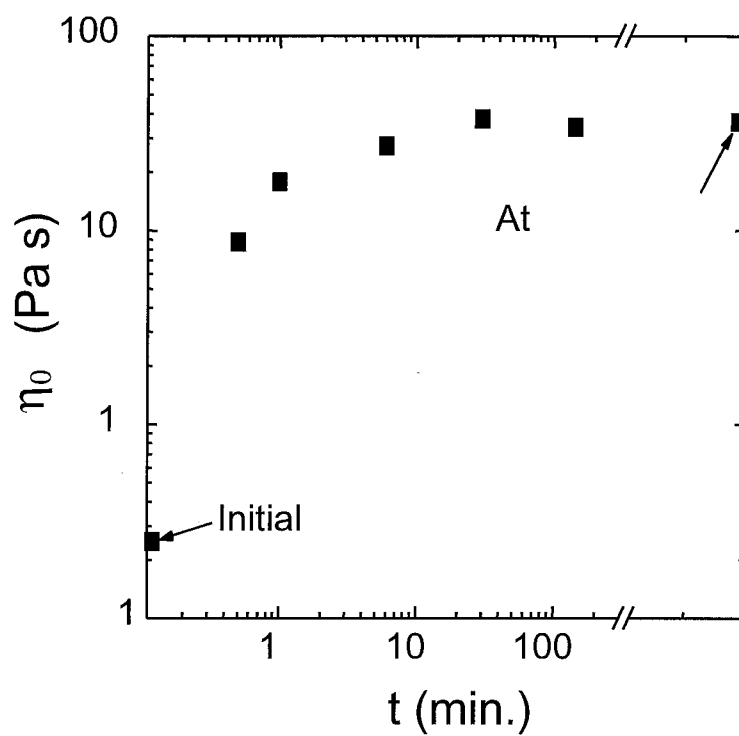


Figure 4.2 Restoration of injectable depot into hydrogel state of 10KC8 solution by being exposed to a water reservoir. Injectable formulation was 1:1 of NMP:polymer by weight, and initial thickness was c.a. 0.15 cm.

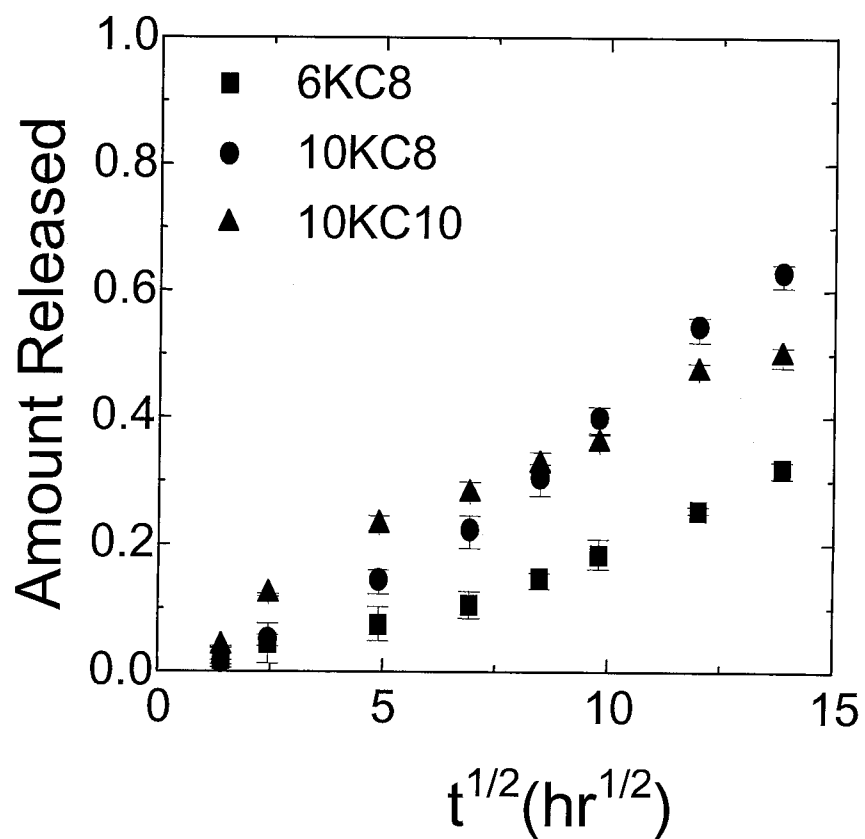


Figure 4.3 BSA release from the pre-made gel state (composition of 10:15:1 of polymer:buffer solution:BSA by weight) for various R<sub>f</sub>-PEGs at 37 °C. The gel thickness was c.a. 0.2 cm for 6KC8 and c.a. 0.3 cm for 10KC8 and 10KC10.

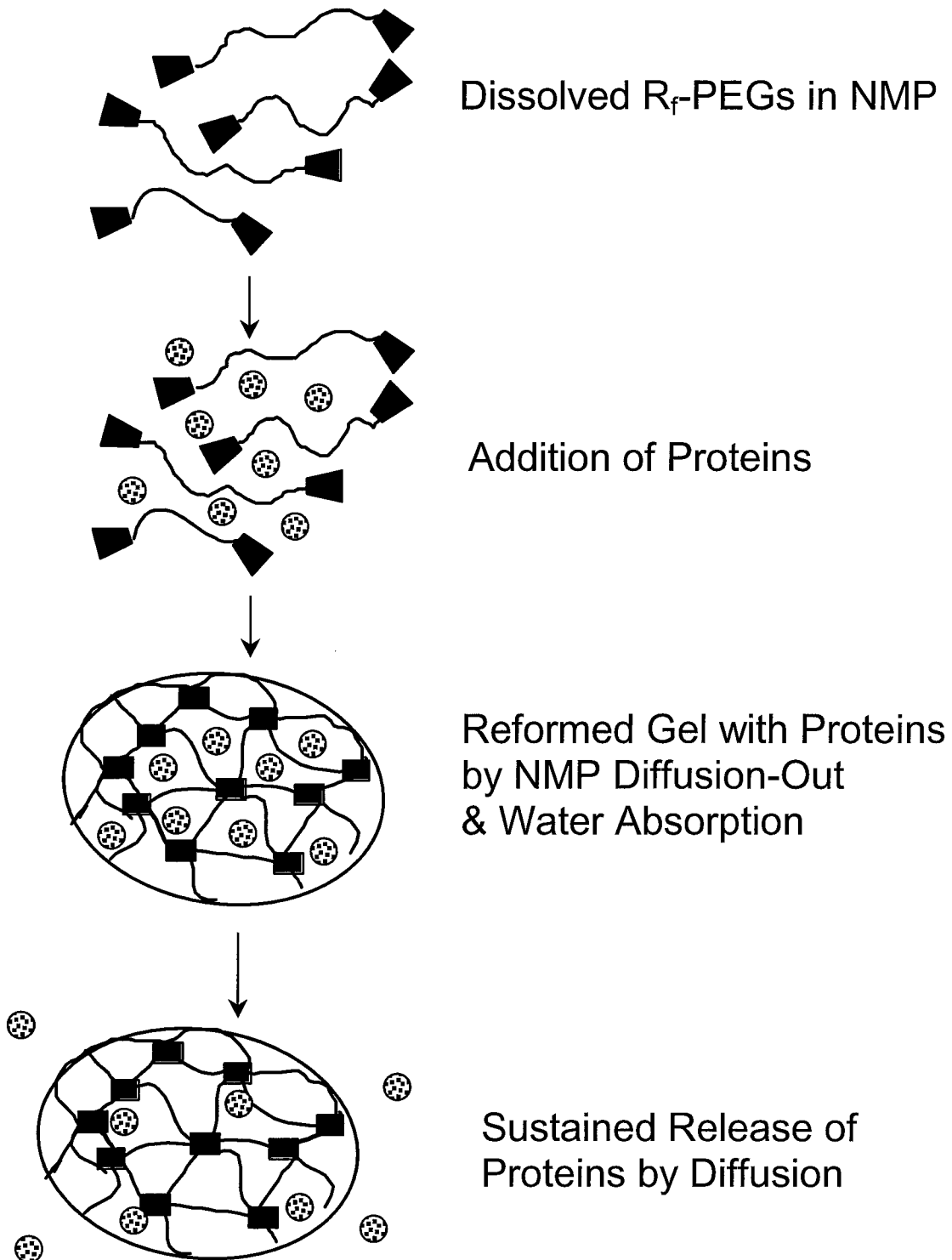


Figure 4.4 Schematic depiction of application of the present *in situ* forming hydrogel system as an injectable depot for sustained release of proteins.

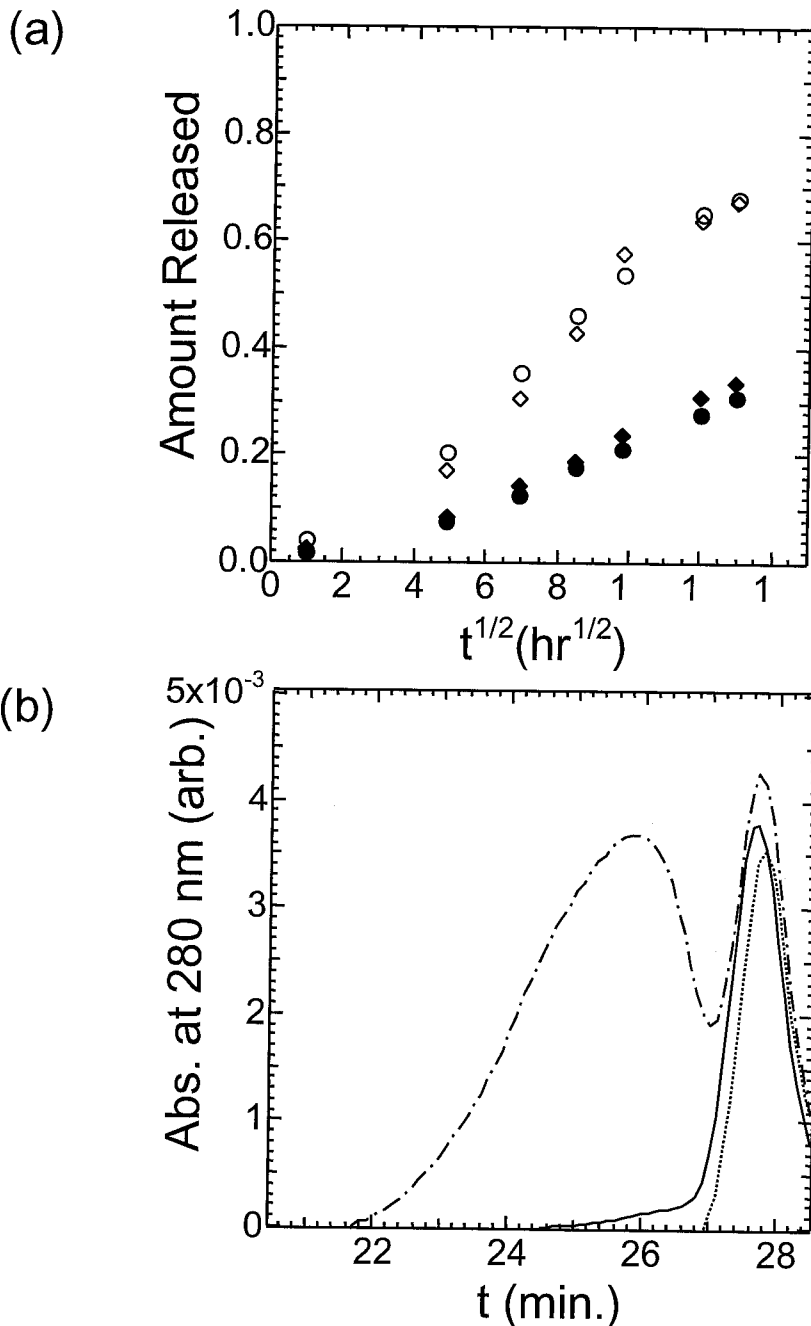


Figure 4.5 hGH release from 6KC8 hydrogel without Zn-pretreatment of hGH. (a) Release profiles at 37 °C from the pre-made gel state (filled symbols, composition of 10:15:1 of 6KC8:buffer solution:hGH by weight) and the injectable formulation (emptied symbols, composition of 10:10:1 of 6KC8:NMP:hGH by weight). In both cases, the gel thicknesses were c.a. 0.2 cm after initial equilibration. (b) HPLC analysis of released hGH using aqueous size exclusion columns (SEC) (---: injectable formulation, -.-.-: pre-made gel state, —: hGH standard). 1 ml/min. of 10 mM phosphate buffer with 30 mM of NaCl was used as a mobile phase, and absorption at 280 nm was used to detect the protein.

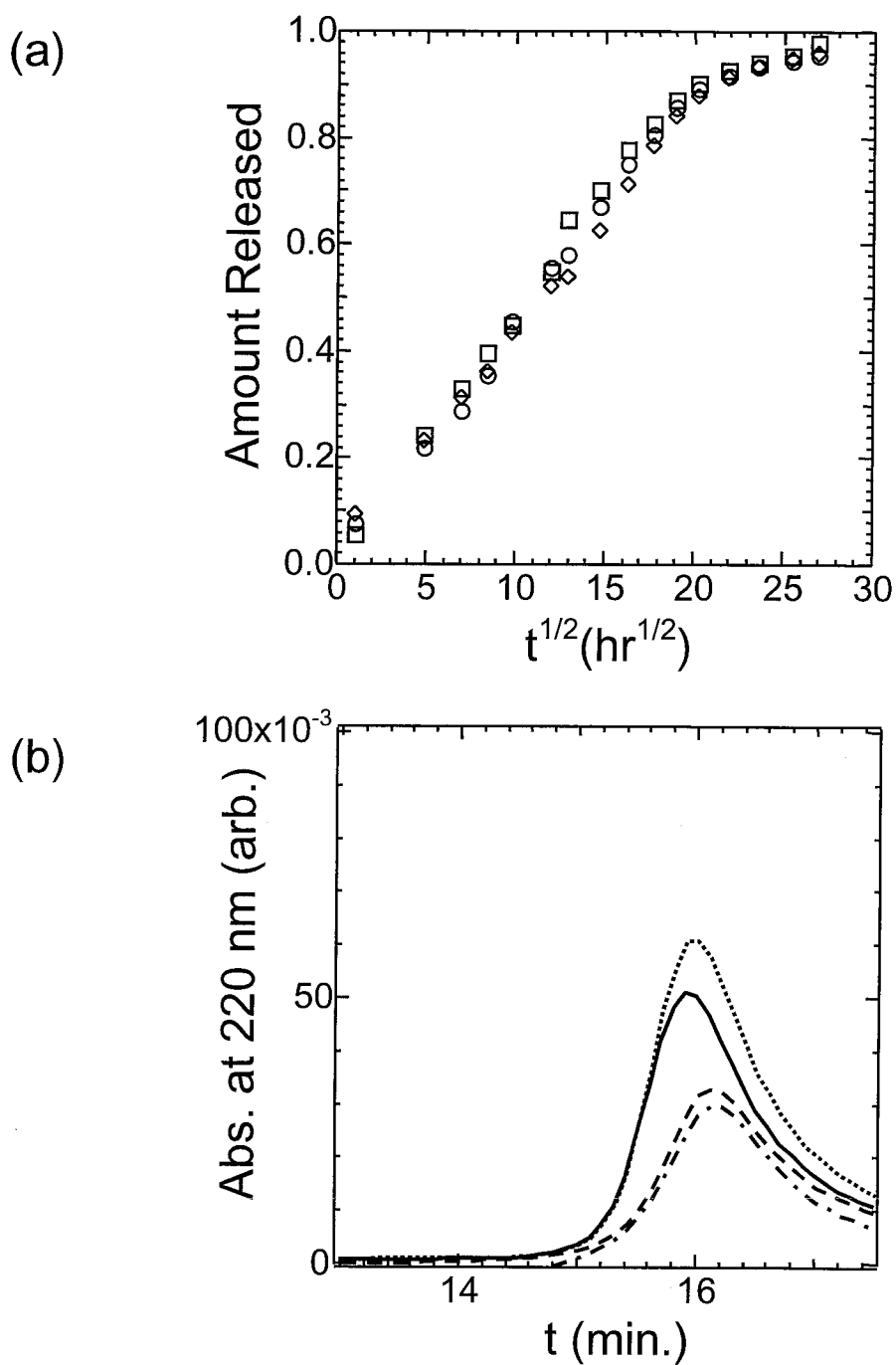


Figure 4.6 hGH release from 6KC8 hydrogel with Zn-complexed hGH. (a) Release profiles at 37 °C from the injectable formulation (composition of 10:10:1 of 6KC8:NMP:hGH by weight). Each symbol represents the individual run, and the gel thicknesses were c.a. 0.2 cm after initial equilibration. (b) HPLC analysis of released hGH using aqueous size exclusion columns (SEC) (..... : day 2, ----- : day 6, - · - · - : day 9, \_\_\_\_ : hGH standard). 1 ml/min. of 10 mM phosphate buffer with 30 mM of NaCl was used as a mobile phase, and absorption at 220 nm was used to detect the protein.



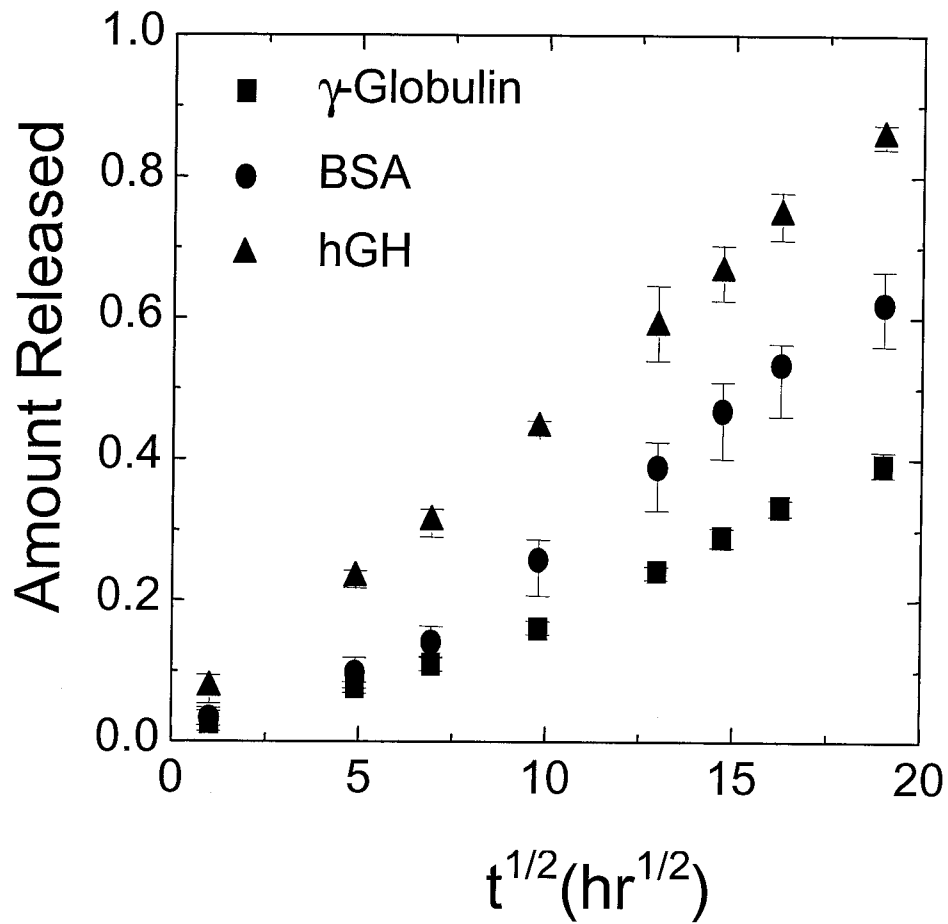


Figure 4.7 Protein release from the injectable formulation (composition of 10:10:1 of 6KC8:NMP:protein by weight) of 6KC8 hydrogel. The gel thicknesses were c.a. 0.2 cm after initial equilibration.

## Chapter 5. Surface Modification of Poly(Tetrafluoroethylene) (PTFE) Using R<sub>F</sub>-PEGs

### Abstract

A simple way to modify the surface of poly(tetrafluoroethylene) (PTFE) using physisorption of PEG modified with fluorocarbon ends (R<sub>F</sub>-PEGs) is presented. The PTFE substrate is immersed in a solution of R<sub>F</sub>-PEG in ethanol (1 wt %), and then immersed into water, which induces the stable adsorption of R<sub>F</sub>-PEG onto PTFE. This physisorption makes the surface of the PTFE hydrophilic, as observed by the capillary rise method. The stability of the adsorbed PEG layer under flow of water depends on the phase behavior and erosion rate of the bulk gel state of the R<sub>F</sub>-PEG. When PTFE is functionalized using an R<sub>F</sub>-PEG that exhibits sol-gel equilibrium, the hydrophilicity of the surface decays on a time scale of 1-10 hr, which correlates with the known erosion kinetics of the specific R<sub>F</sub>-PEG, insensitive to the shear stress applied by flow. On the other hand, when the PTFE surface is modified by an R<sub>F</sub>-PEG (6 kD PEG with C10 fluorocarbon ends) that is insoluble in water, it exhibits stable surface properties over the time scale of the experiment (2 wk). Therefore, this method can provide a simple, economic way to modify the surface properties of PTFE-based devices.

## Introduction

Poly(tetrafluoroethylene) (PTFE) is extensively used in medical devices and accounts for approximately one-half of the synthetic grafts used in vascular surgery.<sup>1</sup> One of those applications is a vascular graft that uses an expanded PTFE (ePTFE) form. Despite their successful use for replacement of large diameter blood vessels, ePTFE vascular grafts with internal diameter of less than 6 mm uniformly fail as a result of blood clot formation (thrombosis).<sup>2</sup> Also, the poor wettability of ePTFE graft is a problem in utilization of currently used sealants to reduce blood leakage.<sup>3</sup> The blood response to the hydrophobic ePTFE graft is believed to be initiated by protein adsorption via hydrophobic interaction.<sup>4</sup>

Several approaches have been attempted to minimize protein adsorption by the surface modification of ePTFE; most commonly, chemical derivatization of the PTFE surface was done either by wet etching,<sup>5</sup> plasma<sup>6</sup> or ion beam treatments,<sup>7</sup> or photoexcited electron transfer reaction.<sup>1</sup> Then, graft copolymerization was added for biological functionalization.<sup>8</sup> Alternatively, construction of a protective thin polymer membrane<sup>9</sup> or PEG-layer<sup>10</sup> were suggested. All of these methods have shown limited success, requiring further improvement to be practical, mainly due to the complicated processes/equipment used to achieve the surface modification. Therefore, it is desired to develop a simple way to modify PTFE surfaces.

The ability of PEG to reduce protein adsorption by virtue of its strong hydrophilicity and large excluded volume is well known and a subject of much interest in the biomedical community.<sup>11</sup> So, the surface modification of biomaterials with PEG is an effective way to eliminate protein adsorption and, therefore, prevent thrombosis on

materials in contact with blood.<sup>12</sup> However, the difficulty (or complexity) of applying this method to PTFE modification lies in the chemical inertness of PTFE.

PEGs modified with hydrophobes at both ends have been investigated widely as model associative polymers.<sup>13,14</sup> The majority of alkyl-ended PEGs form micelle-like clusters in aqueous solution and as the concentration of polymer increases, the size of the connected clusters of associative polymers grows continuously and finally forms an infinite gel-like cluster. However, phase separation is found for some cases of PEG modified with fluorocarbons ( $R_f$ -PEGs) or alky groups (R-PEGs) when the relative length of hydrophobic end group is sufficiently large relative to the PEG midblock length; specifically, PEG of 6 kD modified with  $C_8F_{17}CH_2CH_2$  and PEG of 10 kD modified with  $C_nF_{2n+1}CH_2CH_2$ ,  $n = 8$  or  $10$  using isophorone diurethane linkage show sol-gel coexistence, where the sol phase is very dilute ( $< 0.1$  wt %), and the gel phase is a hydrogel composed of connected micelles. Furthermore, 6 kD PEG modified with  $C_{10}F_{21}CH_2CH_2$  does not dissolve to any detectable level in water, but exist as a swollen precipitate.<sup>15</sup>


The gels of sol-gel coexisting species exhibit surface erosion,<sup>15</sup> and the erosion rate is mainly determined by the end group length in an open system ( $\sim 10^{-4}$  mg/cm<sup>2</sup>/hr for PEG of 6 or 10 kD modified with  $C_8F_{17}CH_2CH_2$ , and  $\ll 10^{-5}$  mg/cm<sup>2</sup>/hr for PEG of 10 kD modified with  $C_{10}F_{21}CH_2CH_2$ ). The insoluble  $R_f$ -PEG (PEG of 6 kD modified with  $C_{10}F_{21}CH_2CH_2$ ) showed no sign of erosion. Since these  $R_f$ -PEGs show such slow erosion rates, the purpose of this chapter is 1) to apply these  $R_f$ -PEGs as surface-modifying coating materials for PTFE, and 2) to characterize the stability of these physisorbed layers of  $R_f$ -PEG on PTFE under flow.

## Experimental Section

**Materials ( $R_f$ -PEGs).** Poly(ethylene glycol) (PEG) (with alcohol functionality at both ends) of nominal molecular weight 6000 g/mol (6 kD) and 10 kD were modified at both ends with fluorocarbon ends (-IPDU-(CH<sub>2</sub>)<sub>2</sub>-C<sub>n</sub>F<sub>2n+1</sub>, n = 8, or 10) using isophorone diurethane (IPDU) linkage. Syntheses and characterizations were done as described previously.<sup>15</sup> The samples used for this study are described in Table 5.1, where the abbreviation nKCm denotes a polymer with a PEG midblock MW of n kg/mol and with m-carbon fluoroalkyl end groups.

**Table 5.1.  $R_f$ -PEGs**

Sample	PEG-block	End Group <sup>a</sup>
10KC8	10 kg/mol	-C <sub>8</sub> F <sub>17</sub>
10KC10		-C <sub>10</sub> F <sub>21</sub>
6KC8	6 kg/mol	-C <sub>8</sub> F <sub>17</sub>
6KC10		-C <sub>10</sub> F <sub>21</sub>

<sup>a</sup> Full end group is -IPDU-(CH<sub>2</sub>)<sub>2</sub>-C<sub>n</sub>F<sub>2n+1</sub>, where IPDU is -NHC(O)-

**Surface modification of PTFE with  $R_f$ -PEGs.** The physisorption of  $R_f$ -PEGs onto PTFE was made by two steps. First, the PTFE part was immersed in a solution of  $R_f$ -PEG in ethanol (1 wt %). The PTFE part was removed after ~1 hr, and then without complete drying immersed in a water reservoir for 10 min. During the second step, the  $R_f$ -PEG molecules are expected to rearrange to adsorb onto the PTFE surface. Then, the PTFE part was washed several times with clean water. The low concentration of  $R_f$ -PEG

in ethanol used in the first step was chosen not to make a thick gel layer on the PTFE surface. When a high concentration (10 wt %) was used to modify a narrow PTFE tube described later, the tube was found to be partially filled with hydrogel in some occasions. Time interval between the first step and the second step was maintained minimal to achieve a uniform physisorbed layer on the PTFE part.

**Characterization of surface properties of PTFE.** When a capillary is located at the liquid-air interface, the capillary rise of the capillary,  $h$ , is determined by

$$h = 2 \gamma \cos\theta / (\Delta\rho g r)$$

where  $\gamma$  is the surface tension,  $\theta$  is the angle between the wall of capillary and the interface at the contact point,  $\Delta\rho$  is the difference in density between the liquid and gas phase,  $g$  is the gravity constant, and  $r$  is the diameter of the capillary. When the liquid wets the wall of capillary (when the surface is hydrophilic),  $\cos\theta$  is positive, so  $h$  is also positive. As the surface becomes less hydrophilic,  $\cos\theta$  becomes small, so  $h$  decreases. When the surface becomes more hydrophobic, so the liquid does not wet the wall of capillary,  $\cos\theta$  becomes negative, which results in capillary depression ( $h < 0$ ) instead of the capillary rise (Figure 5.1). Therefore, the capillary rise is indicative of the hydrophobicity of the wall of the capillary for a given fluid and capillary geometry.

To monitor the hydrophobicity of the modified PTFE, this capillary rise method was used. Small diameter PTFE tubing (I.D.  $\approx$  1.35 mm, Waters) was cut into 3 cm lengths and surface modified with R<sub>f</sub>-PEGs as described. The capillary rise was measured by slowly raising the PTFE tube after immersing it in distilled, deionized water. Before modification, the PTFE tube shows capillary depression as expected, and after modification, a positive value of  $h$  is observed (Figure 5.1).

**Stability of R<sub>f</sub>-PEG adsorption under flow condition.** The stability of R<sub>f</sub>-PEG adsorption onto PTFE was investigated under flow condition by attaching the surface modified PTFE tube to a water pump. Distilled, deionized water was run through the system at ambient temperature. The flow rate was controlled to set the shear stress at the wall ( $\tau_w$ ) to a selected value between 0.3 and 2 Pa. At the measurement time, the tube was disconnected from the flow system, and the surface properties were monitored by the capillary rise method as described above and re-connected to the flow system.

**Electron Spectroscopy for Chemical Analysis (ESCA).** ESCA was performed with an M-Probe Surface Spectrometer (Surface Science Instruments, Mountain View, CA). A monochromatic Al K- $\alpha$  X-ray source was employed, and measurements were taken with a resolution 4 at 55° take-off angle. A flood gun was employed for charge neutralization on the polymer surfaces, using the minimum energy feed possible.

## Results and Discussion

**R<sub>f</sub>-PEG adsorption onto PTFE.** Physisorption of R<sub>f</sub>-PEGs dramatically changes the surface properties of PTFE from being hydrophobic to hydrophilic. When the PTFE tube is placed at the air-water interface, the surface properties change from capillary depression ( $h \approx -2$  mm) before modification to capillary rise ( $h > 0$ ) after R<sub>f</sub>-PEG adsorption. The magnitude of the initial capillary rise ( $h_0$ ) is insensitive to the R<sub>f</sub>-PEG used:  $h_0 \approx 16$  mm for 6KC10 and 10KC10, and  $h_0 \approx 12$  mm for 6KC8 and 10KC8. Thus, a PTFE tube modified with any of R<sub>f</sub>-PEG wets effectively.

The stability of R<sub>f</sub>-PEG adsorption onto PTFE under flow depends on the molecular structure of R<sub>f</sub>-PEGs in accord with their phase behavior and erosion kinetics. First,

surface modification by the sol-gel coexisting species shows the gradual change in the hydrophobicity with time. Surface modification by 6KC8 and 10KC8 show similar gradual decrease in the capillary rise on a timescale of one day (Figure 5.2 (a), (b)). Increasing the length of the fluorocarbon ends (10KC10) increases the apparent lifetime of the adsorbed layer (Figure 5.2 (c)). The desorption tendency is insensitive to the shear stress applied by the flow in the range of  $\tau_w$  from 0.3 to 1.3 Pa. Second, surface modification by the insoluble R<sub>f</sub>-PEG is much more stable than by the sol-gel coexisting species. The surface modification by PEG of 6 kD with C10 fluorocarbon end (6KC10) shows very stable modification for long times; at low shear rate ( $\tau_w = 0.3$  Pa), no sign of a change in the capillary rise was observed in 2 wk (Figure 5.2. (d)). Some changes in the capillary rise were observed in ~80 hr at high shear rates (1.2 or 2.0 Pa), but the vibration of the PTFE tube connected to the high capacity pump required to provide the high flow rates might contribute to the partial desorption observed at high wall shear stresses.

The order of the stability of R<sub>f</sub>-PEG adsorption onto PTFE can be understood qualitatively in terms of the phase behavior (sol-gel coexistence or precipitate) and erosion rates of the bulk phases.<sup>15</sup> However, the four fold difference in the desorption time scale between 10KC8 and 10KC10 (it takes ~20 hr to drop to  $h \approx 6$  mm for 10KC8, and ~80 hr for 10KC10) is smaller than the difference in the end-group relaxation time (~40 fold) or the difference in the erosion rate of the bulk gels ( $\gg 100$  fold). This difference in behavior of the physisorbed layers relative to the bulk gels implies that the interaction among the fluorocarbon end groups cannot directly be compared to the interaction between fluorocarbon end groups and the PTFE surface (Figure 5.3).



Adsorption/desorption of hydrophobically modified PEGs on hydrophobic surface under flow in a closed circuit was previously reported.<sup>16</sup> In that experiment, the concentration of free chains in the flowing stream is stepped up or down and the approach to a new equilibrium state is monitored. The modified PEGs investigated (12 kD to 120 kD PEG modified with C16 hydrocarbon at both ends) do not show sol-gel coexistence in water, but instead are soluble in the entire concentration range. Their desorption from polystyrene under flow are governed both by the kinetics of desorption and the diffusive-convective mass transfer. Fillipova found that the process was mass transfer limited; consequently, for a fixed end group (C16 hydrocarbon end), the desorption rate slowed with increasing length of the polymer. The desorption transient following a step down in concentration required from 1s to ~1 hr for the longest PEG studied, depending on the initial surface concentration of the adsorbed layer. This provides a conservative estimate of the lifetime of such layers if they were placed in contact with a flowing stream with no dissolved polymer, as in the present experiments. The dramatic difference in lifetime of their layers (<1 hr) compared to the present polymers (>100 hr) is in accord with the relative magnitude of the erosion rates of single-phase type  $R_f$ -PEG associative polymers compared to  $R_f$ -PEG that exhibit sol-gel coexistence.<sup>15</sup>

We also compared the behavior of telechelic  $R_f$ -PEGs to monofunctional  $R_f$ -PEGs. The desorption of monofunctional  $R_f$ -PEGs was very rapid; the monofunctional  $R_f$ -PEGs were apparently almost completely removed during washing with fresh water after dip coating from ethanol as described above (the PTFE surface remains hydrophobic). This fast desorption correlates with the absence of a thermodynamic barrier for desorption for

monofunctional  $R_f$ -PEG molecules (they can simply form micelles and dissolve in the aqueous phase).

Further study is required to determine if the stability of the surface modification of PTFE by  $R_f$ -PEGs adsorption is long enough to be applied to the small diameter PTFE vascular graft for permanent implantation. However, over 80 hr patency up to 2 Pa wall shear stress or over 2 week patency at 0.03 Pa wall shear stress obtained for 6KC10 adsorption indicates that this adsorption can be applied at least for the surface treatment of PTFE or any hydrophobic biomaterials for relatively short periods (e.g., catheters, short-term use of small diameter grafts in reconstructive surgery and extracorporeal blood contact devices),<sup>10</sup> with the advantages including the simplicity of the process, the versatility to cover any shape, and the low cost of the materials and the coating operation.

**Characterization of  $R_f$ -PEG adsorption by ESCA.** ESCA is an effective way to analyze the chemically modified PTFE surface.<sup>1,8</sup> So, the PTFE surface modification by physisorption of  $R_f$ -PEGs was also analyzed using ESCA. Surprisingly, even after physisorption was made, F atom signal was still detected from ESCA survey spectrum and also  $CF_2$  peak from the high-resolution ESCA C1s spectra, as summarized in Table 5.2. From the detection of  $CF_2$  peak, it may be thought that  $R_f$ -PEG adsorption cannot effectively cover the PTFE surface. However, not only  $CF_2$  peak but also  $CF_3$  peak, which cannot be detected from the bare PTFE surface, was observed from the high-resolution ESCA C1s spectra, and also N atom signal, which is present only at the linker of the  $R_f$ -PEG was detected from the survey spectrum. Therefore, it means that the hydrophobic end group parts were detected. The contribution of end group parts was also confirmed by characterizing the cast thick film of  $R_f$ -PEG on a glass slide, so no fluorine

signal is possible from the substrate, and it still revealed both CF<sub>2</sub> peak and CF<sub>3</sub> peak in the high-resolution ESCA C1s spectra. Considering that ESCA is sensitive only at the surface composition, the detection of CF<sub>2</sub> peak and CF<sub>3</sub> peak in the high-resolution ESCA C1s spectra means that the end groups of R<sub>f</sub>-PEG are not all bound to PTFE surface, but located toward the surface of PTFE during the ESCA analysis. In other words, R<sub>f</sub>-PEG molecules are rearranged from the state where some of the end groups are bound to PTFE surface at the aqueous environment to the state where the end groups are toward air during drying and also at the vacuum state, in which ESCA analysis are performed (Figure 5.4). This highly surface-active state of perfluorocarbon end group and the localization of end groups toward polymer-air interface was reported for the PEGs (from 2 kD to 12 kD) with C8 fluorocarbon end groups.<sup>17</sup> While ESCA is a preferred method of characterization of covalent surface modification of PTFE,<sup>1,5-8</sup> the method does not extend to the present systems, since the structure rearranges upon drying to present a fluoroalkyl signal even when the R<sub>f</sub>-PEG layer is present.

**Table 5.2. ESCA Analysis of R<sub>f</sub>-PEG Modified PTFE Sheet**

Adsorbed species	Sample state	Atom ratio (%) from survey spectrum				Carbon species (%) from high resolution C1s spectra		
		F	O	N	C	CF <sub>3</sub>	CF <sub>2</sub>	CH <sub>x</sub>
Control	bare PTFE	68.4	0	0	31.6	0	100	0
6KC10	adsorption onto PTFE sheet	48.9	9.6	3.1	38.4	8.6	35.0	43.5
10KC10	adsorption onto PTFE sheet	28.1	23.5	0	48.4	0	11.2	88.8
6KC10	casting on glass slide	not measured				7.1	39.8	53.1

## Conclusions

The surface adsorption of R<sub>f</sub>-PEGs onto PTFE effectively modifies the surface from being hydrophobic to hydrophilic. The capillary rise method is a sensitive tool to monitor the change in the surface properties of a narrow tube. The stability of this physisorption under flow of water correlates with the phase behavior and erosion rate of the bulk state of R<sub>f</sub>-PEGs. In particular, an R<sub>f</sub>-PEG that is insoluble in water provides the most stable modification.

## References

- [1] Noh, I.; Chittur, K.; Goodman, S.L.; Hubbell, J.A. *J. Polym. Sci. Pol. Chem.* **1997**, *35*, 1499
- [2] Haimovich, B.; Difazio, L.; Katz, D.; Zhang, L.; Greco, R.S.; Dror, Y.; Freeman, A. *J. Appl. Polym. Sci.* **1997**, *63*, 1393
- [3] Zdrahala, R.J. *J. Biomat. Appl.* **1996**, *10*, 309
- [4] Andrade, J.D.; Hlady, V. *Adv. Polym. Ser.* **1986**, *79*, 1
- [5] Brecht, V.H.; Mayer, F.; Binder, M. *Angew. Makromol. Chem.* **1973**, *33*, 89
- [6] Rong, C.J.; Wakida, T. *J. Appl. Polym. Sci.* **1997**, *63*, 1933
- [7] Koh, S.K.; Park, S.C.; Kim, S.R.; Choi, W.K.; Jung, H.J.; Pae, K.D. *J. Appl. Polym. Sci.* **1997**, *64*, 1913
- [8] Noh, I.; Hubbell, J.A. *J. Polym. Sci. Pol. Chem.* **1997**, *35*, 3467
- [9] Haimovich, B.; Difazio, L.; Katz, D.; Zhang, L.; Greco, R.S.; Dror, Y.; Freeman, A. *J. Appl. Polym. Sci.* **1997**, *63*, 1393
- [10] Deible, C.R.; Petrosko, P.; Johnson, P.C., Beckman, E.J.; Russell, A.J.; Wagner, W.R. *Biomaterials*, **1999**, *20*, 101
- [11] Harris, J.M. Ed. "Poly(Ethylene Glycol) Chemistry, Biotechnical and Biomedical Applications," Plenum New York, **1992**
- [12] Bergstrom, K.; Osterberg, E.; Holmberg, K; Hoffman, A.S.; Schuman, T.P.; Kozlowski, A.; Harris, J.M. *J. Biomater. Sci. Polymer Edn.* **1994**, *6*, 123
- [13] Annable, T.; Buscall, R.; Ettelaie, R. *J. Rheo.* **1993**, *37(4)*, 695
- [14] Xu, B.; Li, L.; Yekta, A.; Masoumi, A.; Kanagalingam, S.; Winnik, M. A.; Zhang, K.; Macdonald, P.M.; Menchen, S. *Langmuir* **1997**, *13(9)*, 2447

- [15] Tae, G.; Kornfield, J.A.; Hubbell, J.A.; HogenEsch, T.E.; Johannsmann, D.  
*Macromolecules* **2001**, *34*, 6409
- [16] Filippova, N.L. *Langmuir* **1998**, *14*, 5929
- [17] Su, Z.; Wu, D.; Hsu, S.L.; McCarthy, T.J. *Macromolecules* **1997**, *30*, 840

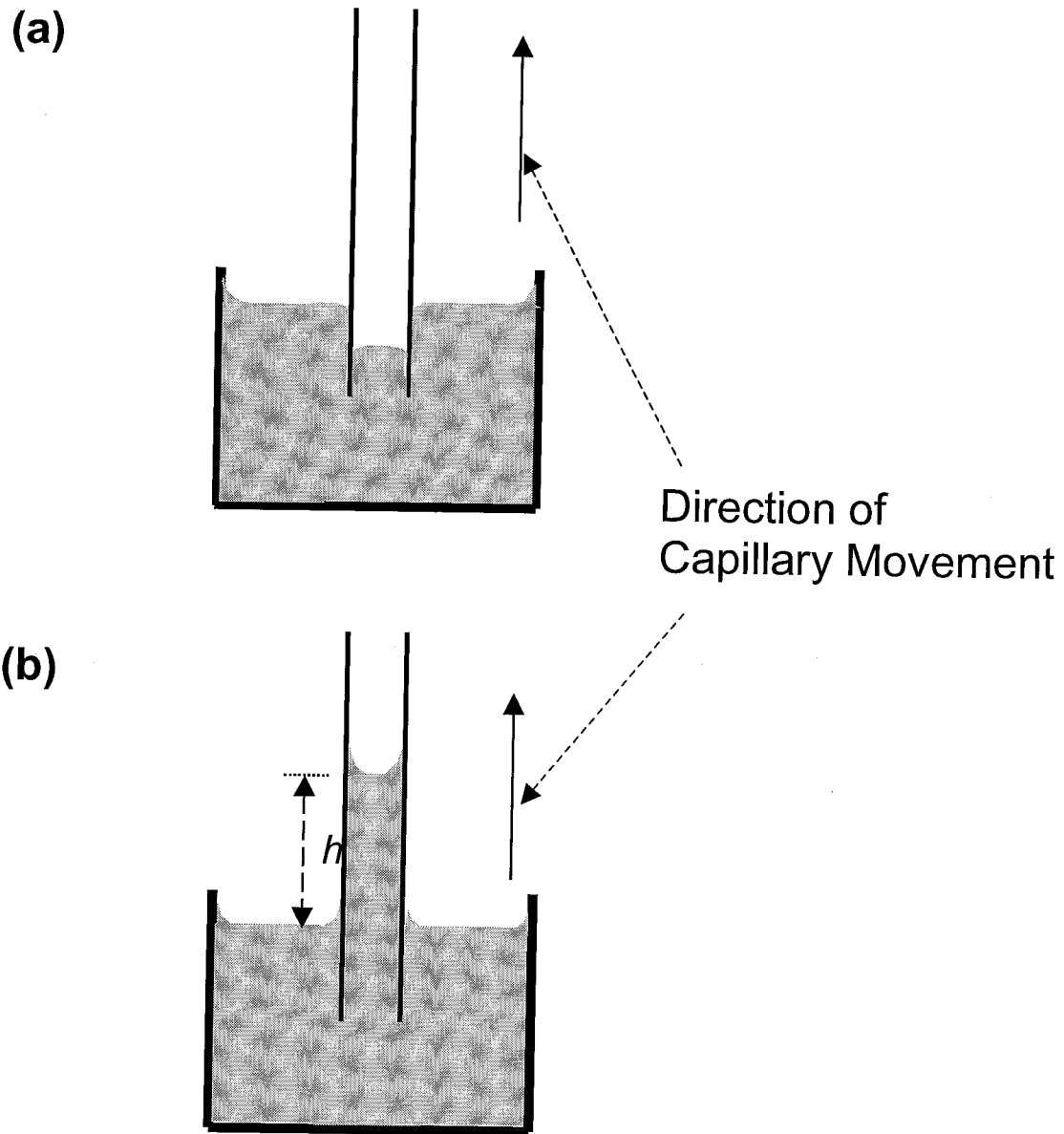
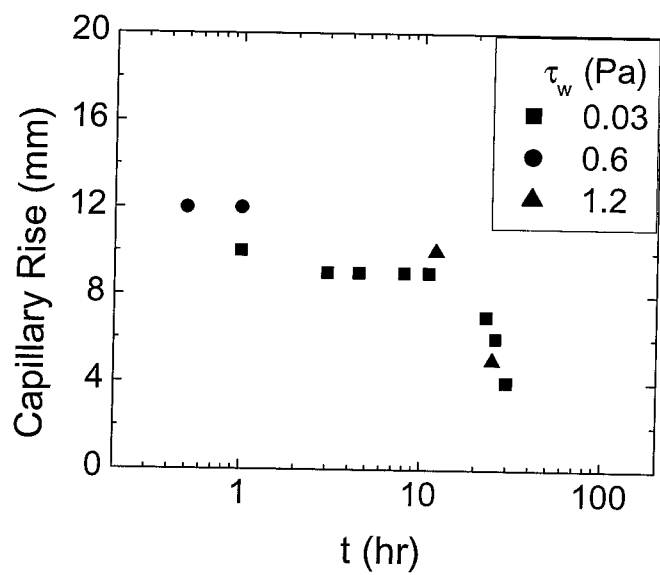
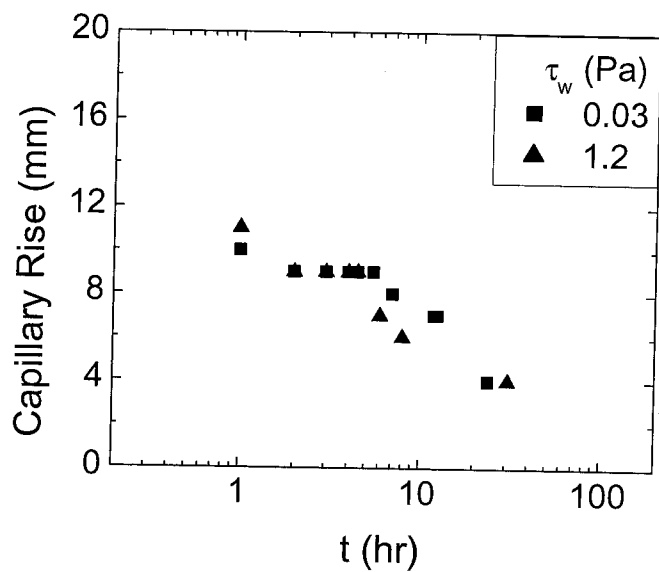


Figure 5.1 The change in the capillary rise by the hydrophobicity of the surface of the capillary that is located at the air-water interface. (a) capillary depression for hydrophobic surface (bare PTFE), (b) capillary rise for hydrophilic surface (modified PTFE).

(a) 10KC8

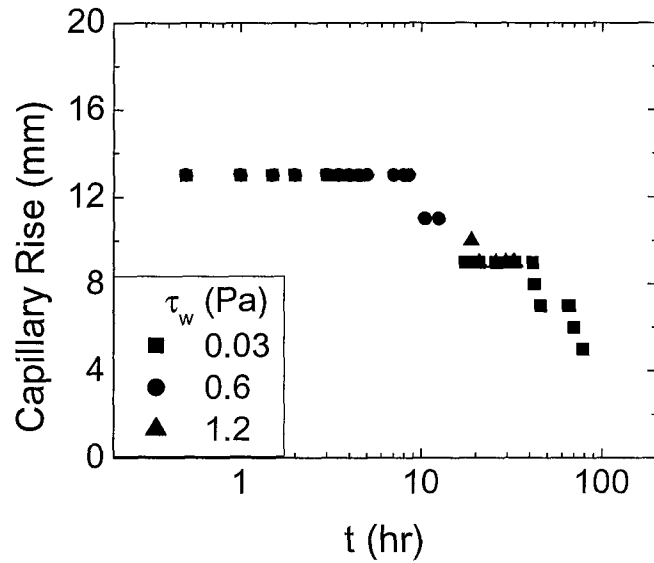


(b) 6KC8





## (c) 10KC10



## (d) 6KC10

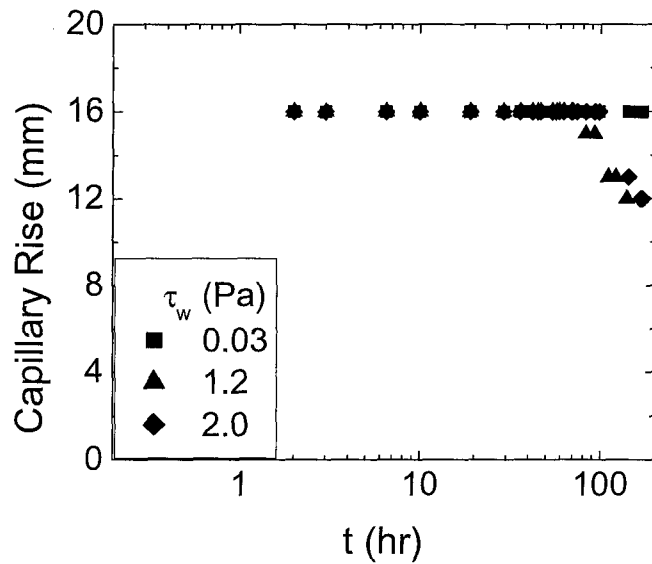
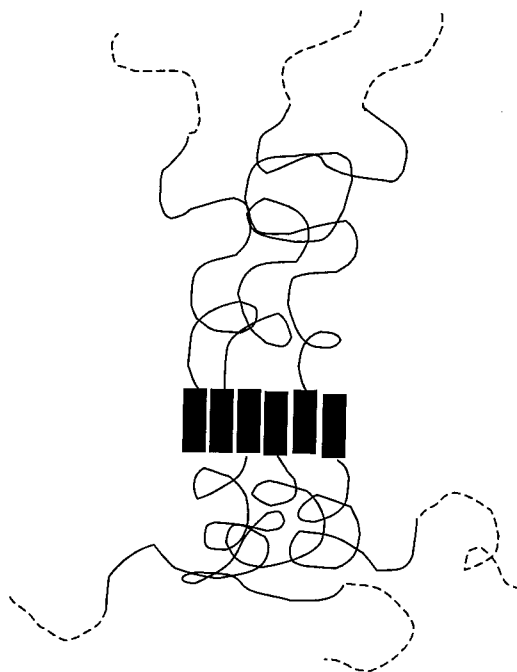


Figure 5.2 The change of the capillary rise of the R<sub>f</sub>-PEG modified PTFE tube (I.D.≈1.35 mm) with time when the tube is exposed to the flow of water for various wall shear stresses. (a) PTFE tube modified with 10KC8, (b) 6KC8, (c) 10KC10, (d) 6KC10.

(a)



(b)

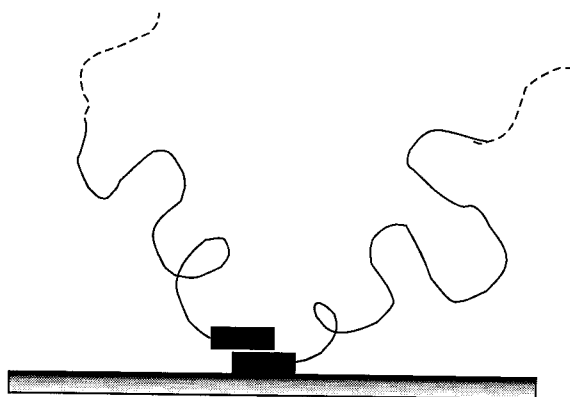
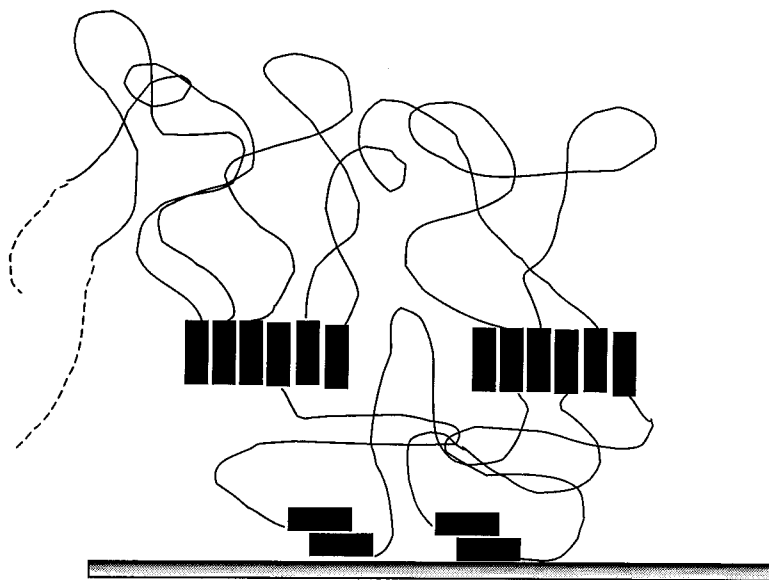


Figure 5.3 The schematic representation showing the physical junction state of fluorocarbon endgroups of  $R_f$ -PEG molecules. (a) in the bulk gel state, (b) in the physisorbed state on PTFE surface.

(a)



(b)

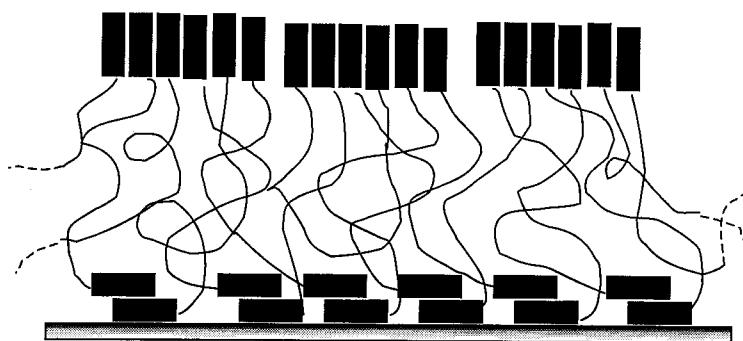


Figure 5.4 The schematic representation showing the physically aggregated state of  $R_f$ -PEG molecules on PTFE surface. (a) in aqueous media, (b) in a dried state.

## Chapter 6. Swelling Behavior of Thin Films of R<sub>f</sub>-PEGs Under Controlled Humidity

### Abstract

The swelling behavior of thin films of fluoroalkyl-ended polyethyleneglycol (R<sub>f</sub>-PEG) (~100 nm thick), observed using a quartz crystal resonator, shows abnormalities under controlled humidity. In a humidity ramp test, it shows an unusual hysteresis: as humidity increases, little swelling occurs until ~85% humidity, then the film swells rapidly; as the humidity decreases, a rapid deswelling occurs near ~75% humidity. This behavior is explained by the semicrystalline nature of dry PEG: once the humidity is high enough to drive melting, abrupt swelling occurs; on cooling, once a sufficient supersaturation is reached, crystals nucleate and grow, expelling water. In response to a step increase in humidity, there is an overshoot in the mass increase, then a gradual reduction to the equilibrium value. In contrast, the response to a step down in humidity is rapid and monotonic. The overshoot and subsequent slow equilibration is attributed to the transient development of the physical network in the gel state.

## Introduction

Absorption, desorption and swelling behavior of polymers play important roles in polymer processing and performance, ranging from issues of dimensional stability and permeability, to controlling adhesion. Rich, nonlinear phenomena are associated with transient swelling and drying of glassy and semi-crystalline polymers. Anomalous, non-Fickian behaviors are broadly associated with the non-linear effects of penetrant on the dynamics of the polymers. Here we describe anomalous behavior of a different type that is associated with a sorbent-triggered first-order phase transition. The system of interest is a hydrophilic, semi-crystalline polymer with hydrophobic end groups, placed in contact with humid air. Due to the strong tendency to absorb water, the melting transition of the crystallites can be induced by contact with sufficiently humid air; during desorption, a sufficient supersaturation must be reached before nucleation and regrowth of crystals occurs. This leads to very different hysteresis behavior than has been previously described. In addition, the transient absorption behavior upon a jump into the swollen state shows a unique overshoot followed by a gradual approach to equilibrium that appears to reflect the time required for assembly and equilibration of the physical gel.

Hysteresis during sorption/desorption has been reported for both glassy polymers and semi-crystalline polymers. The sorption isotherm of glassy polymers has lower swelling ratio during absorption than during desorption at the same fugacity (or partial pressure) of the penetrant.<sup>1</sup> Desorption starts from the removal of the penetrant from the rubbery state of polymer, whereas absorption starts from the addition of the penetrant to the glassy state of polymer, so different volumetric and sorption behavior is expected for mechanically non-equilibrium glassy polymer.<sup>1</sup> Moreover, during drying, the material layer next to the

vapor-polymer interface is the driest part of the sample and can act as a barrier blocking further solvent to the interface.<sup>2</sup> In the case of semi-crystalline polymers, the crystalline part of polymer gives an additional barrier for the penetrant transport.<sup>3</sup> Sorption isotherms have been reported for small amount of penetrant adsorbed (less than a few percent by mass), so the materials maintained their crystallinity during the experiments.<sup>3,4,5</sup> Therefore, the sorption isotherm has been modeled by considering the crystalline regions to be completely non-permeable,<sup>4</sup> and the effect of melting/crystallization of polymers has not been investigated. For the kinetics of sorption and desorption, semi-crystalline polymers and glassy polymers show similar asymmetry in their responses to step-up vs. step-down transients (following a step-up the transient is initially slow and becomes more rapid; following a step-down the transient is initially rapid and slows), attributed to different diffusivity and permeation during absorption and desorption.<sup>6,7,8</sup>

Overshoot sorption has also been reported for glassy polymers;<sup>9-13</sup> following either immersion in solvent or a step-up in vapor pressure, plots of swelling vs. time exhibit an uptake that passes through a maximum and then decreases to a final equilibrium value. The overshoots were interpreted to be related with the different time scales of penetrant transport and polymer relaxation,<sup>9,10,11</sup> as well as the soluble fractions in the polymers<sup>12</sup> or penetrant-induced crystallization<sup>13</sup> in some cases. However, the relaxation phenomena occurring during swelling from a glassy to a solvent-induced rubbery state are very different than the relaxation phenomena involved in the overshoot behavior in our system.

Poly(ethylene glycol)s (PEGs) modified with hydrophobes at both ends have been investigated widely as model associative polymers.<sup>14,15</sup> In aqueous systems, they form physical gels held together by micelle-like clusters of their hydrophobic end groups. In contrast to the previously examined, glassy polymers in which anomalous penetrant transport has been investigated, PEG has a very low glass transition temperature,<sup>16</sup> and thus R<sub>f</sub>-PEGs do as well.<sup>17</sup> Therefore, complexities associated with the glass transition are not expected to play a role. On the other hand, the sorption behavior of R<sub>f</sub>-PEGs may be influenced by relaxation processes associated with the crystallization/melting of PEG midblock and with the network formation/deformation during swelling/deswelling.

Here, we investigate the swelling/deswelling behaviors of thin films of (~0.1 μm) of R<sub>f</sub>-PEG using a quartz crystal resonance (QCR) in humidity ramp and humidity step tests. The humidity range investigated is sufficiently wide to probe the complete melting or crystallization of the PEG midblock.


## Experimental Section

**Materials (R<sub>f</sub>-PEGs).** Poly(ethylene glycol) (PEG) (with alcohol functionality at both ends) of nominal molecular weight 6000 g/mol (6 kD) and 10 kD were modified at both ends with fluorocarbon ends (-C<sub>q</sub>F<sub>2q+1</sub>CH<sub>2</sub>CH<sub>2</sub>, q = 8 or 10) using di-isocyanate linkage. Synthesis and characterizations were done as described previously.<sup>18</sup>

The samples used for this study are described in Table 6.1, where the abbreviation nKCm denotes a polymer with a PEG midblock MW of n kg/mol and with m-carbon fluoroalkyl end groups.

**Table 6.1. R<sub>f</sub>-PEGs**

Sample	PEG-bock	End Group <sup>a</sup>
10KC8	10 kg/mol	-C <sub>8</sub> F <sub>17</sub>
10KC10		-C <sub>10</sub> F <sub>21</sub>
6KC8	6 kg/mol	-C <sub>8</sub> F <sub>17</sub>

<sup>a</sup> Full end group is -IPDU-(CH<sub>2</sub>)<sub>2</sub>-C<sub>n</sub>F<sub>2n+1</sub>, where IPDU is -C(O)NH  NHC(O)-

**Mass determination by QCR with control of humidity.** The fundamental principle of QCR with a viscoelastic load is the shift of the resonance frequency with the mass and dynamic compliance of the load. Neglecting the effect of electrodes, the frequency shift is

$$\delta f^* = (if/\pi)(Z^*/Z_q)$$

where  $\delta f^* = \delta f + i\delta\Gamma$  is the shift of the complex resonance frequency  $f^* = f + i\Gamma$ , with  $2\Gamma$  the bandwidth.  $Z_q$  is the acoustic impedance and  $f_f$  the fundamental frequency. For a film of thickness  $d$  and density  $\rho$ ,

$$\delta f^*/f \approx -(2if_f/Z_q)m[1 + J^*(\omega)(4\pi^2 m^2/3\rho)f_f^2]$$

where  $m = \rho d$  is the mass per unit area, and  $J^*$  is the shear compliance. From the intercept of  $\delta f/f$  vs.  $f^2$ ,  $m$  can be obtained, and from the slope of  $\delta f/f$  vs.  $f^2$  and  $\delta\Gamma/f$  vs.  $f^2$ , even the elastic compliance ( $J'$ ) and viscous compliance ( $J''$ ) can be obtained, respectively.<sup>19</sup>

QCR placed in the humidity-controlled chamber was used to measure the change of mass at a controlled humidity.<sup>2</sup> AT-cut, plane parallel quartz, optically polished, with fundamental frequency of 4 MHz was used. The polymer film was spin-coated onto the



quartz from  $\sim 1$  wt % polymer solution in ethanol. The data acquisition has been described elsewhere,<sup>20</sup> and humidity was feed-back controlled by two air-flows, one that is saturated by passing through the water reservoir, and the other that is dried by passing through desiccant. Temperature was controlled at 24 °C.

## Results

**Humidity ramp test.** With increase of relative humidity, the thin film absorbs water and swells. However, instead of gradual increase of mass from the low fugacity of penetrant (or relative humidity for this case) that is common for the most cases of absorption process, almost no absorption is observed at low relative humidity. Then, a rapid swelling starts at  $\sim 85\%$  relative humidity, followed by further increase of mass at higher humidity. In addition, even with a sufficiently slow rate of humidity ramp (2%/hr), the swelling behavior shows hysteresis; thin film starts to show a rapid swelling from  $\sim 85\%$  humidity when humidity goes up, but a rapid deswelling occurs from  $\sim 75\%$  humidity when humidity goes down (Figure 6.1 (a)).

Successive cycling sorption-desorption experiment was done with increasing ramp rate. During absorption, with increasing ramp rate in each successive run, the overall sorption curve shifts slightly to lower humidity, so the critical humidity where the thin film starts to show a rapid swelling also shifts to a somewhat lower value, and the thin film shows a little higher swelling ratio at a given humidity (Figure 6.2 (b)). During desorption, with increasing a ramp rate in successive runs, the overall desorption curve changes from the sudden deswelling at  $\sim 75\%$  humidity to more gradual deswelling behavior.

With change of film thickness from  $\sim 1.0 \times 10^2$  to  $1.5 \times 10^2$  nm, the thicker film shows a slightly higher swelling than the thinner film in the high humidity range (Figure 6.3). However, with relatively similar film thicknesses ( $\sim 1.5 \times 10^2$  nm and  $\sim 1.8 \times 10^2$  nm), no effect of end group length for the same PEG midblock length (10KC10 vs. 10KC8) is found (Figure 6.4 (a)), but increasing the molecular weight of the PEG midblock slightly increases swelling (10KC10 vs. 6KC8) in the high humidity regime for similar film thicknesses ( $\sim 1.0 \times 10^2$  nm) (Figure 6.4 (b)).

**Humidity step test.** Following a step increase of humidity from a level well below the swelling transition to a level above it, overshoot is observed in the mass change, followed by the slow reduction to the equilibrium state, similarly reminiscent of previous observations in glassy polymers.<sup>9-13</sup> In contrast, following a step down from high to low humidity, the film tracks the equilibrium state very rapidly and monotonically (Figure 6.5). With increase in the high humidity value, the magnitude of the overshoot, the time it takes to reach the maximum overshoot, and the time to reach the equilibrium swollen state all increase (Figure 6.6). With increasing film thickness from  $\sim 1.0 \times 10^2$  to  $\sim 1.5 \times 10^2$  nm, the approach to the equilibrium state after overshoot appears to be somewhat faster (Figure 6.7).

## Discussion

**Sorption isotherm.** The plausible cause of the peculiar sorption curve of R<sub>f</sub>-PEG thin films is the crystallinity of the PEG midblock at low humidity conditions. The hysteresis of sorption curve cannot be explained in terms of the transition between the glassy state and the rubbery state because the experiment temperature is well above the

glass transition of temperature of PEG. However, this hysteresis could result from the transition between the crystal state and the rubbery state of the PEG midblock. The melting of semi-crystalline PEG induced by the sorbent (water vapor) during absorption might result in the abrupt increase in swelling around the critical humidity. Upon drying, a substantial supersaturation may be required before nucleation and growth of crystals of PEG occur during desorption, producing a substantial expulsion of water at a threshold humidity that is lower than the critical value upon swelling.

The effects of increasing ramp rate in successive sorption/desorption experiments also accord with an explanation based on crystallization: the decrease in the tendency of abrupt deswelling and the shift of the threshold humidity for deswelling to lower values are both anticipated by the hypothesis that the deswelling is governed by nucleation and growth. The shift to lower humidity with increasing ramp rate corresponds to reaching a low enough humidity (high enough supersaturation) that significant nucleation occurs during the time the system spends at that supersaturation. The smoothing of the deswelling transition suggests that the integrated amount of crystallization by the time a given humidity is reached decreases with increasing ramp rate, due to the reduced time available for nucleation and growth.

It is interesting that prior studies of sorption behavior in covalently crosslinked PEG did not show abrupt transitions in swelling and deswelling.<sup>21</sup> The sorption isotherm of the crosslinked PEG resin shows significant absorption of water even in the low humidity regime (from ~1.05 swelling ratio at 10% humidity to ~1.20 swelling ratio at ~65% humidity), and a somewhat steeper increase in sorption in the high humidity regime (from ~1.20 swelling ratio at ~65% humidity to ~1.35 swelling ratio at ~75% humidity) at 20

°C. Insignificant hysteresis was found during sorption/desorption. Chemical crosslinking tends to suppress crystallization of semi-crystalline polymers in the dried state. Reduced crystallinity, likely obtained for the crosslinked PEG resin, could permit swelling in the low humidity regime. Further, crosslinking tends to lock in locally heterogeneous environments, causing the distribution of crystallite sizes to be very broad. A broad distribution of crystallite sizes would cause the enhanced sorption associated with their melting to be spread over a broad range of humidity. The strong increase in sorption at high humidity might reflect the melting of crystallites present in the crosslinked PEG resin. The absence of significant hysteresis in crosslinked PEG materials is in accord with the observation that much of the swelling appears to be associated with amorphous material in the network, and what effects of crystallinity may be present are smoothed out by local heterogeneities in the material. Therefore, the abrupt swelling and deswelling, and pronounced hysteresis of the sorption isotherm observed in our system, appear to be distinctive characteristics of a physically crosslinked semi-crystalline polymer.

**Transient sorption.** There are two intriguing features of the transient swelling behavior: first, there is a striking overshoot in mass uptake following a step up in relative humidity that crosses the threshold for abrupt swelling; second, the subsequent relaxation to equilibrium takes a remarkably long time. The overshoot behavior indicates that physical structure in the hydrated state immediately after swelling is compatible with a substantially higher swelling than the equilibrium value. Having swollen from a dry state to a gel with a swelling ratio of  $\sim 2$ , the crystals can be considered fully melted and the PEG chains well solvated. The fluoralkyl groups are likely to have formed clusters, but these micelle-cores may not have reached their equilibrium size ( $N_{ag} \sim 50$  for C10 R<sub>f</sub>

groups and  $\sim 30$  for C8 R<sub>f</sub> groups in each hydrophobic core). Irregularities in the physical network may allow this transient state to swell much more substantially than the equilibrium gel would.

The subsequent approach to equilibrium takes a few hr, which is quite surprising in a system in which the crystallites are melted, *i.e.*, in which all the chains are highly mobile and the individual end-group relaxation time is less than one min. On the other hand, the relaxation of the network structure to equilibrium requires sufficient time for the system to probe a substantial portion of the configuration space of all the end groups among all the micelle cores. We believe that the gradual shuffling of fluoroalkyl ends among hydrophobic aggregates allows the system to move progressively toward the equilibrium aggregation number, loop-to-bridge ratio, etc. As the configuration of the network becomes tighter and more uniform, water is forced out and the swelling ratio drops gradually to its equilibrium value.

Therefore, our proposed model for the whole relaxation process is as follows: Upon the sudden increase of humidity, first, PEG midblocks melt from the semi-crystalline state and start to absorb water vapors before the end groups are fully connected to each other. (The time scale associated with the melting of PEG crystallites can be regarded as relatively short, because humidity ramp rates from 10%/hr to 160%/hr showed very similar sorption curves, Figure 6.2b.<sup>22</sup>) Then, the connectivity among end groups increases and becomes saturated toward the more densely crosslinked gel state, which leads to the partial exclusion of the absorbed water molecules. Therefore, the mass uptake during the process may reveal the underlying change of the crosslinking density of the physical network.

The effect of the set value of high humidity in the step change can also be explained by the proposed model; the higher set value means that the higher driving force for the water absorption for the PEG midblock before the full connectivity among end groups are made, so the peak value is higher and it takes more time to reach the maximum sorption.

Qualitatively similar overshoot sorption behavior was found when the dried thin films of the R<sub>f</sub>-PEGs used in this study (sol-gel coexisting species) were exposed to the flow of water. The polymer concentration in the film shows an initial rapid drop that swings below the value corresponding to the equilibrium state, and then slowly increases to the equilibrium value.<sup>18</sup>

The proposed mechanisms for the abnormal sorption suggest structural studies for the future. To clarify the origin of the hysteresis observed in the humidity ramp test, *in situ* observation of crystallinity of the thin film under the controlled humidity ramp in both directions would be valuable. Similarly, to prove the mechanism of the overshoot sorption following a humidity step, *in situ* observation of the aggregated state of R<sub>f</sub>-PEGs will be needed. However, it is very challenging to obtain adequate signal-to-noise ratio when investigating thin films *in situ*, particularly for transient phenomena.

## Conclusion

The swelling behaviors of thin films of R<sub>f</sub>-PEGs, observed using quartz crystal resonator, show abnormalities that can be attributed to the melting or crystallization of PEG midblock. For the humidity ramp test, thin films of R<sub>f</sub>-PEG shows a peculiar sorption curve; as humidity increases, little swelling occurs until ~85% humidity, then the film swells rapidly; as the humidity decreases, a rapid deswelling occurs near ~75%

humidity. The transition between the semi-crystalline state and rubbery state is proposed as a plausible cause. For the humidity step-up test, an overshoot of mass increase, followed by the slow reduction to the equilibrium value, is observed. The change of the aggregated state of R<sub>f</sub>-PEG molecules (increase in connectivity among end groups) is proposed as a mechanism.

## **Acknowledgement**

We acknowledge Diethem Johansmann in Max Planck Institute for Polymer Research at Mainz, Germany, for the supply of experimental setup of QCR measurements.

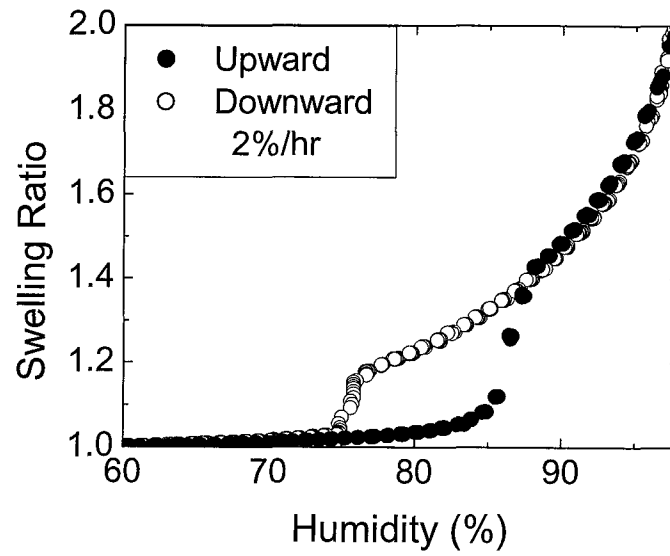
## References

- [1] Vrentas, J.S.; Vrentas, C.M. *Macromolecules* **1996**, *29*, 4391
- [2] Bouchard, C.; Guerrier, B.; Allain, C.; Laschitsch, A.; Saby, A.-C.; Johannsmann, D. *J. Appl. Poly. Sci.* **1998**, *69*, 2235
- [3] Sato, Y.; Yurugi, M.; Yamabiki, T.; Takishima, S.; Masuoka, H. *J. Appl. Poly. Sci.* **2001**, *79*, 1134
- [4] Pope, D.S.; Koros, W.J. *J. Poly. Sci.: Poly. Phys.* **1996**, *34*, 1861
- [5] Hsu, W.-P.; Myerson, A.S.; Kwei, T.K. *J. Appl. Poly. Sci.* **1998**, *70*, 39
- [6] Ngui, M.O.; Mallaparagada, S.K. *Polymer* **1999**, *40*, 5393
- [7] Crank, J.; Park, G.S. "Diffusion in Polymers," Academic Press, New York, USA, **1968**
- [8] Hedenqvist, M.; Johnsson, G.; Trankner, T.; Gedde, U.W. *Poly. Eng. Sci.* **1996**, *36*, 271
- [9] Vrentas, J.S.; Duda, J.L.; Hou, A.-C. *J. Appl. Poly. Sci.* **1984**, *29*, 399
- [10] Smith, M.J.; Peppas, N.A. *Polymer* **1985**, *26*, 569
- [11] Kim, D.; Caruthers, J.M.; Peppas, N.A. *Macromolecules* **1993**, *26*, 1841
- [12] Scranton, A.B.; Klier, J.; Peppas, N.A. *Polymer* **1990**, *31*, 1288
- [13] Titow, W.V.; Braden, M.; Currell, B.R.; Loneragan, R.J. *J. Appl. Poly. Sci.* **1974**, *18*, 867
- [14] Annable, T.; Buscall, R.; Ettelaie, R. *J. Rheo.* **1993**, *37(4)*, 695
- [15] Xu, B.; Li, L.; Yekta, A.; Masoumi, A.; Kanagalingam, S.; Winnik, M. A.; Zhang, K.; Macdonald, P.M.; Menchen, S. *Langmuir* **1997**, *13(9)*, 2447



- [16] 206 K, Young, R.J.; Lowell, P.A. "Introduction to polymers," 2<sup>nd</sup> Ed., Chapman & Hall, London, UK, **1991**
- [17] Glass transition temperatures of R<sub>f</sub>-PEGs have not been measured directly, but melting temperatures of R<sub>f</sub>-PEGs are lower than those of unmodified PEGs, so low glass transition temperatures are expected for R<sub>f</sub>-PEGs.
- [18] Tae, G; Kornfield, J.A.; Hubbell, J.A.; HogenEsch, T.E.; Johannsmann, D. *Macromolecules*, **2001**, *34*, 6409
- [19] Wolf, O.; Seydel, E.; Johannsmann, D. *Faraday Discuss*, **1997**, *107*, 91
- [20] Johannsmann, D.; Mathauer, K.; Wagner, G.; Knoll, W. *Phys. Rev. B*, **1996**, *46*, 7808
- [21] Ranucci, E., Opelli, P., Ferruti, P. *Poly. Gel. Net.* **1994**, *2*, 119
- [22] See Chapter 3.

(a)



(b)

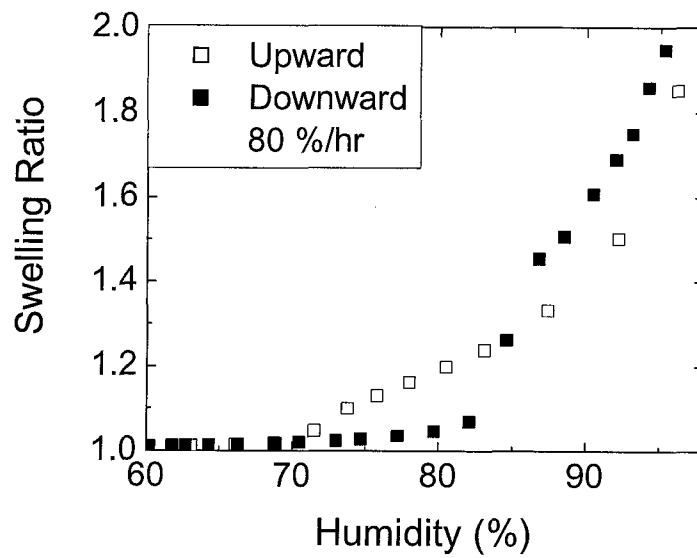
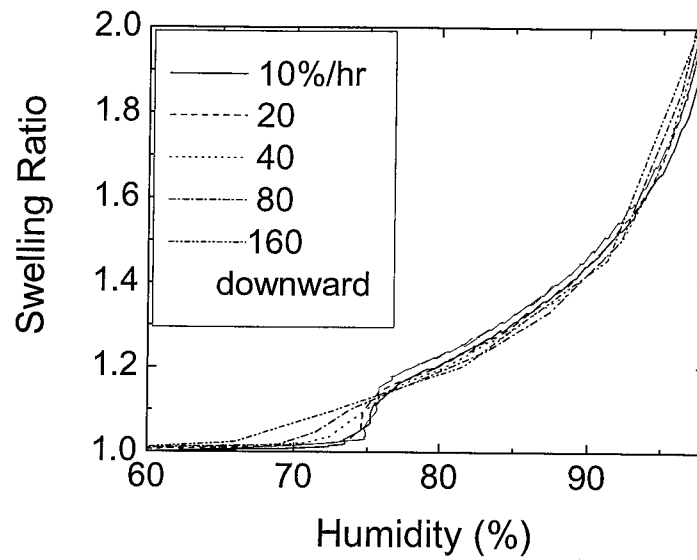


Figure 6.1 Change of swelling state of 6KC8 thin film ( $\sim 1.0 \times 10^2$  nm when dry) for the change in humidity (a) at 2%/hr (b) 80%/hr.

(a)



(b)

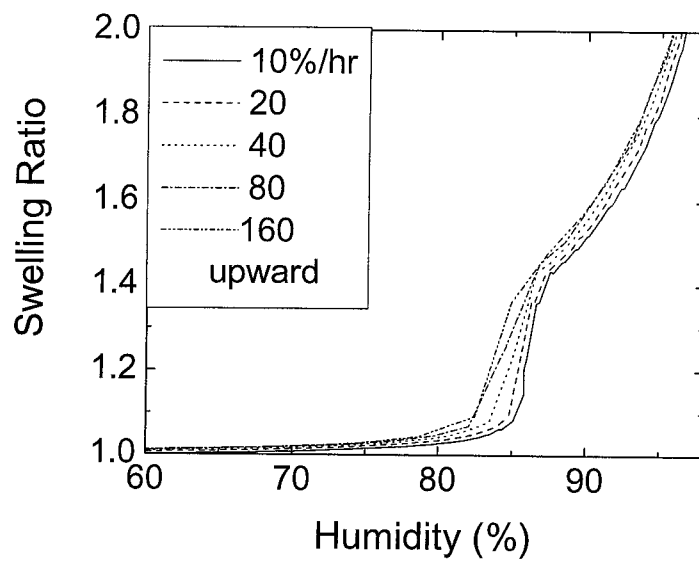
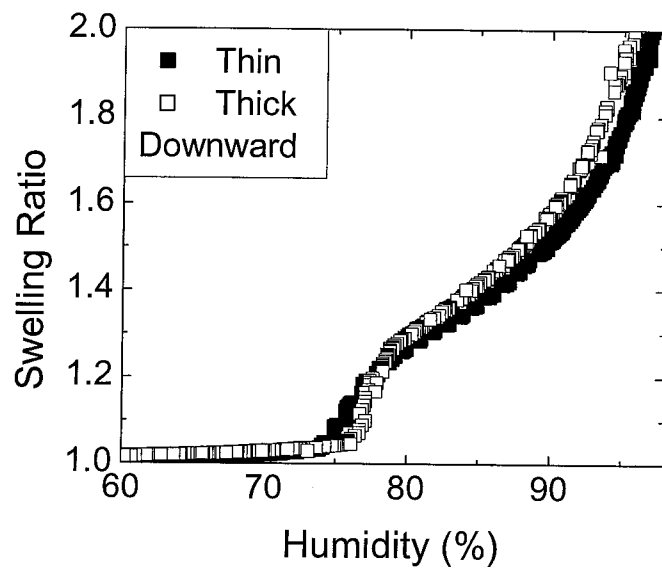


Figure 6.2 Change of swelling state of 6KC8 thin film ( $\sim 1.0 \times 10^2$  nm when dry) for various rates of humidity ramp rates. (a) with decreasing humidity, (b) with increasing humidity.

(a)



(b)

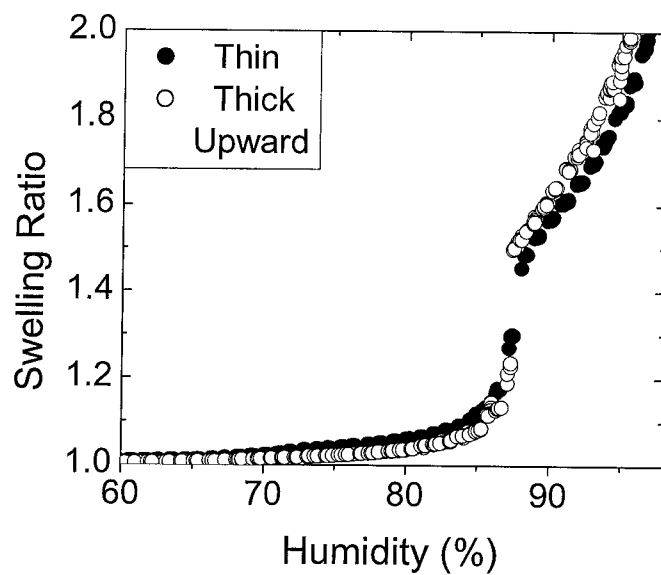
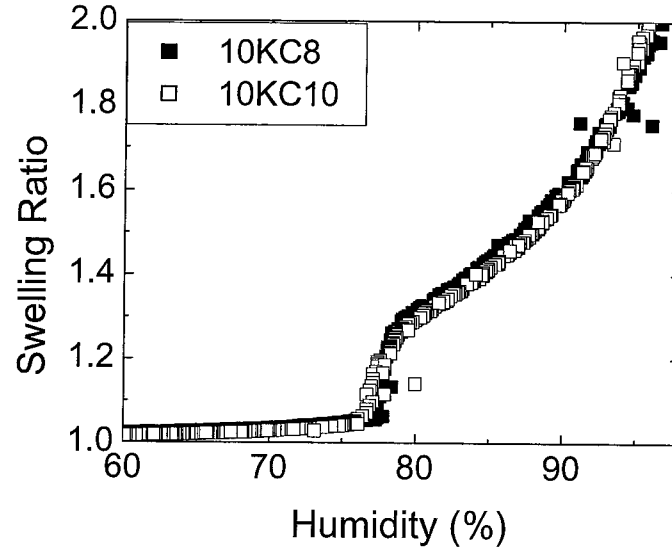


Figure 6.3 Changes of swelling states of two different 10KC10 thin films, one of  $\sim 1.0 \times 10^2$  nm thickness and the other of  $\sim 1.5 \times 10^2$  nm thickness, for the change of humidity at 2%/hr.

(a)



(b)

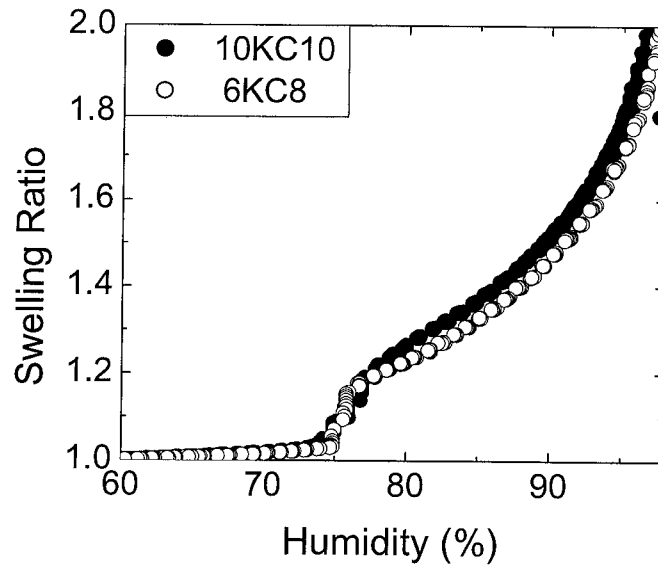


Figure 6.4 Changes of swelling states with decreasing humidity at 2%/hr. (a) comparison of 10KC10 thin film ( $\sim 1.5 \times 10^2$  nm) and 10KC8 thin film ( $\sim 1.8 \times 10^2$  nm), (b) comparison of 10KC10 thin film ( $\sim 1.0 \times 10^2$  nm) and 6KC8 thin film ( $\sim 1.0 \times 10^2$  nm).

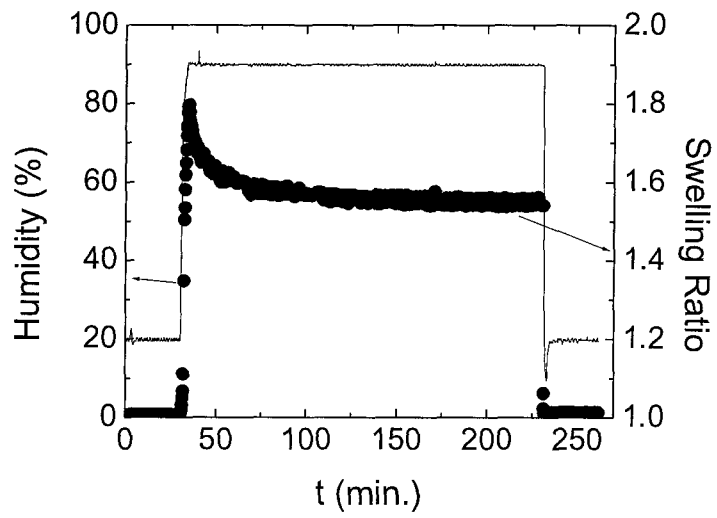


Figure 6.5 Change of swelling state of 6KC8 thin film ( $\sim 1.0 \times 10^2$  nm) for the step change of humidity from 20% to 90%.

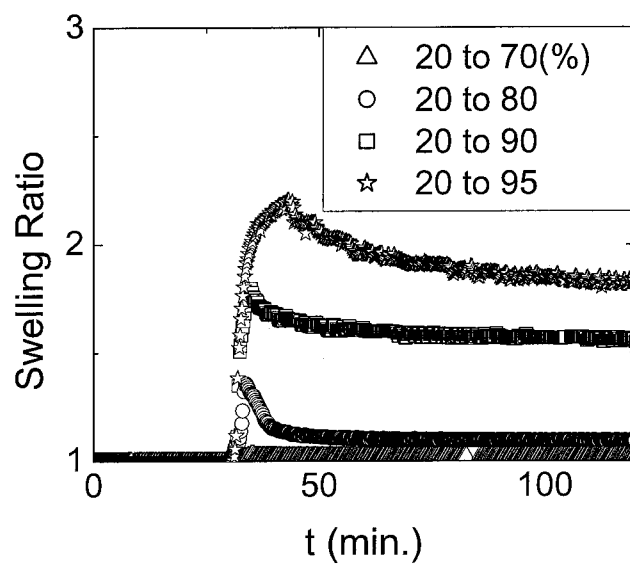


Figure 6.6 Changes of swelling states of 6KC8 thin films ( $\sim 1.0 \times 10^2$  nm) for the step changes of humidity from 20% to various states.

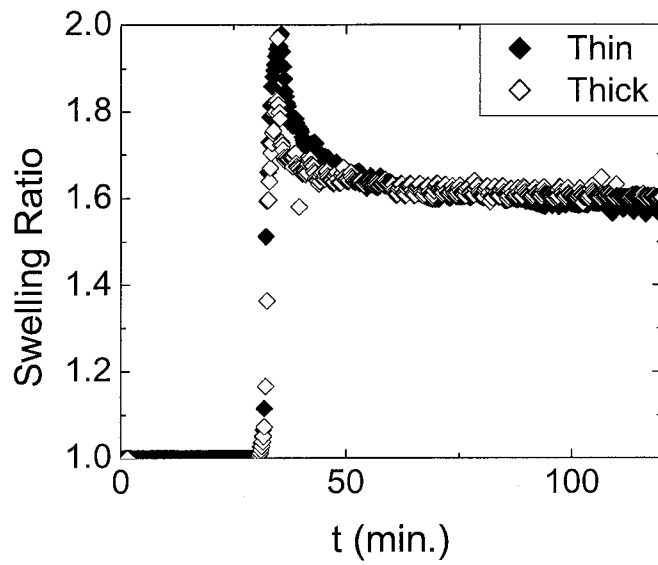


Figure 6.7 Changes of swelling states of two different 10KC10 thin films, one of  $\sim 1.0 \times 10^2$  nm thickness and the other of  $\sim 1.5 \times 10^2$  nm thickness, for the step change of humidity from 20% to 90%.